ABSTRACT

Title of Dissertation:	PHYSICAL-BIOLOGICAL INTERACTIONS DRIVING THE DISTRIBUTION OF THE PELAGIC MACROALGAE SARGASSUM
	Maureen Therese Brooks, Doctor of Philosophy, 2019
Dissertation directed by:	Associate Professor Victoria J. Coles, Marine Estuarine and Environmental Sciences Program

The holopelagic macroalgae of the genus *Sargassum* are the ecosystem engineers of a unique open-ocean rafting ecosystem in the subtropical North Atlantic and tropical Atlantic. Over the last decade, increases in biomass in the tropics and Caribbean Sea have been observed. The underlying causes of this regime shift have been difficult to discern without a baseline understanding of the drivers of *Sargassum* distribution. The objective of this dissertation is to fill this knowledge gap using remote and *in situ* observations, and coupled ocean circulation, biogeochemical, Lagrangian particle, and *Sargassum* physiology models. A satellite-derived *Sargassum* abundance climatology shows the center-of-mass of *Sargassum* shifting between the tropics, Caribbean, Gulf of Mexico, and Sargasso Sea throughout the year. Model experiments demonstrate that advection alone can explain up to 60% of the observed distribution at time scales shorter than two months. At longer time scales, the growth and reproductive strategy of the macroalgae interact with physical processes to drive

the overall observed pattern. *Sargassum* populations in the Western Tropical Atlantic and Gulf of Mexico appear to exert disproportionate influence over the basin-wide distribution. One key physical process influencing both transport and growth is inertia. A novel inverse method, developed from remote sensing to determine the effective radius of *Sargassum* rafts, facilitates modeling inertial effects. The effective radius is on the order of 0.95 m, much closer to the size of an individual plant than that of aggregations which can span kilometers. The inclusion of inertia alters modeled distributions of *Sargassum* by increasing retention in the Gulf of Mexico and the Caribbean, while increasing export from the Sargasso Sea by up to 20%. Inertia acting on buoyant *Sargassum* rafts also leads to their increased entrainment in cyclonic eddies. These eddies propagate toward the north-west in the northern hemisphere providing transport for *Sargassum* from the tropics through the Caribbean to the Gulf of Mexico and leading to increased biomass due to transport into regions with better growing conditions. *Sargassum* biology and its interaction with ocean circulation and mesoscale features is central to improving understanding of the changes in its distribution and for prediction of costly beaching events.

PHYSICAL-BIOLOGICAL INTERACTIONS DRIVING THE DISTRIBUTION OF THE PELAGIC MACROALGAE SARGASSUM

by

Maureen Therese Brooks

Dissertation submitted to the Faculty of the Graduate School of the
University of Maryland, College Park, in partial fulfillment
of the requirements for the degree of
Doctor of Philosophy
2019

Advisory Committee:
Professor Victoria J. Coles, Chair
Dr. Raleigh R. Hood
Dr. Louis A. Codispoti
Dr. Judith M. O'Neil
Dr. Zulema D. Garraffo

Preface

What sweetest macroalgae floats upon

Oligotrophic waves in central gyre

That hosts such plankton, turtles and fish spawn

Who cycle nutrients as they respire

Yet golden seaweed also stands as foe,

A sight that coastal dwellers might abhor

For sweet *Sargassum* causes ample woe

When thalli cast themselves upon the shore

Now I convert this algae into bytes

To drift computer currents far from sea

Lagrangian pathways matched with satellites

Show Western Gulf and tropics are the key

I'll rush to share this news, the hour is late

Write! Write! And publish all, then graduate

-Maureen T. Brooks, 2017

Dedication

For David, whose loving support and boundless patience made this work possible.

Acknowledgements

I must express my deepest and most heartfelt gratitude to my advisor, Victoria Coles. Her example inspired me to pursue my Ph.D., and her guidance and expert mentoring helped me succeed. I thank her for being so generous with her patience, her knowledge, and her time, and for always giving me a safe space to learn and grow. I am also incredibly grateful to have a fantastic committee in Raleigh Hood, Lou Codispoti, Judy O'Neil, and Zulema Garraffo. Discussions with Raleigh helped fuel the hypotheses behind my early work, and his insights and advice have been helpful every step of the way. Judy and Lou have always been ready with constructive suggestions and have been generous with their time whenever I had questions. Zulema been wonderfully supportive, and she helped me decipher the workings of the Lagrangian particles that are the foundation of all of my research.

I have been fortunate enough to work with other generous collaborators throughout this project. I wish to thank Jim Gower for providing MERIS observations of *Sargassum* and the wisdom to interpret them. Likewise I thank Chuanmin Hu for granting permission to use the Sargassum Early Warning System VIIRS images. Thank you to William Coles for his assistance providing field measurements of *Sargassum* in the Caribbean. Tom Cortese was an extremely helpful HPC mentor. I am also grateful to Libby Johns, Scott James, and Mengqiu Wang for fruitful discussions about *Sargassum* distribution, growth, and modeling. Chapters 2 and 3 have also benefited from the suggestions of several anonymous reviewers. Finally I would like to thank the faculty, students, and staff of Horn Point Laboratory.

I am honored to have been a part of such a vibrant and encouraging academic community.

This research is part of the Blue Waters sustained-petascale computing project, which is supported by the National Science Foundation (awards OCI-0725070 and ACI-1238993) and the state of Illinois. Blue Waters is a joint effort of the University of Illinois at Urbana-Champaign and its National Center for Supercomputing Applications. The Izaak Walton League of America Mid-Shore Chapter provided funds for travel and equipment. This work was also funded in part by a University of Maryland Center for Environmental Science Horn Point Laboratory Bay and Rivers Fellowship. Additional support was provided by UMCP College of Computer, Mathematical and Natural Sciences Dean's and Merit Fellowships.

Table of Contents

List of Tables

Chapter 2

Chapter 4

Appendix I

Appendix II

anticyclonic, and the *Sargassum* line position relative to the center for the eddy is also shown. Quality Control (QC) values indicate the following quality requirements: clarity of the *Sargassum* lines in the satellite image, whether the lines were straight for >= 20 km, and whether they were touching a FLSE line. A QC value of 1 indicates the *Sargassum* line met all three criteria, a value of 2 indicates the line failed one criterion, and a value of 3 indicates it failed 2 of the criteria. Lines failing all three criteria were not considered in this analysis.

List of Figures

Chapter 2

Chapter 4

Appendix II

Figure A2.3 *Seasonal effect of inertia on connectivity of Sargassum throughout its range*. Connectivity was calculated at a particle age of 90 d. Colors indicate the % change in connectivity from source region on the x-axis to each receiving region on the y-axis. Small sub-boxes are for particles launched in Fbruary, May, August, and November (clockwise from top left) for each source-receiving region pair.

Chapter 1: Introduction to pelagic *Sargassum* and its habitat

1.1 Introduction

The macroalgae commonly known as "gulf weed", *Sargassum fluitans and Sargassum natans*, are keystone species in the Atlantic Ocean and Gulf of Mexico (Laffoley et al. 2011). Pelagic *Sargassum* serves as habitat and forage for a diverse floating ecosystem including fish, reptiles, and invertebrates (Butler et al. 1983; Hoffmayer et al. 2005; Huffard et al. 2014). Recent unexplained changes in *Sargassum* biomass and extent (Gower et al. 2013; Schell et al. 2015) coincide with increasing reports of wash-ups on beaches in Africa, the Caribbean, and the Gulf of Mexico which negatively impact fishing and tourism (Smetacek and Zingone, 2013). In this dissertation, I aim to understand the physical, biological, and biogeochemical factors that influence *Sargassum's* distribution in the Atlantic.

Satellite observations starting in 2002 highlight the Gulf of Mexico, Sargasso Sea, and western tropical Atlantic as regions with high *Sargassum* biomass, but there is high variability in that biomass from year to year (Gower and King 2011). *Sargassum* areal coverage in the western tropical Atlantic, for example, has varied by as much as a factor of 20 over the last decade (Wang and Hu 2016). However, the underlying factors that contribute to this variability are still not well understood. These factors must be described in order to give context to the recent anomalous events, determine whether they are related to long-term trends, and help local governments in the region adapt their management strategies for these species.

1.2 Ecology and physiology

Pelagic *Sargassum* is a brown macroalgae (Phaeophyceae) found throughout the tropical and subtropical north Atlantic Ocean and its sub-basins. It has been described as early as Columbus' journey from Europe to the Americas in 1492, with other scientific observations dating back centuries (Dickson 1894). *Sargassum*, commonly known as "gulf weed", forms grape-like pneumatocysts which allow it to float at or near the ocean surface. The abundance of *Sargassum* in the western portion of the North Atlantic Subtropical Gyre led the region to be dubbed the Sargasso Sea.

There has been much debate over the origins and life cycle of pelagic *Sargassum* because of its unique open ocean habitat (Deacon 1942). It is now considered to be the world's only true holopelagic macroalgae, having no benthic attached stage in its life cycle and reproducing solely vegetatively via fragmentation (Butler et al. 1983, Stoner 1983). Pelagic *Sargassum* is adapted to its pelagic life cycle via gas vesicles or air bladders which grow up to10mm in diameter (Deacon 1942).

Pelagic *Sargassum* is comprised of two species, *Sargassum fluitans* and *Sargassum natans*. The pelagic *Sargassum* species exhibit physiological characteristics that are distinct from their benthic attached cousins. Pelagic *Sargassum* favors higher salinity environments, and functions better in high light conditions (Hanisak & Samuel 1987). *S. fluitans* has a higher maximum growth rate than *S. natans*, while *S. natans* has a broader optimum temperature range (Hanisak & Samuel 1987). The ranges of the two species overlap, and they often co-occur in samples (e.g. Oyesiku & Egunyomi 2014, Lapointe et al. 2014, Schell et al. 2015).

The two pelagic species can be further classified into distinct morphological forms, *S. fluitans III* and *X,* and *S. natans I, II, VIII,* and *IX* (Winge 1923, Parr 1939). Historically *S. fluitans III* and *S. natans I* have been considered the dominant forms, however the previously-rare *S. natans VIII* has increased in abundance in the tropical Atlantic (Schell et al. 2015, Amaral-Zettler et al. 2017). *S. natans VIII* and *S. fluitans III* are visually similar, with broad blades compared to *S. natans I,* and can be differentiated by the presence or absence of thorns and spines (Parr 1939). Molecular techniques have revealed that the three are genetically distinct (Amaral-Zettler et al. 2017).

Oceanic rafting, which *Sargassum* provides, is key in the propagation and dispersal of many marine organisms (Thiel and Gutow, 2005; Fraser et al 2011). The communities of epi-flora and -fauna that grow within and around floating *Sargassum* include some species endemic to this system (Coston-Clements et al. 1991; Hemphill 2005). *Sargassum* mats are associated with higher abundance and diversity of fish than surrounding waters (Casazza and Ross 2008; Hoffmayer et al. 2005), with up to 110 different species of fish and invertebrates living in close association with *Sargassum* in the Gulf of Mexico and Sargasso Sea (Dooley 1972; Bortone et al. 1977; Butler et al. 1983, Huffard et al. 2014).

Sargassum also plays a role in the migration of juvenile green, hawksbill, loggerhead, and Kemp's Ridley sea turtles (Carr and Meylan 1980; Carr 1987; Schwartz 1988; Witherington et al. 2012). Because of the ecological services they provide and their association with endangered species, *Sargassum fluitans* and *S. natans* are considered keystone species (Laffoley et al. 2011). They are also managed

species in the United States with a Total Allowable Catch of 5,000 pounds wet weight (South Atlantic Fishery Management Council 2002).

Sargassum has a doubling time on the order of 10 days (Carpenter and Cox 1974). It is adapted to environmental conditions in the tropics and Sargasso Sea, and experiences a steep decline in growth rate at temperatures lower than 18°C (Hanisak and Samuel 1987; Carpenter and Cox 1974; Winge 1923). Maximum growth rates of *Sargassum* are achieved at salinities greater than 33 in culture (Hanisak and Samuel 1987). *Sargassum* primary production varies across its range (Carpenter & Cox 1974), and is generally higher in neritic waters with higher nutrient availability (Lapointe 1995).

The pelagic *Sargassum* species, which are largely constrained to the upper meters of clear, oligotrophic waters, have a higher light requirement than their benthic counterparts. They have a light saturation of between 200-300 umol m^{-2} sec^{-1} (Hanisak and Samuel, 1987). In the oligotrophic tropical Atlantic in June 2010, PAR at 5m depth ranges from 0-175 Einsteins m^{-2} sec^{-1} depending on time of day and incident radiation, so the potential for *Sargassum* photosynthetic activity declines rapidly with depth even in the clearest waters. The presence of gas-filled bladders gives *Sargassum* a positive buoyancy, with a rate of rise up to 6 cm/s at the ocean surface (Johnson and Richardson 1977) and allows a range of organisms to colonize *Sargassum* mats. *Sargassum* buoyancy can be compromised by excursions to depths below 35m, due to failure of the buoyant pneumatocysts at pressures experienced at depths between 35 and 100m (Johnson and Richardson, 1977). This means that

Sargassum can only thrive in regions like the Sargasso Sea, with stratified water columns and relatively little mixing.

However, conditions in the Sargasso Sea appear unfavorable to algal growth, with inorganic nitrogen < 0.1 μmol kg^{-1} over most of the year, N:P ratios that indicate potential for phosphorus limitation (Michaels et al. 1994; Cavender-Bares et al. 2001) and even potential iron limitation (Menzel and Ryther 1961; Moore et al. 2006; Wu and Boyle 2002). These overall nutrient conditions and corresponding low primary productivity are similar over much of the Sargasso Sea (Ryther and Menzel 1969; Lomas et al. 2013). It is possible that *Sargassum* acts as an ecosystem engineer, supporting the growth of a community that alters the immediate environment to enhance *Sargassum* growth. The N:P ratio of *Sargassum* itself can vary, from near Redfield ratios (Redfield et al. 1963) of 16 to as low as 10 (Lapointe 1995). *Sargassum* mats host epiphytic cyanobacteria that fix nitrogen (Carpenter 1972; Carpenter and Cox 1974), increasing nutrient availability in otherwise oligotrophic conditions and making *Sargassum* isotopically distinct from surrounding phytoplankton (Rooker et al. 2004). Epiphyte load varies over *Sargassum's* range, and *Sargassum* prevents some fouling by producing and exuding antimicrobial compounds (Conover and Sieburth 1964). In addition to diazotrophic epiphytes, excretion by fish foraging in and around *Sargassum* can provide excess nitrogen and especially phosphorus to the macroalgae, and this mutualistic relationship has the potential to increase *Sargassum* growth (Lapointe et al. 2014).

Sargassum has three primary fates; grazing, sinking, and beaching (Rothäusler et al. 2012; Schoener and Rowe 1970). Grazed *Sargassum* contributes to the growth

of its associated community and nutrient cycling in the euphotic zone. *Sargassum* which sinks to the sea floor can serve as substrate and forage for benthic organisms, and eventually contribute to carbon burial (Schoener and Rowe 1970; Wolff 1979; Wei et al. 2012). Beached *Sargassum* can play positive and negative roles, enhancing dune plant growth (Williams and Feagin 2010) but also causing economic hardship for coastal residents (Ackah-Baidoo 2013; Smetacek and Zingone 2013). The ways in which *Sargassum* responds to ocean physics and chemistry thus have implications for ecology and species disperal, biogeochemical cycling, and the economic and environmental health of coastal communities.

1.3 Sargassum distribution and seasonal cycle

Systematic observations of pelagic *Sargassum* date back centuries, and it was understood as occurring mainly in the Gulf of Mexico and Sargasso Sea (Dickson 1894; Parr 1939). Only within recent decades has the larger geographic extent of *Sargassum* been confirmed (de Széchy et al. 2012; Gower et al. 2006; Gower and King 2011; Siuda 2011). *Sargassum* has been found in the surface Atlantic from the equator to at least 50°N, and spans the basin from the Gulf of Mexico in the west to the Gulf of Guinea in the east. Recent MODIS satellite observations also suggest *Sargassum* presence south of the equator off the coast of Brazil (Mengqiu Wang, *pers. comm.*).

Although the Gulf Stream provides a pathway for *Sargassum* to reach the Sargasso Sea from the Gulf of Mexico, early studies suggested that these two regions hosted distinct populations (Parr 1939). Studies in other organisms such as copepods show large differences in diversity and community composition between the Gulf

Stream and the remainder of the North Atlantic (Beaugrand et al. 2002). Analysis of community composition showed differences in species diversity and variation in abundance in the Sargasso Sea compared to the Gulf Stream, which may relate to the relative age of *Sargassum* mats in the two regions (Stoner and Greening 1984). More recent work by Schell et al. (2015) shows that both *Sargassum fluitans* and *S. natans* can be found from the Western Tropical Atlantic, through the Sargasso Sea and farther to the north, but even within species, morphology differs with latitude. These studies raise questions about how connected populations of *Sargassum* are throughout its range, and what mechanisms might create barriers that could lead to the kinds of morphological and community variability observed.

Studies in the late 20th century hypothesized that *Sargassum* experienced a long term decline, since tows from the 1970s contained only ~6% of the biomass seen in the 1930s (Stoner 1983). However that inference was shown to be the result of insufficient seasonal and spatial coverage in the data (Butler and Stoner 1984), so the historical trend of *Sargassum* biomass remains unclear. More recent observations show a wide range of variability, with densities ranging from 0 - 0.3 g/m^2 in the same location and season from year to year (Siuda 2011). Even though the biomass is variable, the spatial extent is relatively consistent over the seasonal cycle from year to year (Gower and King 2011). The exception to this is in the tropics. High biomass in the tropics like that seen in the summer of 2011 (Gower et al. 2013) is not an annual occurrence, although the trend appears to be one of increase (Wang and Hu 2016). Some years *Sargassum* is absent from the satellite observations in the region and

other years record densities occur, with differences that range over an order of magnitude from 2009 - present day (Wang and Hu 2016).

The seasonal cycle of *Sargassum* detected via remote sensing appears to initiate in the spring following a minimum in biomass in the Sargasso Sea and Gulf of Mexico. The spring bloom yields increasing detections in the Gulf of Mexico and in the tropics south of 10°N. As the year progresses, this biomass is reduced, while *Sargassum* in the Sargasso Sea increases to a peak in the late fall. Ship-based observations in fall and spring dating back over 30 years also show higher abundances to the south of 30°N in the spring, and higher to the north in the fall (Siuda 2011). Gower and King (2011) hypothesized that *Sargassum's* seasonal cycle initiated in the Gulf of Mexico, and that this population is advected out to the Sargasso Sea as the year progresses.

Since 2011 there appears to be a regime shift in *Sargassum* distribution detected via direct and remote sensing observations, with increased biomass now found in equatorial regions in most years (Gower & King 2011, de Széchy et al. 2012, Gower et al. 2013, Oyesiku & Egunyomi 2014, Wang & Hu 2016, Sissini et al. 2017). These recent unexplained changes in *Sargassum* biomass and extent coincide with increasing reports of wash-ups on beaches in Africa, the Caribbean, and Gulf of Mexico which negatively impact fishing and tourism (Smetacek and Zingone, 2013). *Sargassum* areal coverage in the western tropical Atlantic, for example, has varied by as much as a factor of 20 over the last decade (Wang and Hu 2016). Field observations suggest this may also be influencing species and morphotype composition in the Caribbean (Schell et al. 2015). Multiple detection and early

warning systems have been developed to alert residents to incoming *Sargassum* beaching events (Hu 2009; Webster & Linton, 2013; SaWS 2018), however, the underlying factors that contribute to these changes are still not well understood. These factors must be described in order to give context to the recent anomalous events, determine whether they are related to long-term trends, and help local governments in the region adapt their management strategies for these species.

1.4 Regional circulation features affecting Sargassum

Sargassum is free-floating and buoyant, and thus primarily subject to two dimensional lateral surface ocean circulation. The largest area of *Sargassum* habitat, and the region most associated with *Sargassum* is the Sargasso Sea. This sea is defined by the North Atlantic Subtropical Gyre. It is bounded by the Gulf Stream on the west, North Atlantic and Azores Currents to the north, the Canary Current on the east, and the North Equatorial Current to the south. Mesoscale activity is far higher in these boundary regions than in the gyre interior (Wyrtki et al. 1976; Ducet and Traon 2001; Häkkinen et al. 2008). The eddy kinetic energy (EKE) of the Gulf Stream region also varies seasonally, with higher EKE in the summer and lower EKE in winter months (Zhai et al. 2008). Ekman transport helps drive warm temperatures and low nutrient conditions in the highly stratified water column within the convergent gyre over much of the year (Michaels and Knapp 1996).

By contrast, the Gulf of Mexico experiences more eddy activity due to meanders in the Loop Current and seasonal formation of Loop Current rings which propagate from east to west across the Gulf (Elliott 1982; Sturges and Leben 2000). The mean flow in the Gulf is from east to west, with evidence for downwelling in the

western Gulf that could contribute to buoyant *Sargassum* accumulation there (Sturges 2016). The timing of winter mixing differs in the Gulf, and surface irradiance is higher year-round then in the Sargasso Sea, which allows earlier onset of spring bloom conditions than in the subtropical gyre (Xue et al. 2013; Muller-Karger et al. 2015). Major features of the tropical Atlantic include the Inter-Tropical Convergence Zone (ITCZ) which experiences a seasonal north-south shift and associated seasonal changes in the North Equatorial Countercurrent (Richardson and Reverdin 1987; Mitchell and Wallace 1992), and the equatorial upwelling which acts as a barrier to cross-equatorial transport (Stramma and Schott 1999), while increasing nutrient availability.

Eddies have been shown to impact not only overall surface chlorophyll values (Gaube et al. 2014) but also the dominance of different phytoplankton functional groups (d'Ovidio et al. 2010). The same mechanisms that drive these patterns should also apply to *Sargassum*. Lagrangian trajectory analysis suggests that some mesoscale eddies can have retention times as long as months (d'Ovidio et al. 2013), long enough to impact *Sargassum* based on measured growth rates (Carpenter and Cox 1974; Hanisak and Samuel 1987). Conditions within eddies can differ from those outside because they can impact temperature and nutrient concentrations through increased vertical velocities via Ekman pumping (Gaube et al. 2015). This study will examine whether these consequences of eddy activity in the Atlantic and Gulf of Mexico have a measurable impact on modeled *Sargassum* growth and distribution.

1.5 Research focus

This study examines *Sargassum* biomass and distribution across scales, from the processes that influence the mean seasonal *Sargassum* distribution to the high frequency interaction between mesoscale circulation features and *Sargassum* growth and dispersal. A coupled modeling approach that includes ocean circulation, biogeochemistry, and a Lagrangian particle individual-based model of *Sargassum* is used to study the *Sargassum* seasonal cycle. A novel inverse method is developed to estimate physical characteristics of *Sargassum* aggregations from remote sensing imagery. These results are then applied to examine the effects of eddies and inertia on *Sargassum* distribution and growth. The results of this study will inform present day management of *Sargassum*, and help predict how these species will respond to changing oceanic conditions in the Anthropocene.

Chapter 2: Factors controlling the seasonal distribution of pelagic *Sargassum*[1]

2.1 Abstract

Pelagic *Sargassum* (*S. fluitans and S. natans*) is endemic to the tropical and subtropical North Atlantic, where it provides habitat for a diverse and economically important ecosystem. Here, we investigate what controls the *Sargassum* seasonal distribution using a coupled modelling approach that integrates output from a data-assimilating 1/12° HYCOM simulation, a 1/4° coupled HYCOM−biogeochemical model, and individual-based Lagrangian *Sargassum* growth models. Passively advected, buoyant particles with no *Sargassum* physiology aggregate in the central North Atlantic Subtropical Gyre at annual time scales and do not show distributions consistent with satellite observations of *Sargassum*. However, at shorter time scales, advection alone can explain up to 60% of the following month observed distribution during some periods of the year. Connectivity between the tropical Atlantic and Sargasso Sea is largely one-way, with the Sargasso Sea acting as a 'dead end' for *Sargassum*. Adding growth, mortality and a simple formulation of reproduction through fragmentation to the passive advection of *Sargassum* particles generates distributions that match observations with 65 to 75%

---

[1]Published as: Brooks, M.T., Coles, V.J., Hood, R.R., & Gower, J.F.R. (2018). Factors controlling the seasonal distribution of pelagic *Sargassum*. Mar. Ecol. Prog. Ser., 599, 1–18. https://doi.org/10.3354/meps12646

accuracy across all seasons. Incorporating both ocean circulation and *Sargassum* physiology appears to be key in successfully reproducing the seasonal distribution of biomass. We propose a conceptual model of the *Sargassum* seasonal cycle that incorporates new information about a population in the tropical Atlantic. Additionally, we suggest that the Gulf of Mexico and Western Tropical Atlantic are regions whose *Sargassum* populations may disproportionately influence the basin-wide biomass.

2.2 Introduction

Observations of pelagic *Sargassum* date back centuries (Dickson 1894), sparking debate over its origins and life history for much of that time (Deacon 1942). The species of the brown macroalgae (Phaeophyceae) *Sargassum, S. fluitans* and *S. natans*, form floating aggregations or 'rafts' over much of the tropical and subtropical North Atlantic. Both species are holopelagic, having no attached benthic stage in their life cycle, and reproduce solely vegetatively by fragmentation (Butler et al. 1983, Stoner 1983).

Changes in *Sargassum* abundance from the early to the late 20th century have been suggested but have proven difficult to verify (Parr 1939, Stoner 1983). Seasonal variability in *Sargassum* distribution and biomass coupled with seasonality in the sparse observations led to this perceived decline (Butler & Stoner 1984). More recently, *Sargassum* distribution throughout the annual cycle has been mapped via satellite (Gower & King 2011, Gower et al. 2013, Wang & Hu 2016). The remote sensing derived distributions also suggest that changes in biomass and southern range

expansion have occurred in recent years (Gower et al. 2013, Wang & Hu 2016), and field observations suggest this may be influencing species and morphotype composition in the Caribbean (Schell et al. 2015). *In situ* observations confirm that *Sargassum fluitans* and *Sargassum natans* occur off the coast of Brazil, south of the presumed range (Széchy et al. 2012, Sissini et al. 2017). Franks et al. (2016) suggest this is related to a recirculation in the tropical gyre. These range and biomass changes coincide with an increase in reports of beaching events affecting fishing and tourism from Africa to the Caribbean (Franks et al. 2011, Smetacek & Zingone 2013), which prompted the development of a satellite-based *Sargassum* early warning system for the region (Webster & Linton 2013). Understanding what environmental factors are controlling recent variability is difficult, however, without a better understanding of what is driving variability in *Sargassum* distribution on seasonal time scales.

Remote sensing algorithms for *Sargassum* exist for sensors such as the Medium Resolution Imaging Spectrometer (MERIS) and Moderate Resolution Imaging Spectroradiometer (MODIS) satellites because floating vegetation causes enhanced reflectance in the near-infrared (Gower et al. 2006, Hu et al. 2015). Satellite observations (Gower et al. 2006, Gower & King 2011) from 2002 through 2010 demonstrate a seasonal cycle in *Sargassum* distribution initiating in April when integrated basin-wide biomass is at a minimum. High abundances occur in the Gulf of Mexico in the spring and early summer, in the Gulf Stream extension region in late summer and early fall, and in the southern Sargasso Sea in the winter and early spring (Fig. 2.1). High abundances are also suggested (but with little direct validation) in the

tropical gyre in late spring through fall. Subsequent years show the influence of the high biomass seen in the western tropics (Gower et al. 2013, Wang & Hu 2016).

Buoyant *Sargassum* is expected to passively follow surface currents and local eddy fields (Zhong et al. 2012), although there are suggestions that inertial effects acting directly on *Sargassum* rafts could cause their trajectories to differ from that of the surrounding water and influence their distribution (Beron-Vera et al. 2015). However, pelagic *Sargassum* has a minimum doubling time of 9 to 13 d, depending on species (Hanisak & Samuel 1987), which is short relative to advection time scales. Thus, *Sargassum* may not act as an entirely passive tracer, since its distribution can be influenced by growth and mortality in addition to advection. *Sargassum* primary production varies across its range (Carpenter & Cox 1974), and is generally higher in neritic waters with higher nutrient availability (Lapointe 1995). Pelagic *Sargassum* underpins a diverse ecosystem (Butler et al. 1983, Laffoley et al. 2011, Huffard et al. 2014) supporting a wide range of fish species (Hoffmayer et al. 2005) and playing a role in the migration of juvenile sea turtles (Carr & Meylan 1980, Witherington et al. 2012). Some evidence suggests that the macroalgae may even be responsive to excretion of ammonium and phosphorus from associated fish species (Lapointe et al. 2014). This raises the question of the extent to which the observed seasonal pattern is a result of passive advection of *Sargassum* around the Atlantic, versus due to growth and mortality of *Sargassum* rafts as they encounter changing environmental conditions.

In this study we use a numerical model to investigate what controls the distribution and seasonal cycle of *Sargassum* in the North Atlantic and Gulf of

Mexico. Physical circulation and Lagrangian particle advection models are used to estimate the contribution of advection to the *Sargassum* seasonal distribution. This is accomplished via analysis of particle trajectories, particle densities, and regional connectivity. The influence of *Sargassum* growth and mortality is examined by adding an algal physiology model, coupled to a biogeochemical model embedded within the circulation. The simulations suggest spatial and temporal variability in *Sargassum* growth regions strongly influences basin-wide seasonal biomass patterns.

2.4 Methods

2.4.1 Data description and validation

Sargassum biomass is derived from satellite imagery from the European Space Agency MERIS sensor (Rast et al. 1999). A climatology of *Sargassum* biomass is generated from monthly 1° gridded MERIS counts from 2002 to 2012, with an estimated 1400 t (wet weight) of *Sargassum* per grid per MERIS count (Gower & King 2011, Gower et al. 2013). The resulting distribution is smoothed with an adjustable-tension continuous curvature spline with a tension factor of 0.25 (Fig. 2.1). The climatology illustrates the seasonal changes in *Sargassum* biomass in the key habitat regions of the Gulf of Mexico and Sargasso Sea, as well as potentially high *Sargassum* abundance in the tropics.

Both MERIS and MODIS observations show what appears to be a regime shift in *Sargassum* in the tropics, initiating with a high biomass event in 2011 (Gower et al. 2013, Wang & Hu 2016). However, smaller amounts of *Sargassum* have been detected in the region over the entire satellite record (Gower & King 2011, Wang &

Hu 2016). A second climatology using only the period 2002 to 2010 shows a similar overall seasonal pattern and phenology, though with reduced tropical biomass. Thus, here we use the full 2002 to 2012 climatology, which gives a robust description of the seasonality in the subtropics and also includes the signal of the modern tropical regime.

Only limited observations were available to Gower & King (2011) for algorithm validation. Anomalies such as satellite detection of Maximum Chlorophyll Index (MCI) signal in the Pacific outside of the known range of *Sargassum*, and the large biomass in the tropics where there had been few direct observations of *Sargassum* until recently (Széchy et al. 2012) motivate further validation. The Sea Education Association has performed neuston tows from 1973 to 2010 (Siuda 2011). In spring, low to no *Sargassum* is found in tows along 65° W from 20 to 40° N and higher densities are found south of 32° N and west of 65° W (Siuda 2011). This pattern is consistent with the May satellite climatology (Fig. 2.1), which has the lowest densities in the Sargasso Sea, with some moderate biomass to the south and west. In fall, low densities are found in tows south of 30° N along 55 to 60°W, and higher densities (0 to 3 g m^{-2}) are found between 30 and 40°N and extending towards the US East Coast from 55 to 70°W. This is broadly consistent with the September to November satellite climatologies, when moderate to high density regions of *Sargassum*, defined as having greater than 1% of maximum possible MCI signal, extend over the largest area of the Sargasso Sea. This band of high biomass stretches from 35° N to nearly 50° N, beyond the range of direct observations. Satellite detection of abundant *Sargassum* stretching north from the eastern Caribbean to near

24° N from 60 to 65° W in September is less consistent with the limited ship-based data, which suggests low *Sargassum* biomass in this location.

Within the Gulf of Mexico, higher satellite observed densities are seen in spring (March) and increase to over half the area of the Gulf in July (Fig. 2.1) and August (not shown). Like the Sargasso Sea, the Gulf of Mexico also experiences seasonal periods of low or undetectable *Sargassum* densities, but in January rather than May. In contrast, the Caribbean and central tropics (east of 60°W, south of 15° N) have *Sargassum* year-round. In these regions, the extent of the moderate to high densities are the largest in the late summer (September).

2.4.2 Physical model description

Daily output from a data-assimilating Hybrid Coordinate Ocean Model (HYCOM) simulation (Chassignet et al. 2009) is used to advect Lagrangian particles. This is an eddy-resolving (1/12° ~7 km resolution) global model run by the Naval Research Laboratory (HYCOM.org GLBa0.08 expt_ 90.9). The model has 32 hybrid vertical layers, 11 of which are fixed-depth in the upper 60 m of the water column including a 1 m thick surface layer. The high surface vertical resolution is ideal for modeling *Sargassum*, whose buoyancy begins to diminish at depths below 35 m and is fully compromised below 120 m (Johnson & Richardson 1977). Surface forcing, including wind speed, wind stress, precipitation and heat flux is from the Navy Operational Global Atmospheric Prediction System. The short-wave radiation forcing has an analytic diurnal cycle superimposed. Three-dimensional multivariate data assimilation is performed via the Navy Coupled Ocean Data Assimilation system (Cummings 2005, Cummings & Smedstad 2013).

The HYCOM particle-tracking code (Halliwell et al. 2003), based on particle advection schemes from the Miami Isopycnal Coordinate Ocean Model (Garraffo et al. 2001) is used to advect idealized *Sargassum* rafts. Daily instantaneous model velocities, interpolated to 4 h intervals using second-order Runge−Kutta, are used as input for the Lagrangian particle model, which treats particles as water parcels with respect to inertial forces. Solutions are insensitive to realistic values of diffusion (< 1% difference in pairwise particle density at 60 d time scales with added horizontal turbulence velocity variance of 4.63×10^{-6} m^2 s^{-2}). The code is modified for this study to allow specification of float buoyancy (here set to 0.1 m s^{-1} following Johnson & Richardson 1977). This is achieved by adding this rate of rise to the vertical velocity after interpolation of the velocity fields from HYCOM to the particle location. Additional modifications allow for running particles backwards in time by reversing the time step and velocities. All particles in this study are initialized in the uppermost meter to represent buoyant healthy *Sargassum* rafts. Experimental information, including particle release dates and tracking times are specified in Table 2.1. To mitigate the effects of interannual variability, we launch particles in a total of 8 different model years, 2 at 1/12° resolution for physics-only experiments and 6 at 1/4° resolution (Table 2.1). We track individual particles for 2 yr after initialization. Following best practices for particle models of biological–physical interactions we quantitatively evaluate the optimum particle number for model experiments (North et al. 2009). The number of model particles required to obtain stable statistics is determined using the fraction of unexplained variance (FUV) method described by Simons et al. (2013). Particle initializations range from 20 to 280 particles daily,

randomly distributed over the domain of interest over 2 yr (Fig. 2.2). Particle density distribution (PDD) is calculated as the number of particles of a given age in a 2° box divided by the total number of particles released. The FUV is calculated as $1 - r^2$ of the linear correlation coefficient between the PDD at each intermediate total particle count and the final total count of particles. At 60 d (Fig. 2.2a) FUV does not reach the acceptable threshold of 0.05 until there are more than 30000 particles. As particles approach a year of deployment time variability decreases and FUV is <0.025 with only 15000 particles. Low particle number leads to variability in FUV, with a decreasing trend as particles age (Fig. 2.2b). At particle numbers over 50000, FUV is within acceptable limits and shows little change with particle age. An initialization of 51 100 particles (140 d^{-1}) is used as a baseline particle number for our simulations because it is highly correlated (FUV < 0.01) with a larger doubled distribution of 280 particles d^{-1} over particle ages ranging from 30 to 360 d in the region of interest.

2.4.3 Biogeochemical model description

To understand the impact of processes such as light and nutrient availability on *Sargassum*, we developed a biogeochemical model. This is nested within a 1/4° HYCOM simulation with an Atlantic domain from 15° S to 62°N and 100°W to 15°E. A 6-hourly surface forcing is based on the European Centre for Medium-Range Weather Forecasts (ECM-WF) reanalysis (Uppala et al. 2005) and simulations are run for years 1983 to 1988.

The biogeochemical model consists of 2 nitrogen species (NO_3, NH_4), dissolved inorganic phosphorus (DIP), 2 phytoplankton (an open-ocean phytoplankton assemblage, and a diazotroph modeled on *Trichodesmium*), 1

zooplankton, and 2 detrital compartments of different sizes and remineralization rates. All of the living compartments have fixed N:P ratios, while the detrital compartments are allowed variable stoichiometry. Model structure is adapted from the work of Fennel et al. (2006), with addition of inorganic phosphorus, diazotrophy, and changes to phytoplankton light response after Hood et al. (2001) and Coles & Hood (2007). The Polar Science Center Hydrographic Climatology (Steele et al. 2001) is used for nutrient initial conditions and boundary relaxation. Model equations are described in Appendix I. Normalized root mean square (RMS) error between model fields and SeaWiFS monthly chl a climatologies ranged from 0.009 to 0.016 (O'Reilly et al. 2000, SeaWiFS Project 2003). These residuals are slightly lower than those for sea surface temperature.

2.4.4 *Sargassum* model description

A *Sargassum* model runs within each Lagrangian particle, with each particle representing a super- individual aggregate of *Sargassum*. At each time step, *Sargassum* is advected by the particle model, and then growth and mortality are calculated based on ambient conditions at the particle location. This physiology model represents a functional group of pelagic *Sargassum* rather than either species specifically, so rates are selected from the range for both *S. fluitans* and *S. natans* during parameter optimization. *Sargassum* super-individuals within each Lagrangian particle are modeled with a macroalgal framework that includes light (I), temperature (T), and nutrient conditions (N) based on the biogeochemical model.

$$\frac{dSarg}{dt} = Sarg * f(I) * f(T) * f(N) * \mu max_S - m * Sarg \qquad \text{(Eqn 2.1)}$$

Mortality (m) here is the aggregate effect of senescence and grazing, where μmax_S is *Sargassum* maximum growth rate and m is *Sargassum* mortality rate.

Because the Lagrangian approach allows for tracking the fate of discrete aggregations of *Sargassum*, modeled light availability accounts for the growth of epiflora and epifauna as a function of super-individual age:

$$f(I) = (1 - e^{-I/I_k}) * f(age) , \quad \text{(Eqn 2.2)}$$

with an exponential decay in light response at increasing ages:

$$f(age) = e^{-age/a_{ref}} . \quad \text{(Eqn 2.3)}$$

where a_{ref} is the reference age for *Sargassum* light limitation due to colonization by epifloral and epifauna.

Nutrient uptake is modeled as a Monod function,

$$f(N) = \frac{(N)}{k_{sarg}+(N)} , \quad \text{(Eqn 2.4)}$$

where N is the limiting nutrient (NO_3, NH_4, or DIP).

Growth experiments suggest little effect of temperature on *Sargassum* growth above 18°C (Carpenter & Cox 1974), with reduced growth below this temperature for both species (Hanisak & Samuel 1987). *S. fluitans* may experience low-temperature stress starting at 24°C (Hanisak & Samuel 1987), however observations of *Sargassum* below 18°C showed signs of distress and wilting (Winge 1923). For this reason, we implement a temperature dependence with a threshold for growth at 18°C.

$$f(T) = \begin{cases} 1, & Temp \geq T_{ref} \\ 0, & Temp < T_{ref} \end{cases} \quad \text{(Eqn 2.5)}$$

The *Sargassum* model also includes pressure-induced sinking. Buoyancy of *Sargassum* floats is diminished at relatively shallow depths, and they are fully

compromised by excursions to 120 m (Johnson & Richardson 1977, Woodcock 1993). Any *Sargassum* particle that descends below the maximum depth of float integrity (z_{max}) becomes too dense to recover and all biomass is lost via sinking.

We perform parameter optimization because several model parameters have few or no reported values in the literature for pelagic *Sargassum*, and because we are using a *Sargassum* functional group rather than explicitly modeling both species. A 3-way optimization tests 12 possible values for each parameter (1728 total parameter combinations) to select the parameter values that minimize error with satellite fields. Each model solution is compared with observations by binning both the satellite climatologies and model output onto an identical 2° grid and computing the RMS difference. This RMS error is averaged over the model domain monthly. The optimal parameter values, used in all subsequent simulations, are shown in Table 2.2. Note that the nutrient half saturation value is likely biased to be low because the biogeochemical model tends to have slightly low surface nutrient concentrations.

2.4.5 Particle model validation

HYCOM model fields have been widely utilized in studies of particle dispersal (Coles et al. 2013, Putman & He 2013, Rypina et al. 2013, Stukel et al. 2014) and model validation studies have been published for the global domain (Chassignet et al. 2003, 2009). Here we concentrate on how well the model particles compare with the limited set of surface observational drifter data to ensure the surface currents relevant to *Sargassum* dispersal are captured reasonably, and to identify potential regions of divergence. Drifter observations for drogued drifters within the model domain region are obtained from the Global Drifter Program Drifter Data

Assembly Center (Hansen & Poulain 1996). Model particles are launched to match initial drifter observations, with 7 particles initialized on the same day of the year and distributed within 3 km of each observed launch. These particles are tracked for 1 yr (Fig. 2.3).

After 2 mo, the distributions of observed drifters (Fig. 2.3a) and model particles (Fig. 2.3b) differ by less than 1% particle density in any given 2° × 2° bin. At this time scale, there is slightly higher retention of observed drifters in the Gulf of Mexico and near the Bahamas, but both model and observed drifters show the highest densities in the northwest region of the domain off of Georges Bank. Although the number of observed drifters with a full year of tracking data is low (n = 310), there is good agreement between the model and observations (Fig. 2.3c). The bulk of the drifters aggregate in the central gyre after 1 yr. Observed drifters show slightly greater spread, especially in the region northwest of the Gulf Stream, where eddy activity in the model may be resolution- limited. However, because model particles are removed when they go aground, particle density in the model tends to be very low near to the coastline, which explains some of the discrepancy.

2.5 Results and discussion

2.5.1 The role of advection

If *Sargassum* is initially evenly distributed through- out the Atlantic at low densities below satellite detection limits, as a result of winter mixing processes for example, seasonal variations in advection could potentially generate aggregations

similar to the observed seasonal patterns. Lagrangian particle experiment R-ISO (Table 2.1) tests this hypothesis.

Randomly seeded, surface-restricted particles are launched every day for 1 yr over the whole domain (Fig. 2.4a). Transport of particles from the tropics through the Caribbean archipelago helps to maintain some particle density in the Gulf of Mexico at 2 mo time scales (Fig. 2.4b). After 6 mo (Fig. 2.4c), particle density is reduced by half in the Gulf of Mexico. Particle densities are also reduced at the northern and southern extents of the domain, due to loss of particles from the domain to the north, and to inflow of waters devoid of particles from the south. Particles are lost from the coast of Africa and the tropics due to upwelling and divergence in the Tropical Gyre and Guinea Dome (near 20° W, 15° N). After 1 yr, there is a strong tendency for particle aggregation in the North Atlantic Subtropical Gyre (Fig. 2.4d). At this time scale, particle densities in the central gyre have increased by an order of magnitude, while ecologically important regions such as the Caribbean and Gulf of Mexico are almost completely devoid of particles. The particle distribution resembles that of surface plastics in the region (Law et al. 2010) due to convergent Ekman flow, rather than the observed *Sargassum* distribution.

We subsequently examine each of the following assumptions: that *Sargassum* is highly buoyant and surface-restricted, that *Sargassum* exists at low densities throughout the domain, and that *Sargassum* behaves like a passive particle. The assumption that *Sargassum* is surface-restricted is tested first. *Sargassum* aggregations are frequently observed drifting subsurface. Small-scale, wind-driven features such as Langmuir cells can drive them as deep as 100 m (Johnson &

Richardson 1977), and wind speeds as low as 4 m s^{-1} can result in subsurface *Sargassum* (Woodcock 1993). In experiment R-3D, the randomly initialized particles are neutrally buoyant 3-dimensional particles, and experiment R-3DB added positive buoyancy of 0.1 m s^{-1}. Both of these simulations resulted in particles aggregating in the central gyre at long time scales similarly to R-ISO (not shown). Particle density distributions for these 3 experiments converged after 6 mo, with pairwise FUV < 0.05 after 1 yr. At long time scales, particles initialized at the surface aggregate in the central gyre due to Ekman transport whether they are surface-restricted, neutrally buoyant, or slightly positively buoyant.

To test whether the *Sargassum* seasonal cycle is dependent on initial conditions, we initialize model particles based on the derived satellite climatologies. Particles are initialized daily in a randomly generated pattern within contours where MCI > 1% of maximum. Simulations with surface-restricted (C-ISO), neutrally buoyant (C-3D) and positively buoyant (C-3DB) particles initialized in accordance with monthly satellite climatologies of *Sargassum* all yield similar aggregated particle densities in the gyre at time scales of 6 mo or greater. Surface-constrained particles (Fig. 2.5) have slightly higher densities in the northern portion of the subtropical gyre than 3-D positively buoyant particles (not shown) since there are some losses from the surface layers when the 3-D particles experience winter mixing. However, all 3 experiments result in the same pattern of aggregation in the gyre despite their observationally determined initial condition.

At shorter time scales, particles initialized in this way more closely match observations, and we examine monthly distributions to determine the degree of short-

term advective control on *Sargassum*. We track model particles which originate within a given monthly observed distribution over a 2 mo period to determine what fraction remain within the satellite derived contours of *Sargassum* observations 2 mo later (e.g. Fig. 2.6b in September). Observed Global Drifter Program (GDP) drifters (Hansen & Poulain 1996) in the domain are also analyzed with an identical method (Fig. 2.6a).

Match rate for particle location is calculated by counting particles within boundaries defined by a 1 km buffer around the 1% contour of MCI from the satellite climatology. This match rate is normalized to the total number of drifters or particles in the domain. The potential maximum match rate is expected to be below 100% due to discrepancies in comparing individual years to a climatology, limitations of model resolution, and small numbers of observed drifters.

The match rate is bimodal for both observed and modelled drifters (Fig. 2.7), with a peak in late winter and a stronger peak in late summer/early fall. Although the sample size for observed drifters is small (fewer than 10 drifters are present in *Sargassum*-dense areas in some months), the overall pattern is consistent with our Lagrangian particles. These match rates are much higher and more strongly seasonally varying than the distributions for all observed drifters in the domain or for randomly distributed model particles (Fig. 2.7). Examining 3 mo and longer time intervals continues to show a distinct peak in match rate until time scales exceed 6 mo. Beyond that time period, the overall match is low and variable. After a full year, only 15% of the particles initialized in *Sargassum*-dense regions are still consistent

with *Sargassum* observations. Thus, initial *Sargassum* distribution influences the final distribution for up to 6 mo.

The seasonality of the match rate indicates that processes other than advection are influencing the *Sargassum* distribution. Elevated match in the winter (months 2 to 4) is consistent with *Sargassum* experiencing lower temperatures and suppressed growth (Hanisak & Samuel 1987), causing physical transport to explain more of the spatial distribution. A maximum match of 59% of model particles (Fig. 2.7b) occurs in the month of September, indicating another period where advection plays a large role in determining the *Sargassum* distribution. The subtropical water column is strongly stratified in September, leading to low nutrient conditions and reduced vertical mixing which make it more likely that surface transport rather than growth is controlling the *Sargassum* density. Periods of minimum match rate in December and June indicate times when *Sargassum* physiology may be more important in setting its distribution.

Gower & King (2011) proposed that the *Sargassum* seasonal cycle begins in the Gulf of Mexico in March-April with *Sargassum* growth advected out to the Atlantic, where it eventually senesces about a year later in the southern Sargasso Sea. To evaluate this hypothesis, we track buoyant, 3-D particles initialized in the Gulf of Mexico in experiment C-3DB, to quantify what fraction exit into the Atlantic within 1 yr, and whether there is a seasonal pattern. Connectivity between the Gulf of Mexico and the Sargasso Sea (Fig. 2.8) is high, with 29% of particles reaching the Atlantic within 1 yr. Particles are 5 times as likely to make this passage within 3 mo of launch as they are at longer time scales (Fig. 2.8a). The seasonal peak in particles crossing

into the Atlantic in August (Fig. 2.8b) is a result of the large *Sargassum* biomass observed in the Gulf of Mexico in the spring and early summer exiting the region at this 3 mo time scale. However, with less than 1/3 of *Sargassum* exiting the Gulf within 1 yr, there must be robust growth of *Sargassum* after leaving the Gulf or additional seeding from other sources to match the densities seen in the northern Sargasso Sea in the fall.

However, the *Sargassum* originating in the Gulf of Mexico does not contribute to high density of *Sargassum* in the tropics. Trajectories of randomly seeded surface particles initialized in the Gulf of Mexico (Fig. 2.9a) and the Caribbean (Fig. 2.9b) remain exclusively north of 10° N after 1 yr. *Sargassum* originating in the tropics (Fig. 2.9c) does reach the Caribbean and Gulf of Mexico at this time scale. Even accounting for transit times longer than 1 yr, *Sargassum* from the Gulf of Mexico does not reach the tropics, since the convergent North Atlantic Subtropical Gyre is essentially a dead end (Fig. 2.9d). Connectivity analysis shows that over 92% of particles launched in the Caribbean in the spring (that did not run aground) are advected into the subtropical gyre after 1 yr. For the western and eastern Gulf of Mexico 54 % and 81 % of particles, respectively, are found in the subtropical gyre after 1 yr, while the rest remain within the Gulf. None of these regions export particles to the tropics at any time scale from 30 to 360 d. This suggests that a southern or eastern source of *Sargassum* is necessary to account for biomass in the tropics and Caribbean. This is supported by the connectivity between the Western Tropical Atlantic, which exports particles to the tropics (77%), but also to the Gulf of Mexico (5 %) and Caribbean (8 %), with the remainder entering the subtropical gyre.

To better understand the connectivity between regions and to potentially highlight source regions of *Sargassum* we conduct an experiment in which we run particles backwards in time (C-BK). Particles are initialized using the *Sargassum* monthly climatology for each month, and run with a negative time step for 60 d (Fig. 2.10). The central and eastern subtropical gyre is largely devoid of particles, confirming the pattern seen in Fig. 2.9d where particles tend to remain confined to that region. The highest densities of particles are found along the coast of Brazil and along the equator, suggesting again the potential for a southern source for *Sargassum* in the tropics. These results are consistent with recent evidence of links between the equatorial population and beachings of *Sargassum* in the Caribbean (Franks et al. 2016). Of particular interest, our results suggest a pathway for connectivity between the putative large equatorial population (Gower et al. 2013) and the Caribbean and Gulf of Mexico. Even though relatively few particles follow this pathway, over 60% of the particles in the Gulf and Caribbean track back to this hypothetical tropical population.

The time scales associated with the travel of these particles indicate that equatorial *Sargassum* observed between December and February could be contributing to the peak in *Sargassum* biomass in the Gulf of Mexico between May and July. Match percent between particles run backwards for 2 mo and observed *Sargassum* distributions showed that 50% of particles track back to regions that do not match observations. This suggests that low densities of *Sargassum*, invisible to satellites, could contribute to blooms over much of the Atlantic as they are advected into regions with favorable growth conditions.

2.5.2 *Sargassum* model

To determine the role *Sargassum* biology plays in driving its seasonal distribution, we apply the *Sargassum* super-individual model to each particle in a 1/4° HYCOM simulation which is coupled with a biogeochemistry model (simulation R-SAR). We conduct a sensitivity analysis to understand which parameters have the largest impact on the *Sargassum* model. Single parameter model sensitivity is evaluated for all *Sargassum* model parameters (Table 2.2), focused on a range bounded by ± 10% of reported values, where available. Mortality, nutrient uptake half saturation, and reference age for light limitation are the parameters with the greatest impact on model solutions. The combined impact of grazing and mortality is about a 5% loss d^{-1}, and *Sargassum* older than 55 d begins to experience notable light limitation from growth of epiflora and epifauna or from loss of buoyancy.

For *Sargassum* growth experiments, particles are initialized daily across the model domain for 6 yr. Nitrogen, phosphorus, light and temperature are sampled at each daily particle location and input into the *Sargassum* physiology model. Particle density maps are similar to the results from 1/12° physics-only simulations indicating that reducing the horizontal model resolution did not significantly alter the particle dispersion characteristics at the spatiotemporal scale of this analysis (Fig. 2.11a). The match between model (Fig. 2.11b) and observations (Fig. 2.1d) is greatly improved by including *Sargassum* biomass from the *Sargassum* physiology model in the particle density calculation (Fig. 2.11c). Biomass is higher in and near regions of high observed *Sargassum* density, and dramatically reduced in the central gyre where low nutrient conditions are unfavorable for growth. Growth rates approached their

maximum of 0.1 d^{-1} most frequently in the tropics in winter, suggesting a stronger role for nutrients than for light and temperature in controlling *Sargassum* growth. The percent match between model and observations (Fig. 2.12a) is higher when *Sargassum* physiology is included than for any other simulation. The match rate is also consistently high throughout the year, implying that *Sargassum* growth and mortality are large contributors to the observed distribution even during periods when advective control is also high.

Because observed *Sargassum* distribution is patchy, we estimate the best possible model fit to observations by comparing the observed interannual variability to the monthly climatology. We use the root-mean square (RMS) error between satellite derived *Sargassum* biomass for 10 individual years and the climatology to characterize observed variability (Fig. 2.12b). The mean RMS difference between the observations and climatology is 0.44, while the RMS difference between the model and climatology is 0.50. Variability in biomass in the tropics in the spring and summer accounted for the highest differences between individual years of observations and the climatologies. For the model, RMS differences peaked slightly later in the summer and early fall when *Sargassum* biomass is starting to diminish in the tropics. On an annual basis, the model biomass falls within the range of variability of the satellite observations.

2.5.3 *Sargassum* seed populations

This model still underestimates *Sargassum* biomass in the tropics over much of the year even when nutrient, temperature, and light conditions are favorable. Biomass is overestimated elsewhere. Tropical *Sargassum* has high growth rates in the

model, but is advected away too quickly to allow accumulation of biomass. One scenario that accounts for this missing *Sargassum* is import from outside our model domain. Observations of pelagic *Sargassum* off the coast of Africa are relatively recent in the literature (Oyesiku & Egunyomi 2011, Gower & et al. 2013), but evidence from local fishing communities suggests it has been present over at least several decades, although not at current densities (Ackah-Baidoo 2013). A modest export of *Sargassum* from a region such as the Gulf of Guinea, combined with favorable growth conditions, could be contributing to the high biomass across the tropical Atlantic (Franks et al. 2016).

We assess the potential that export from one or several sub-regions of the Atlantic sustains the seasonal distribution of *Sargassum* in a series of model seeding experiments. Particles are initialized daily in 17 sub-regions with average area of 1.32 $\times 10^6$ km^2 in the Sargasso Sea and along the coastlines on both sides of the basin, at the same density as the whole- domain experiments for 6 yr. Notably, seeding in any of the individual sub-regions yields better match with observed *Sargassum* distributions than initializing across the entire domain (Fig. 2.13, gray bars), again suggesting that although *Sargassum* has the potential to be dispersed throughout the Atlantic, these dispersed fragments do not appear to be driving the seasonal cycle. The highest match between model and observations is obtained by seeding particles in the western Gulf of Mexico, west of 90°W (RMS difference = 0.36), the southwestern tropical Atlantic between 5°S to 10°N and 40°W to 60°W (RMS difference = 0.35), or in both of these regions simultaneously (RMS difference = 0.34). A closer examination within individual sub-regions shows that while the basin-

wide average agreement with observations is similar when seeding in either the southwestern tropics or the western Gulf of Mexico, only the experiment that seeded in both simultaneously reproduces the seasonal pattern in those locations (Fig. 2.12a), but still underrepresents peak *Sargassum* biomass, especially in the Sargasso Sea.

Another possible driver for seasonal changes in *Sargassum* biomass is vegetative reproduction. As pelagic *Sargassum* and related species break, new growth is primarily initiated from the residual fragments at apical meristems (Tsukidate 1984, Hanisak & Samuel 1987). We expand the model to include vegetative propagation by tracking when each *Sargassum* particle dies, and resetting its biomass to a small initial condition instead, simulating a small fragment of the *Sargassum* mat breaking off at that location to start a new organism. Since rafting macroalgae can have expected lifetimes on the order of months (Thiel & Gutow 2005), we apply this propagation mode only to *Sargassum* particles over 1 mo old. This avoids over-representation of biomass in regions with high mortality due to seasonal temperature changes or severe nutrient limitation. We apply vegetative propagation only to particles where the *Sargassum* has died because fragmentation and growth at other times is assumed to be aggregated with the other biomass in a given particle.

We repeat the 6-yr, full-domain model experiments with vegetative propagation enabled. Simulations with and without this reproductive strategy added have comparable RMS differences of 0.52 and 0.50 respectively, when compared with the monthly satellite climatologies. However, without vegetative propagation the model has a negative bias in mean relative *Sargassum* biomass of −10 to −40% of the maximum in the western Atlantic and Gulf of Mexico, while the bias with vegetative

propagation is much smaller and more centered about the mean (−7% to +1.5%) (Fig. 2.13, white bars). Vegetative propagation also yields increased match with observations in seeding experiments with sources of *Sargassum* in the Gulf of Mexico and southwestern tropics, while allowing increased accumulation of biomass in the Sargasso Sea (Fig. 2.14). Without vegetative propagation, local patterns are reproduced but the basin-wide distribution is unrealistic without seeding across the domain because of the difference between the mortality rate and the time scale of advection (Fig. 2.14a). The addition of vegetative propagation allows biomass accumulation in the Caribbean and Sargasso Sea from nonlocal sources. Thus, the additive effects of vegetative propagation and localized sources of new *Sargassum* appear to be key in accurately reproducing the *Sargassum* seasonal cycle.

2.6 Conclusions

At short time scales of 2 mo or less, advection alone can be responsible for a 60% match between model particles and *Sargassum* observations, indicating that advection is a central element determining *Sargassum* distributions in the Atlantic. However, at longer time scales, particles, whether surface, neutrally buoyant, or positively buoyant, aggregate in the subtropical gyre. This aggregation occurs regardless of whether particles are initialized throughout the Atlantic or only in regions with observed *Sargassum*. Thus, advection is not sufficient to maintain the seasonal pattern of *Sargassum* biomass across multiple years. This highlights the significance of mortality, growth, and reseeding from putative source regions in maintaining *Sargassum's* seasonal distribution.

Results of seeding experiments with the *Sargassum* growth model highlight that the western Gulf of Mexico and the western tropics, especially south of the equator, appear to have a strong role in generating the seasonal cycle. These regions are associated with 2 of the largest rivers discharging into the Atlantic, the Mississippi and the Amazon. Nutrient loading may enhance *Sargassum* growth locally in these 2 regions, however even under the globally high discharge of the Amazon, inorganic nitrogen falls below detection limits about 200 km from the river mouth (Weber et al. 2017). Neritic waters near the coastline have also been linked with higher growth rates of *Sargassum* than in the central Sargasso Sea in observations (Lapointe et al. 2014). In this model, that growth is what allows for high *Sargassum* biomass even in regions that would otherwise have low accumulation due to the circulation.

It is also noteworthy that due to the circulation patterns in the Atlantic, we are unable to reproduce the seasonal biomass pattern without continuous seeding in both key regions, as there are no purely advective pathways for *Sargassum* from the Gulf of Mexico to reach the tropics at biologically relevant time scales. The backwards-timestep particles and connectivity analysis presented here also support the hypothesis that *Sargassum* in the tropics has a southern source. Different morphological forms of *S. natans* appear to be dominant in the Sargasso Sea versus the Western Tropics (Schell et al. 2015), which is consistent with this two-source hypothesis. Additional observational studies would be helpful in determining if *Sargassum* biomass is present in the proposed seed regions year-round, and whether

the genetic diversity of *Sargassum fluitans* and *Sargassum natans* supports this hypothesis.

The Western Tropical Atlantic source region is of particular interest due to its potential role in fueling beaching events in the Caribbean. Reverse-time modeling and observed drifters suggest that *Sargassum* from recent beaching events in the eastern Caribbean and Brazil may have originated in the equatorial region (Franks et al. 2011, 2016). Biomass in the tropics is highest in the summer, during the period of eastward retroflection of the Amazon River plume in the North Equatorial Counter Current. However, there is also year-round connectivity between the Amazon plume and the Caribbean, with water discharged from the Amazon in the spring having the highest probability of reaching the Caribbean (Coles et al. 2013). The connectivity analysis in this study is consistent with the results of Coles et al. (2013), and also shows that the connectivity from the tropics to the Caribbean is higher than any other potential source in the Atlantic. This provides a mechanism for a direct link between the elevated *Sargassum* biomass in the tropics in recent years and the increased reports of *Sargassum* beaching in the Caribbean.

We propose a scenario where the *Sargassum* seasonal cycle begins in the spring with growth in the tropics and the western Gulf of Mexico, in agreement with analysis of the satellite observations alone (Gower & King 2011). Biomass from the tropics gets advected through the Caribbean to the Gulf, supplementing local growth there into the summer. This model highlights how connectivity between the Gulf of Mexico and the Sargasso Sea, in conjunction with direct inputs from the population in the tropics, fuels growth in the Sargasso Sea in summer and early fall. At this point

temperature and light constrain growth at the northern extent of *Sargassum's* range, and advection works to aggregate biomass toward the Sargasso Sea, where much of the biomass is exported in the late winter. Regions of high *Sargassum* mortality in this model are consistent with observations of *Sargassum* on the sea floor (Schoener & Rowe 1970) and warrant further study as a possible locally important source of carbon export. This enhanced understanding of the drivers of the *Sargassum* seasonal cycle should help inform management of fisheries dependent on *Sargassum* habitat, and forecasting of costly *Sargassum* wash-up events in the Caribbean and Gulf of Mexico.

2.7 Tables and figures

Table 2.1: Lagrangian Particle experiments. Experiments with multiple resolutions listed were replicated at each resolution. The 1/12° model is the global, data-assimilating HYCOM experiment 90.9 for years 2011-2012. The 1/4° model is the Atlantic domain model with coupled biogeochemistry developed for this study, for years 1983-1988.

Experiment Time	Particle	Distribution	Model Resolution(s)	Tracking
R-ISO	Isobaric	Whole domain	1/12°, 1/4°	Forward
R-3D	3-D	Whole domain	1/12°, 1/4°	Forward
R-3DB	3-D, buoyant	Whole domain	1/12°, 1/4°	Forward
C-ISO	Isobaric	Climatology	1/12°, 1/4°	Forward
C-3D	3-D	Climatology	1/12°, 1/4°	Forward
C-3DB	3-D, buoyant	Climatology	1/12°, 1/4°	Forward
C-BK	3-D	Climatology	1/12°, 1/4°	Backwards
R-SAR	3-D, buoyant, growth	Whole domain	1/4°	Forward

Table 2.2: *Sargassum* physiology model parameters

Symbol	Parameter	Value	Unit	Literature range	Source
μmax_S	*Sargassum* maximum growth rate	0.1	d^{-1}	0.029–0.11	Lapointe (1986), Lapointe et al. (2014), Hanisak & Samuel (1987)
m	*Sargassum* mortality rate	0.05	d^{-1}	25–60 % of gross productivity	Carpenter & Cox (1974), Lapointe (1995)
I_k	*Sargassum* growth-irradiance parameter	70	W m^{-2}	33–78	Hanisak & Samuel (1987), Lapointe (1995)
a_{ref}	Reference age for *Sargassum* light limitation	55	d	*	Thiel & Gutow (2005)
k_{SargN}	*Sargassum* nutrient uptake half saturation	0.012	mmol N m^{-3}	**	Lapointe (1986), Lapointe (1995), Carpenter & Cox (1974)
T_{ref}	Minimum temperature for *Sargassum* growth	18	°C	18–24	Carpenter & Cox (1974), Hanisak & Samuel (1987)
z_{max}	Maximum depth before *Sargassum* buoyancy is compromised	120	m	35–135	Johnson & Richardson (1977)

*No literature values are reported for this parameter. Initial estimates for parameter optimization were made based on maximum age of other rafting macroalgae and the growth rates of *Sargassum* epiphytes

**No direct measurements are reported for this parameter; however, see references for examples of growth and nutrient concentrations measured under varying environmental conditions

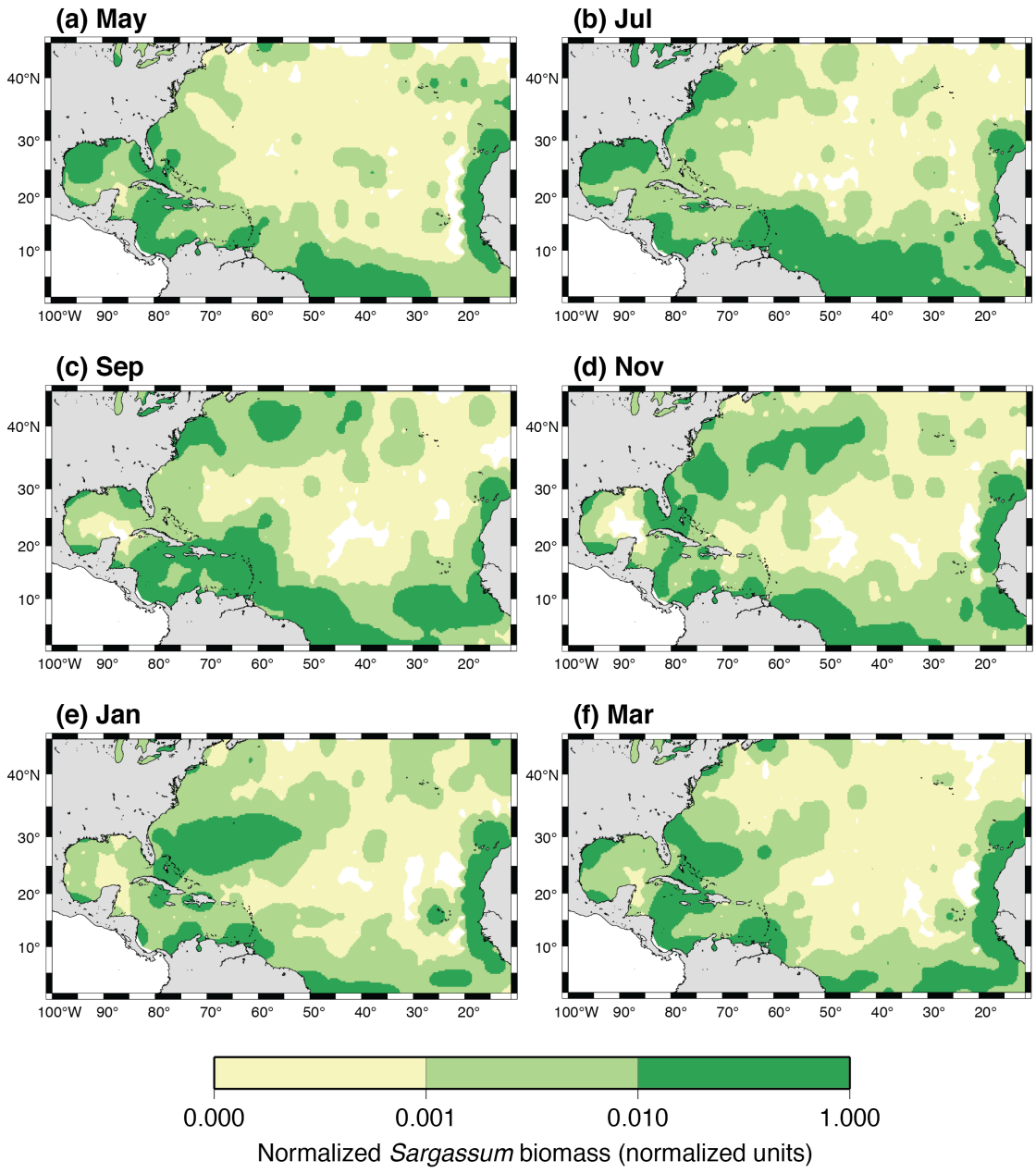

Figure 2.1 Relative *Sargassum* biomass based on monthly satellite climatologies from Gower and King 2011, Gower et al. 2013. Each panel represents a different month, with the seasonal cycle initiating in the spring when integrated basin-wide biomass is at its annual minimum.

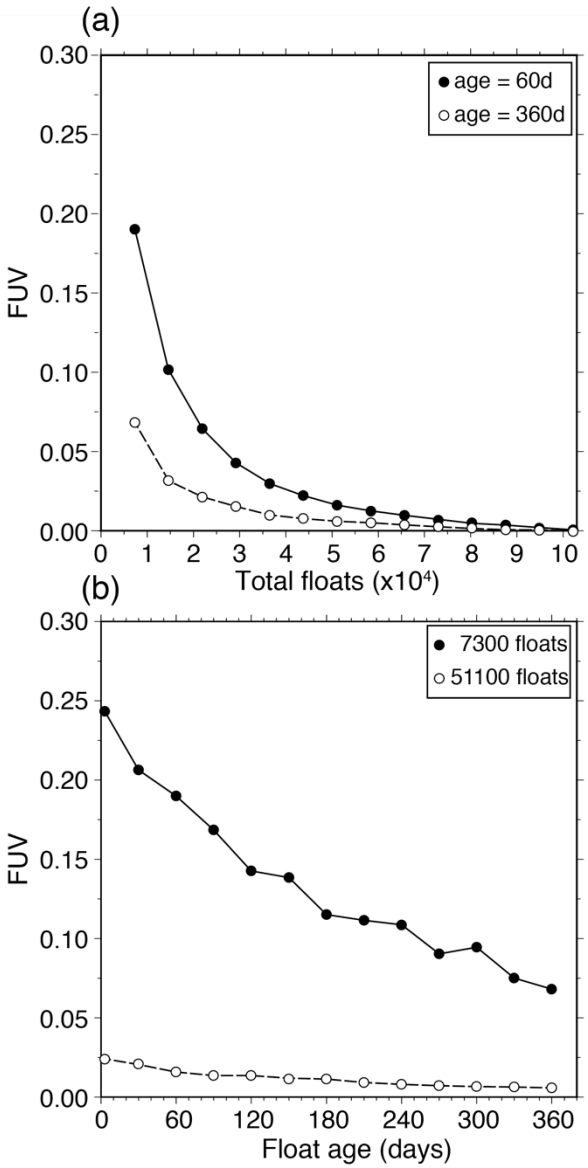

Figure 2.2 Fraction of unexplained variance (FUV) (a) as particle numbers increase, and (b) as a function of particle age. Comparison is with a reference run with 102,200 particles (280 particles released per day).

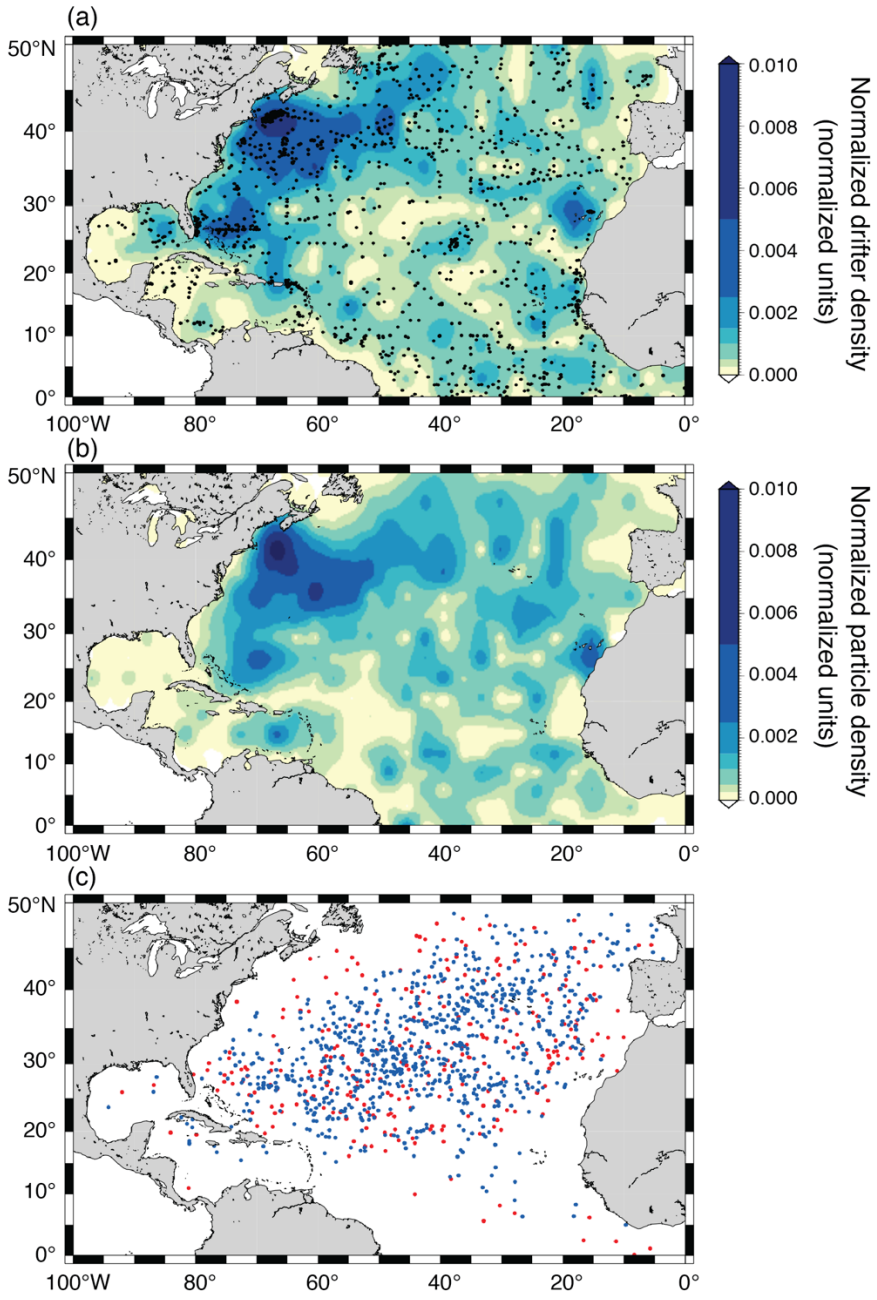

Figure 2.3 Comparison of observed drifters and model particles. Density distributions for (a) observed, and(b) model drifters after 60 d transit time. Black points are model and drifter launch positions. (c) Observed (red) and model (blue) drifter locations after 1 y transit time.

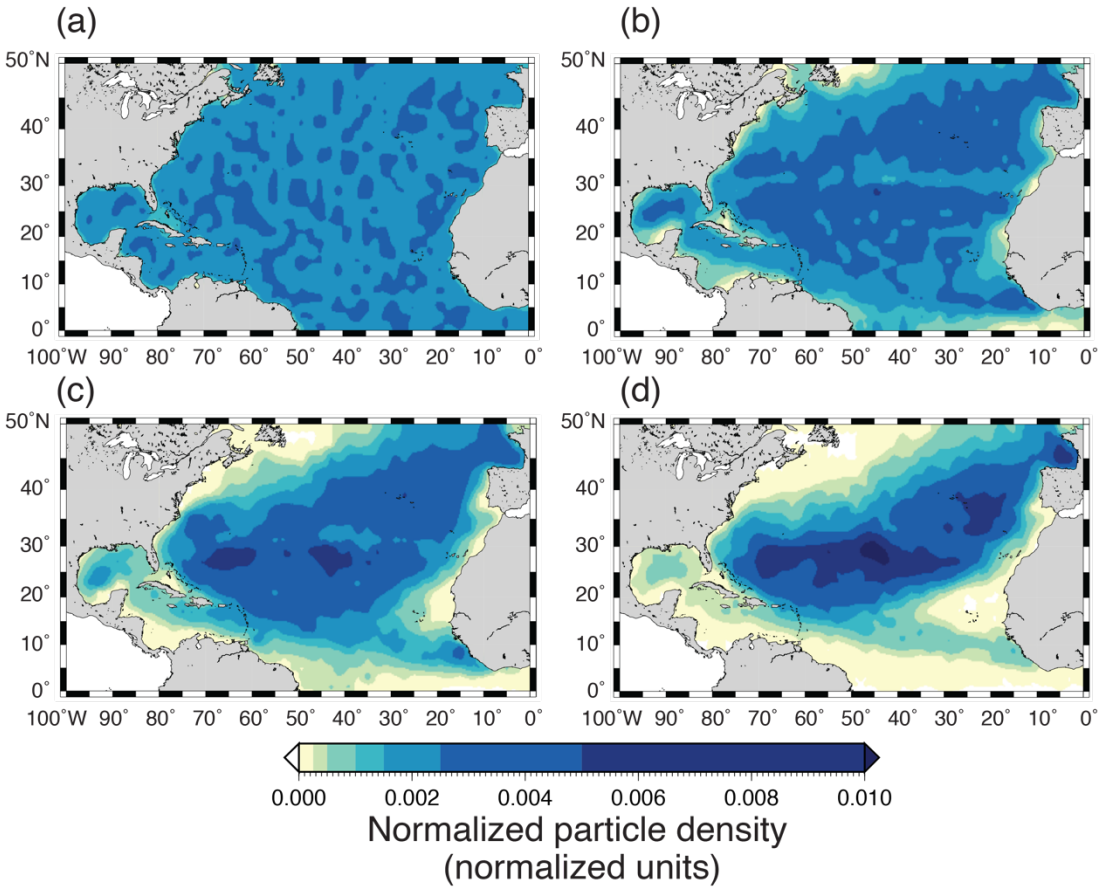

Figure 2.4 Particle Density Distribution for randomly seeded surface particles. Panels show (a) initial condition, and distribution after (b) 60d, (c) 180d, and (d) 360d particle transit time. The initial, randomly-dispersed distribution ends up concentrated in the central gyre at timescales between 60 and 360 days.

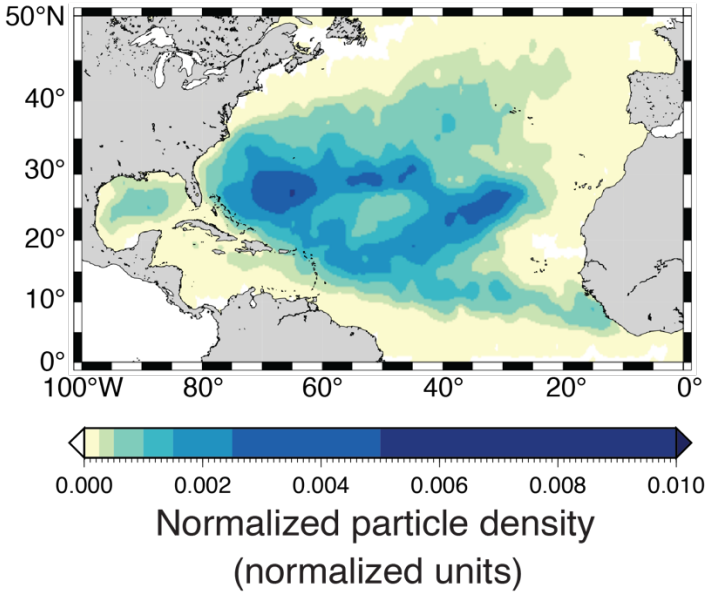

Figure 2.5 Effects of particle motion. Surface-constrained particles initialized according to monthly climatologies of *Sargassum* biomass aggregate in the central gyre after one year.

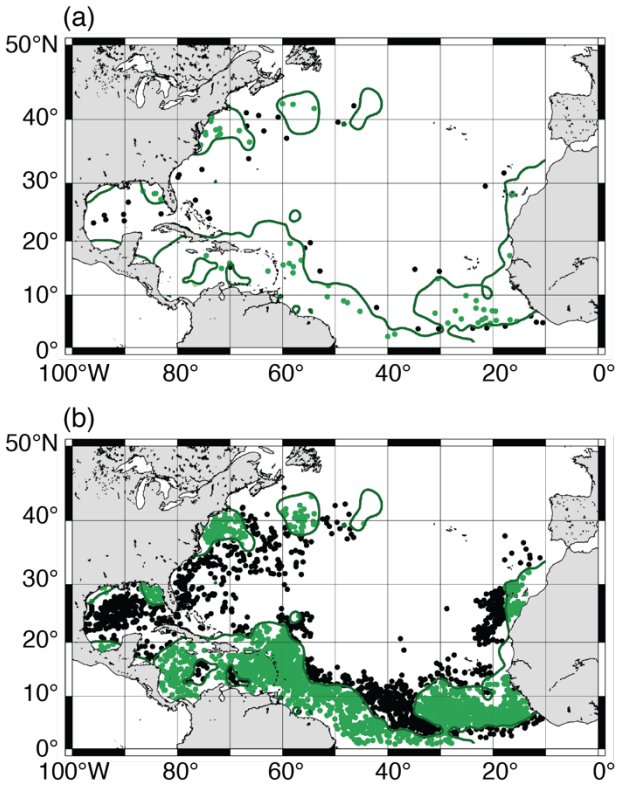

Figure 2.6 Match in September between observed drifters, model floats, and satellite observations after 60d transit time. Only (a) observed drifters and (b) model floats that originated in *Sargassum*-containing regions are shown. Contours are 1% of maximum MCI from *Sargassum* satellite climatology. Green points fall within the bounds of observations, black points represent mismatch.

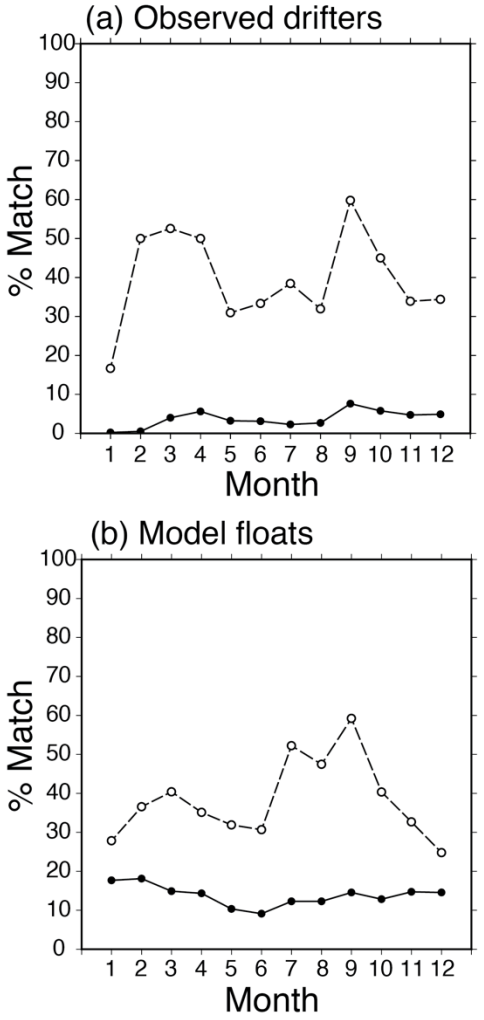

Figure 2.7 Percent match rate with satellite observations of *Sargassum* for (a) observed drifters, and (b) modeled floats. Upper, dashed lines are drifters/floats that originate in regions where *Sargassum* is observed. Lower, solid lines include all observed drifters (a), and all randomly initialized floats (b). Both model and observations show a peak in %match in the fall, indicating high advective control on the *Sargassum* distribution at that time.

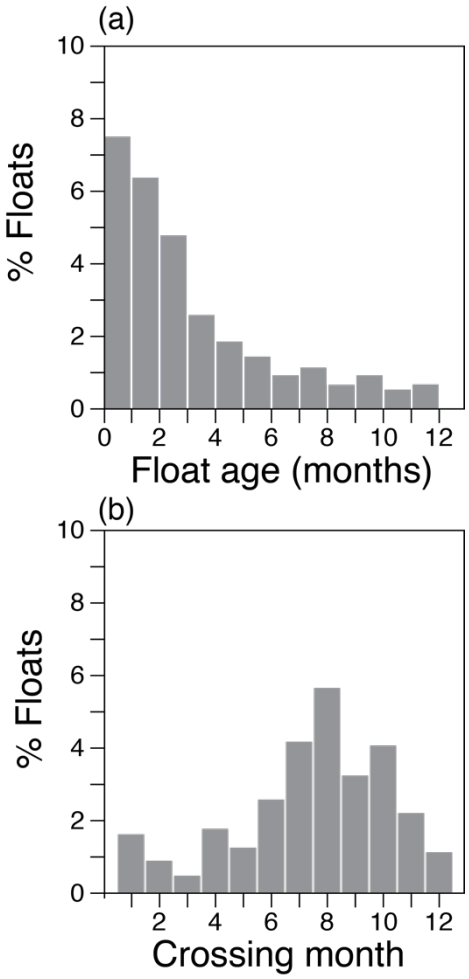

Figure 2.8 Histograms of floats exiting the Gulf of Mexico. (a) Age and(b) month at exit, defined as crossing 81° W, of model floats initialized randomly in the Gulf of Mexico over one model year.

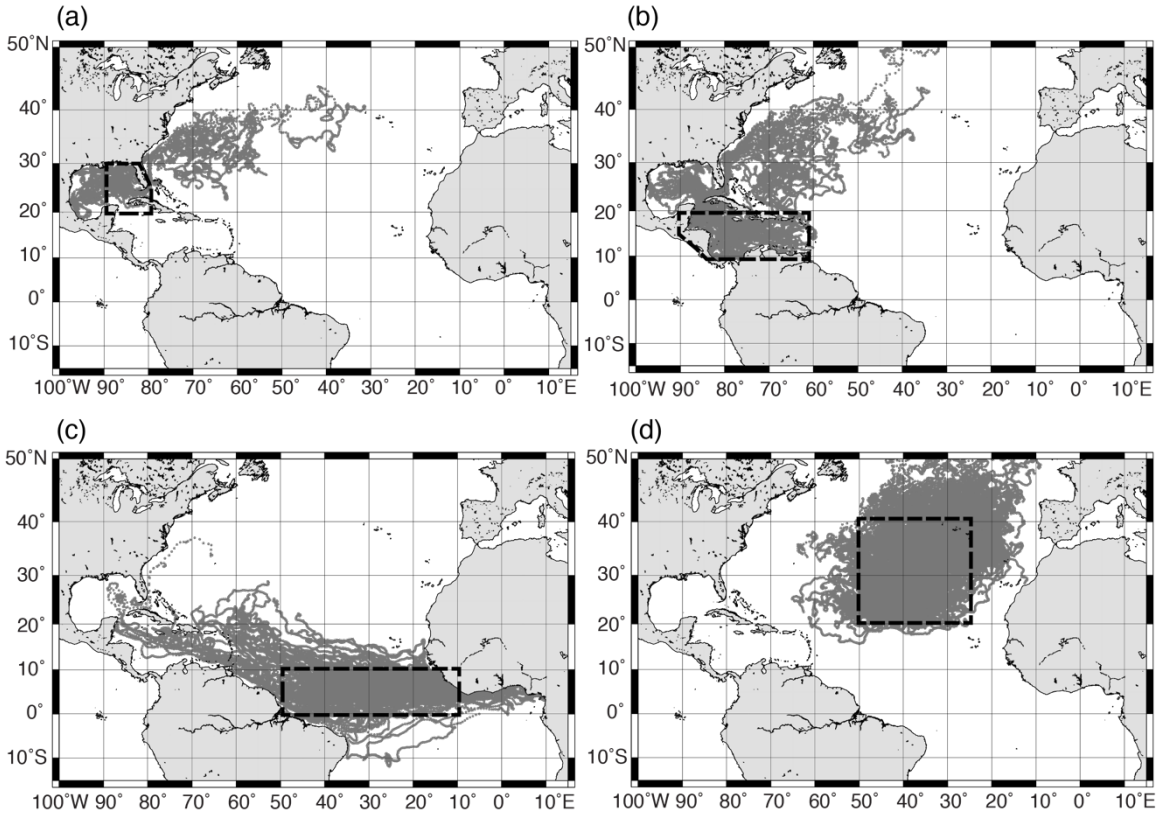

Figure 2.9 A subsample of trajectories over one year for particles launched in (a) the eastern Gulf of Mexico, (b) the Caribbean Sea, (c) the central tropics, and (d) the subtropical gyre. Dashed boxes indicate particle launch regions.

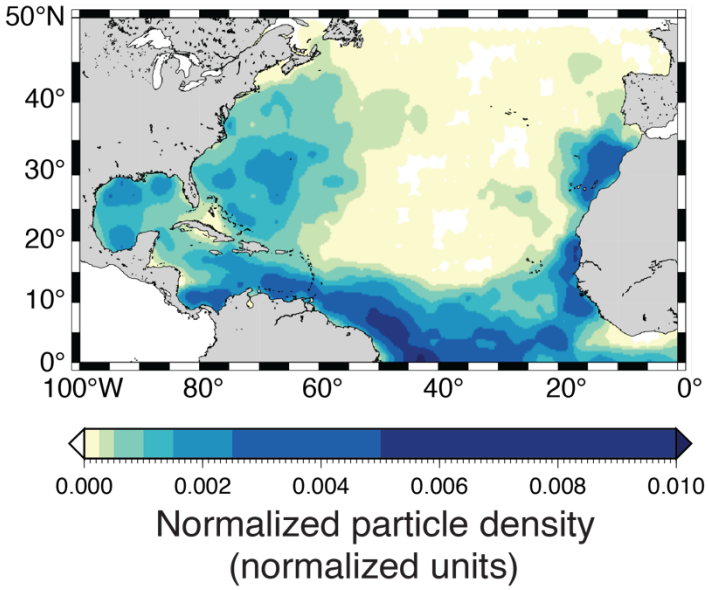

Figure 2.10 Particle density for 3-D particles initialized from *Sargassum* monthly satellite climatologies and run backwards in time. This distribution integrates the seasonal cycle by including all particles of age -60 days.

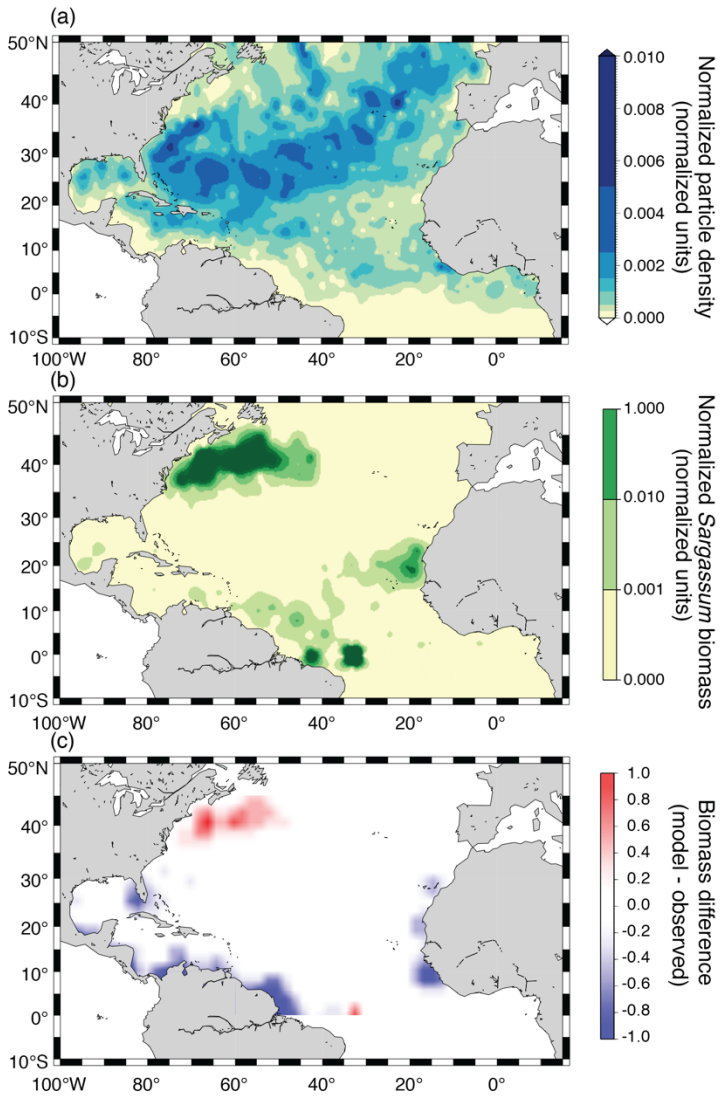

Figure 2.11 (a) Particle density in November without *Sargassum* growth. (b) Normalized *Sargassum* model biomass. (c) Difference between *Sargassum* model and observed normalized biomass. Model *Sargassum* biomass is consistent with observations, in contrast to the high abiotic particle densities in the central gyre.

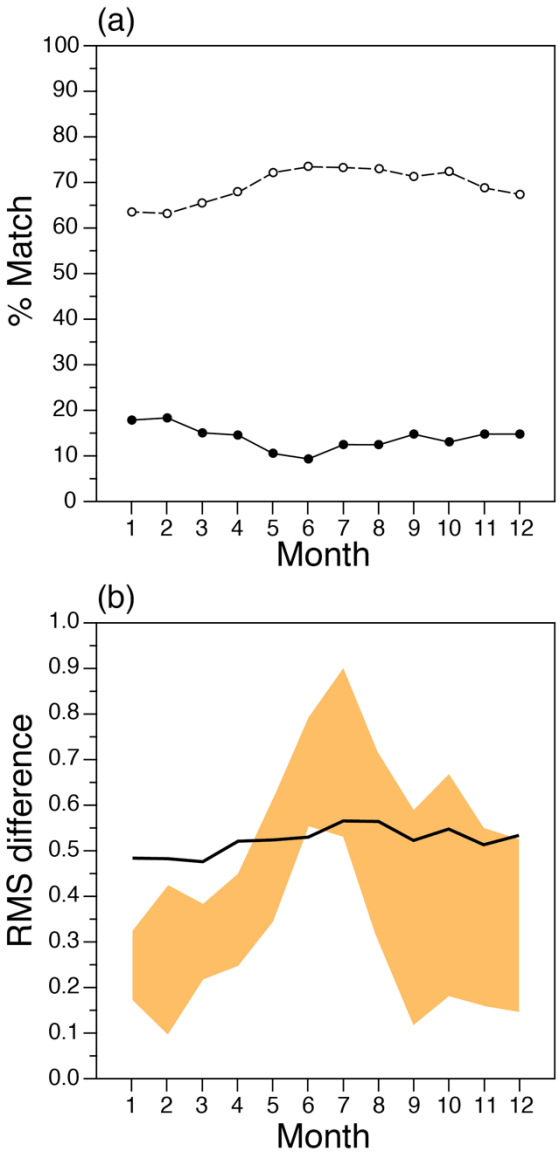

Figure 2.12 Model Performance. (a) Percent match between randomly initialized particles with (dashed line) and without (solid line) accounting for *Sargassum* growth. (b) RMS difference between model and satellite climatologies for the model (black line) and individual years of satellite data (shaded region indicates mean +/- standard deviation). Match with observations is high, consistent throughout the year, and generally within the bounds of observed biomass variability.

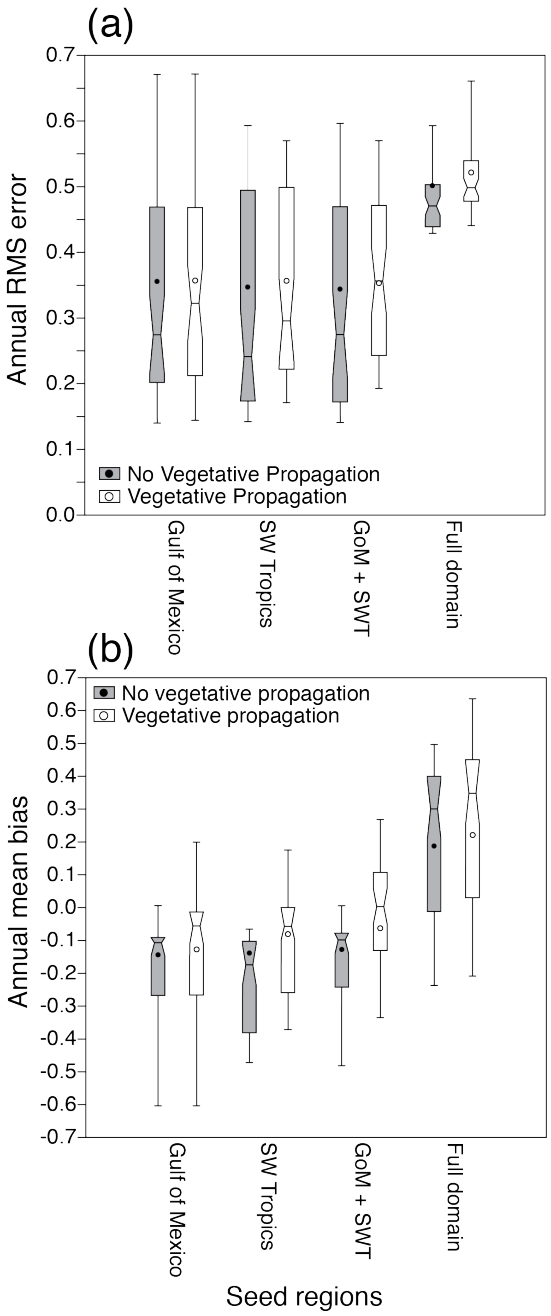

Figure 2.13 (a) RMS difference and (b) mean bias between model and observations for seeding and vegetative propagation experiments. Box-and-whiskers are aggregate results from analysis within individual subregions, circles are the statistic calculated over the full model domain. Seeding in the two subregions reduces error and mean bias, while vegetative propagation further reduces mean bias.

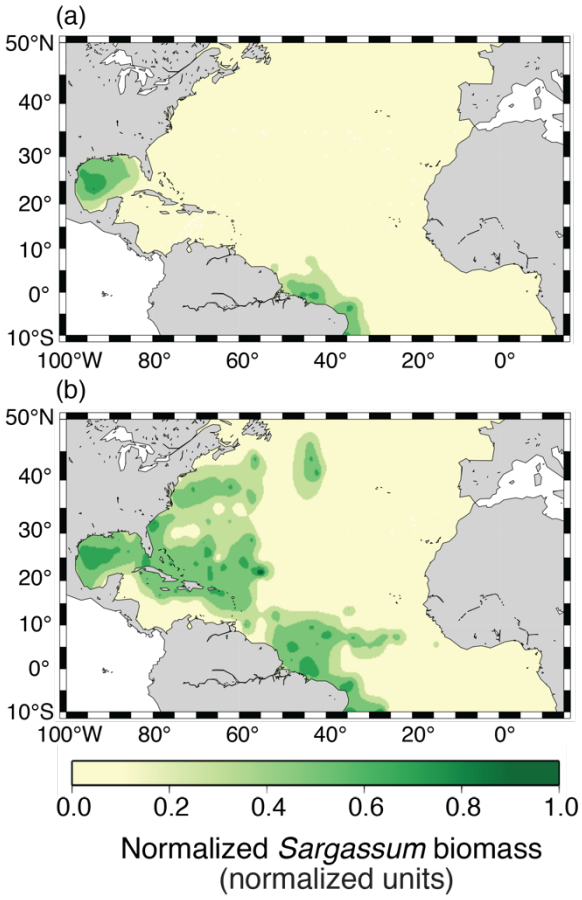

Figure 2.14 Seeding and vegetative propagation experiments. (a) Seeding in the Gulf of Mexico and southwestern tropics reproduces local patterns but underrepresents *Sargassum* biomass elsewhere in the domain. (b) With vegetative propagation, *Sargassum* biomass in the Sargasso Sea can result from advection and growth of nonlocal sources.

Chapter 3: Inertia influences pelagic *Sargassum* advection and distribution[2]

3.1 Abstract

The effect of inertia (resistance to a change in velocity of buoyant finite-sized objects) on the advection of pelagic *Sargassum,* a macroalgae, is a function of the size and density of natural *Sargassum* rafts. Here, we present observations of *Sargassum* density and an approach for estimating an effective radius of *Sargassum* rafts from remote sensing observations. This allows the existing theoretical framework for Lagrangian modeling of inertial effects on spherical particles to be applied to *Sargassum*. Accounting for inertia yields up to a 20% increase in *Sargassum* export from the Sargasso Sea southward, and provides a return pathway to the tropics that may be important to maintaining a self-sustaining population. Resolving inertial effects also leads to increases in retention in the Gulf of Mexico and Caribbean Sea, where *Sargassum* inundation events are increasingly common. Including inertial effects in models of *Sargassum* advection could improve predictions of these events.

---

[2]Published as: Brooks, M.T., Coles, V.J., & Coles, W.C. (2019). Inertia influences pelagic *Sargassum* advection and distribution. Geophys. Res. Let.

DOI:10.1029/2018GL081489

3.2 Introduction

Pelagic macroalgae of the species *Sargassum fluitans* and *Sargassum natans* have been washing up on beaches in the Caribbean, Gulf of Mexico, and western Africa in events of increasing severity and frequency in recent years (Franks et al., 2011; Langin, 2018; Smetacek & Zingone, 2013). This suggests changes have occurred either in *Sargassum* biomass, or its distribution due to surface currents. Because *Sargassum* spends its entire life cycle floating at the ocean surface, it is important to understand how it interacts with ocean currents in order to predict its dispersal and locations of potential landfall.

The *Sargassum* biomass in the Gulf of Mexico and tropical Atlantic exerts a strong influence over basin-wide *Sargassum* distribution (Brooks et al., 2018). Previous studies (Brooks et al., 2018; Franks et al., 2016; Putman et al., 2018) simulating *Sargassum* with Lagrangian particles showed potential pathways for *Sargassum* dispersal, and highlighted the link between *Sargassum* biomass in the tropical Atlantic and the Caribbean Sea. However, these previous models of *Sargassum* drift fail to account for changes in trajectory caused by the size and mass of the floating rafts.

The finite size radius and density of a Lagrangian object, like *Sargassum*, dispersing in ocean currents can influence its trajectory through inertial forces (Maxey & Riley, 1983; see also Beron-Vera et al., 2015; Haller & Sapsis, 2008). Inertia, or an object's resistance to changes in velocity, is dependent on the physical properties of the object. Differences in density create inertia between Lagrangian particles and the surrounding water, and can cause particles to cross material lines and

become entrained in, or expelled from, eddies (Beron-Vera et al., 2015). Particles less dense than the ambient water will tend to deflect to the left of the mean flow. The consequence of this for buoyant *Sargassum* in the tropical North Atlantic is that inertial effects should lead to entrainment in cyclonic eddies and expulsion from anticyclonic eddies.

Differences in entrainment in mesoscale eddies have the potential to impact *Sargassum* dispersal. Eddies in weak background flow propagate westward, with cyclonic eddies tending poleward and anticyclonic tending equatorward (Early et al., 2011; Morrow et al., 2004). Thus, entrainment into a cyclonic eddy will increase the tendency of *Sargassum* rafts to drift northwest in the North Atlantic. Inertial effects are important for correctly modeling these advective responses because inertia may explicitly alter the likelihood of *Sargassum* crossing an eddy boundary (Beron-Vera et al., 2015; Cartwright et al., 2010).

Modeling inertial effects on *Sargassum* advection requires estimates of both raft density and radius. While density can be measured directly, radius is difficult to determine because *Sargassum* rafts are highly non-spherical. The high abundance of *Sargassum* in the Caribbean in 2018 provided a unique opportunity to apply a novel approach to estimating raft radius. In this study, we calculate the density of *Sargassum* from field measurements, and estimate radius using an inverse approach based on comparing the difference between satellite observations of *Sargassum* and of flow streamlines. We then use the density and effective radius to simulate inertial effects on *Sargassum* rafts in the Atlantic to determine the impact on the basin-wide *Sargassum* distribution.

3.3 Materials and methods

3.3.1 Deflection angle definition

We defined the *Sargassum* deflection angle as the angle formed between a fluid trajectory and the *Sargassum* trajectory. Angles that corresponded to the theory for buoyant particles, where the inertial particle deflected to the left of the direction of the flow, were assigned positive values. Those to the right were assigned negative values. This angle is an estimate of the difference between the observed trajectory of a finite sized buoyant object and that of a water parcel with no finite size and a density identical to the surrounding water.

We considered the influence of inertia using the theory for a spherical particle (Maxey & Riley, 1983) as applied to large scale ocean flow by Beron-Vera et al. (2015). Particle velocity, v^p, is a function of the flow velocity v plus an inertial term:

$$v^p = v + \tau(\delta - 1) f v^{\perp} \qquad (3.1)$$

The inertial term is a function of radius (r), latitude, and the ratio of the density of ambient seawater (ρ) to the particle density (ρ^P). For a background flow of velocity v, this inertial component is calculated as

$$\tau(\delta - 1) f v^{\perp} \qquad (3.2)$$

with

$$\tau = \frac{2r^2}{9\nu\delta} \quad , \quad \delta = \frac{\rho}{\rho^P} \qquad (3.3)$$

where ν is the kinematic viscosity, f is the Coriolis parameter, and $\perp$ indicates a 90° rotation anti-clockwise.

Predicted deflection angle can be calculated using this equation and assuming a constant velocity (Figure 3.1). Objects with larger radii or with densities that are differ significantly from ambient water will show the greatest deflection. If the effective radius of *Sargassum* rafts is close to that of an individual plant, then radius alone largely determines the strength of inertial effects. However, if it is larger as a result of aggregation, then both density and effective radius control the strength of the inertial effects.

3.3.2 Density measurements

Samples of *Sargassum* of at least two different morphotypes were collected from Saint Croix, U.S. Virgin Islands to determine the density of the macroalgae. Ten samples were retrieved at each of four locations, Robin Bay and Turner Hole on the south side of the island, and Christiansted Harbor and Hibiscus Beach on the north (Table A2.1 in Appendix II). *Sargassum* was collected by hand in nearshore water of 1 – 2 m depth. Attached flora and fauna was left intact, but free-living organisms and loosely-associated vegetable matter were gently removed. The samples were transferred to plastic storage bins containing ambient water for transport. *Sargassum* density was measured within three hours of collection. Because less buoyant, subsurface *Sargassum* will not be clearly detected by remote sensing, samples showing signs of decay, or loss of structural integrity were excluded from this analysis.

A volume of freshwater was added to a graduated cylinder, and the volume

and mass were recorded. The subsample of *Sargassum* was blotted dry and weighed on a CAS SW-1W electronic balance. This sample was added to the graduated cylinder. A large steel washer (52 mm diameter, 8 ml, 45 g) was placed on the top of the *Sargassum* to ensure the entire sample was submerged, and the cylinder was reweighed. Mass and volume were recorded, and the density ratio between seawater and *Sargassum* was calculated from wet mass and volume of the *Sargassum* samples.

3.3.3 Satellite observations

U.S. National Aeronautics and Space Administration Visible Infrared Imager Radiometer Suite (VIIRS) satellite observations (Ocean Color, 2018) from 2018 were selected for analysis. Images of Alternative Floating Algae Index (AFAI) (Hu, 2009; Wang & Hu, 2018; Wang et al., 2018), which detects red-edge reflectance of floating vegetation, were selected in the Western Tropical Atlantic, Caribbean, and Gulf of Mexico in March – July 2018. These images were examined to locate putative *Sargassum* aggregations (SaWS, 2018). These were referenced against the finite-size Lyapunov exponent (FSLE) field derived from satellite altimetry (AVISO, 2018; d'Ovidio et al., 2004) to find co-occurrences of *Sargassum* with coherent eddies. FSLE contours and AFAI local maxima were independently traced by hand using a Huion 1060PLUS digitizing tablet and Photoshop software (Adobe Photoshop CS5 v12.1, Adobe Systems, 2011).

The FSLE field and AFAI for the same date and location were subsequently overlaid and examined. Where eddies and *Sargassum* co-occurred in space and time, the angle of orientation of lines of *Sargassum* and the nearest FSLE contour were measured and the deflection angle was calculated by difference (Figure 3.2). This

assumes that the AFAI line reflects the orientation of the *Sargassum* advection. A 20-km guide ruler was used for consistent measurements and to provide a minimum scale below which *Sargassum* aggregations were not considered. A total of 91 *Sargassum* lines were measured from four dates with clear images and high regional *Sargassum* abundance, May 28 and 30, and June 7 and 15, 2018. Probability density functions and comparison with model results using the Anderson-Darling k-sample test were calculated using R (R Core Team, 2018).

3.3.4 Modeling

Daily output from a data-assimilating Hybrid Coordinate Ocean Model (HYCOM.org GLBa0.08 experiment 91.2) simulation at 1/12° resolution (Chassignet et al., 2009) was used as input for an offline Lagrangian particle advection model (Garraffo et al., 2001). The study region extended from 15° S – 65° N and from 100° W – 20° E. A tropical sub-region from 5° S – 25° N and from 90° W – 35° E was used for validation with satellite observations, and the full study region was used in subsequent analyses of *Sargassum* dispersal. Code for buoyant *Sargassum* particles (Brooks et al., 2018) was updated to include inertial forces as a function of particle density and effective radius (Beron-Vera et al., 2015). The source code is available at https://github.com/mtbrooks/inertial-particles.

To determine the temporal scope most appropriate for comparison with the satellite observations, the displacement from initial position for 7300 non-inertial particles initialized on a 0.5° grid within the tropical sub-region for 30 days was measured at daily intervals. A duration of 8 days was chosen for subsequent experiments because more than 98% of particles that did not go aground had reached

a minimum displacement of 20 km in 8 days. Note that 20 km was used as the minimum distance for the angle of deflection calculations derived from satellites.

Model sensitivity to particle radius and density was explored to determine best fit to the satellite-derived deflection angle distribution. Particle density was constrained to within ±12% of the field measurements (consistent with the range in variability of those measurements), while radius was varied between 0.05 m (the approximate size of a single *Sargassum* plant) and 2 m. Particles were initialized 8 days prior to the date of the each of the satellite images, so the model and satellite observations could be compared at the same date. All particles that had traveled at least 20 km from their initial position were used in subsequent calculations.

Deflection angle between inertial and non-inertial particles was calculated as the angle between the lines connecting the initial position and the non-inertial end point, and the initial position and the inertial end point. As in the satellite analysis, angles where the inertial particle deflected to the left of the direction of the flow were assigned positive values, those to the right were assigned negative values. The ensemble distribution of each angle was compared with the results of the satellite analysis above to inversely estimate effective *Sargassum* raft radius.

A connectivity model experiment examined the effect of inertia on the *Sargassum* distribution throughout its range. A total of 51,100 non-inertial particles (number determined based on the analysis in Brooks et al., 2018) were initialized randomly throughout the full study region. These particles were launched daily over one year, and each particle was tracked for one year. The study region was divided into 14 sub-regions based on the local circulation and importance to the *Sargassum*

seasonal distribution, and connectivity between each pair of regions was calculated. The simulation was then repeated for particles with inertial characteristics best matching the observed radius and density of *Sargassum* and the difference between the non-inertial and inertial particle distributions was evaluated.

3.4 Results

3.4.1 *Sargassum* density

The density of *Sargassum* was variable, ranging from 0.45 g ml^{-1} (at Robin Bay) to 2.50 g ml^{-1} (at Turner Hole). Density was consistently high at the Turner Hole site, with 6 out of 10 samples being denser than the ambient water. This may be due to the age of the *Sargassum* at the location, or the smaller size of the fragments there. The mean *Sargassum* density from all samples was 1.04 g ml^{-1} (standard deviation of 0.38 g ml^{-1}), unexpectedly high for buoyant, healthy biomass. The highest variability was in the smallest samples, which did not always have a consistent ratio of buoyant pneumatocysts to biomass compared with the larger samples. Excluding those samples with a mass of 15 g or less reduced the standard deviation of the mean from 0.34 g ml^{-1} to 0.12 g ml^{-1}, and resulted in a mean density of 0.94 g ml^{-1}. The ratio of *Sargassum* density to that of ambient water for this subset of samples was 0.92.

3.4.2 Satellite observations

Observed deflection angles ranged from -92.1° to 110.7°, with a mean of 5.6° (Figure 3.3a). The distribution of deflection angles is skewed positive with a peak frequency between 12.5° and 17.5°. While an idealized distribution of deflection angles due only to buoyant particles experiencing inertia should be entirely positive,

other factors such as temporal variability in velocity fields that formed *Sargassum* lines, submesocale processes unresolved by the altimetry, and windage are present in these observations leading to variability in deflection angle. Given that the prevailing winds in the Caribbean blow from east to west, the effect of windage on deflection angle should result in slightly larger angles on the east side of cyclonic eddies and the west side of anticyclonic eddies, where wind and inertia are acting in the same direction, and slightly smaller angles on the corresponding opposite sides. An Anderson-Darling k-sample test found small but significant ($p<0.05$) differences between the angle distributions of these two groups in our observations, with *Sargassum* on the east side of cyclonic eddies and west side of anticyclonic eddies having a peak at a deflection angle of 21° and *Sargassum* in the opposite group having a peak frequency at 10°. Beron-Vera et al. (2016) extended the theory for inertial particles to include windage on a spherical float, however application of windage effects to the complex morphology and predominantly submerged *Sargassum* rafts remains a challenge.

3.4.3 Model validation

Deflection angles in the sensitivity study model simulations were skewed positive, with much less variance than the observations (e.g. Figure 3.3b). This is as expected, as the model does not resolve submesoscale processes, all particles have the same radius, and we did not include the effects of windage. The probability density functions of the distribution of angles for both model experiments and observations were calculated and the positive distributions were compared using the Anderson-Darling k-sample test. Particles with effective radii less than 0.65 m or greater than

1.15 m had deflection angle distributions that were significantly different from the observed *Sargassum* (p values <0.01). The simulation with a density ratio of 0.92 and effective radius of 0.95 m had a peak frequency that most closely matched that of the observations (Figure 3.3b, and see Appendix II for additional details), and these values were selected for the *Sargassum* distribution experiment.

3.4.4 Inertial effects on *Sargassum* distribution

Although *Sargassum* has a density very close to sea water and a relatively modest effective radius, connectivity analysis shows that the cumulative effects of inertial deflection can alter its basin-wide distribution (Figure 3.4, seasonal pattern in supplemental materials). These differences reflect changes in *Sargassum* entrainment in eddies. Over the course of the experiment, 61% of inertial *Sargassum* became entrained in an eddy-like structure, as defined by having > 180° of particle trajectory rotation in a 5-day period. This is a fivefold increase from the non-inertial simulation, which had only 12% entrainment.

Inertial particles are 48% more likely to be retained in the Western Gulf of Mexico (region 1) at time scales of 90 days and longer (Figure 3.4 diagonal elements). The Caribbean (region 3) also retains 36% more *Sargassum* in the inertia experiment, while also experiencing a small annual increase in particles entering from the northern tropics (region 7). There are large seasonal differences in the exchange between the equatorial region (region 10) and the northern tropics (region 7), matching the timing of the North Brazil Current retroflection.

Inertial effects also alter the *Sargassum* distribution in the subtropical gyre. The northern Sargasso Sea (region 8) retains less *Sargassum* when inertia is

considered, though there is more accumulation along the southern boundary (region 7). Western Atlantic regions 4 and 5 export less *Sargassum* eastward into the central gyre (region 8) when inertial effects are accounted for. At the northeast extent of *Sargassum's* range (region 12) annual mean connectivity and retention showed only decreases in the inertia experiment, due to the rafts grounding or exiting the domain more frequently. Along the coast of western Africa in a region of high divergence in the circulation due to upwelling (region 11) there is an equatorward shift in connectivity, away from the central gyre. Additionally, there is a seasonally varying increase in *Sargassum* escaping the gyre to the south (region 7), with an annual mean of 8% and a peak of nearly 20% in November. Broadly, all source regions south of 20° N exported less *Sargassum* to the Sargasso Sea when inertia was accounted for.

There were also changes in connectivity for regions south of the equator. Inertial rafts were more likely to be retained locally (regions 9,13), although there was a slight increase in export from the western side of the basin northward across the equator to the region of the Amazon River plume (region 6). A seasonal 5% increase in connectivity with the northern tropics was also found for *Sargassum* that originated south of the equator in the spring.

3.5 Discussion and conclusions

The density of *Sargassum*, which has not been previously reported, is very close to that of seawater. This is consistent with its relatively slow rate of rise through the water column, and its ability to be mixed to depth during wind events (Johnson & Richardson, 1977; Woodcock, 1993). The size of *Sargassum* rafts can vary

considerably, from just a few centimeters for a small individual plant, to aggregations spanning kilometers (Gower et al., 2006; Lapointe, 1995; Parr, 1939; Schell et al., 2015; Stoner, 1983). However, here we find the effective radius of the rafts is on the order of 90cm. While *Sargassum* observations have been seen as qualitatively consistent with the theory governing inertial particles (Beron-Vera et al., 2015), no validation for effective radius of *Sargassum* aggregations has previously been reported.

The measurements in this study give the first comprehensive indication of whether *Sargassum* rafts are deflected due to inertia when encountering eddies or other sources of acceleration. The equations for these inertial interactions have been described for spherical particles (Beron-Vera et al., 2015; Maxey & Riley, 1983), but this technique for estimating an effective radius could be useful for improving existing models of non-spherical, non-uniform floating objects such as *Sargassum* (Brooks et al., 2018; Franks et al., 2016; Putman et al., 2018) or floating debris (Lebreton et al., 2012). The methods used here could also potentially be used to discriminate between *Sargassum* and other floating algae detected using AFAI such as *Trichodesmium,* which should have very different inertial responses.

Several of the major pathways of *Sargassum* transport are characterized by high eddy activity, such as the Gulf Stream and the North Brazil Current. (Coles et al., 2013; Putman et al., 2018). Inertial forces tend to favor entrainment of *Sargassum* in cyclonic eddies, and we found that inertia caused *Sargassum* to become entrained in eddies five times more frequently than non-inertial particles. Eddies can impact growth by locally raising or lowering the depth of the thermocline, as well as through

localized strong vertical velocities (e.g Falkowski et al., 1991; Lévy et al., 1998; Martin & Richards, 2001), and cause changes in food web structure and consumer growth rates (Shulzitski et al., 2015; Wells et al., 2017). We hypothesize that *Sargassum* entrained in cyclonic eddies may experience increased access to nutrients both directly from upwelling and potentially recycled from fish excretion (Lapointe et al., 2014) and retained by the eddy structure and shoaled thermocline.

In addition to changing the local environmental conditions associated with eddies, inertial effects also alter the trajectories of *Sargassum* rafts. Incorporation into cyclonic eddies will tend to advect Sargassum to the north-west in this region. The modelled increase in retention in the Gulf of Mexico may help maintain the putative seed population there (Brooks et al., 2018). The increase in connectivity from the Sargasso Sea southward into the tropics provides a mechanism for replenishment of the population which most directly influences the Caribbean (Brooks et al., 2018; Franks et al., 2016; Putman et al., 2018). Changes in eddy dynamics and frequency, particularly during spring and summer *Sargassum* growing seasons, could thus influence variability in *Sargassum* wash-ups in the Caribbean.

The estimates of inertial effects in this study assume *Sargassum* has a constant density and effective radius. However, *Sargassum* buoyancy changes as it ages due to colonization by epi-flora and -fauna, and loss of structural integrity of gas-filled pneumatocysts (Johnson & Richardson, 1977). This implies that the influence of inertia is likely to vary seasonally as *Sargassum* ages. Inertial effects should be more pronounced in the spring and summer when production of new *Sargassum* biomass is high. Because of this age effect, estimates in this study of *Sargassum* escaping the

subtropical gyre may be an upper bound. Given that the gyre accumulates *Sargassum* over long time scales there is likely to be a substantial population of older biomass there (Brooks et al., 2018), which would at least partially offset the increased inertial effects due to higher latitude. Wind influence on raft size distribution could also lead to spatial differences in inertial effects.

Inertial effects may be important for efforts aimed at predicting *Sargassum* beaching events such as the *Sargassum* Early Advisory System (Webster & Linton, 2013) and the *Sargassum* Watch System (Maréchal et al., 2017). The difference between inertial particles and a traditional particle model in these experiments often result in differences of tens of kilometers in projected trajectory over just one week. Inertial forces tend to cause more *Sargassum* to enter and be retained in the Caribbean and Gulf of Mexico than non-inertial models would predict.

3.6 Figures

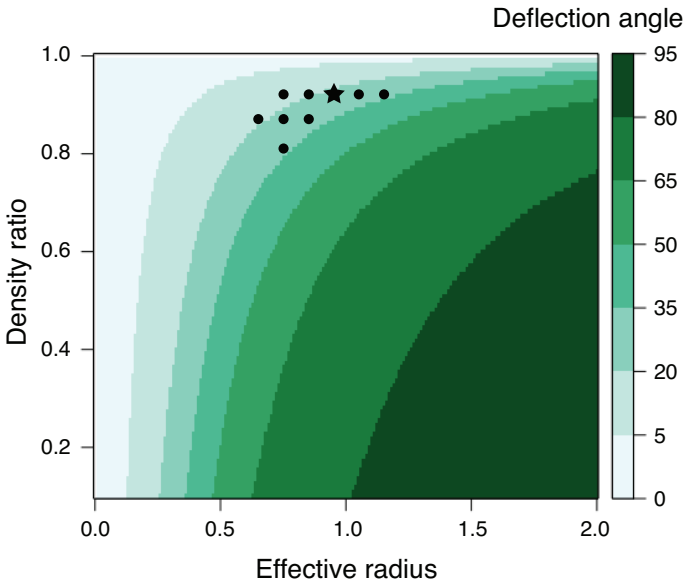

Figure 3.1 Deflection angle derived from inertial equations for buoyant objects with constant velocity at 10° N. Density ratio is the density of the object divided by that of the ambient sea water. Plotted symbols indicate where model and observed deflection angle distributions were not significantly different for a threshold of p = 0.01. The star indicates the effective radius and density ratio of *Sargassum* as determined in this study.

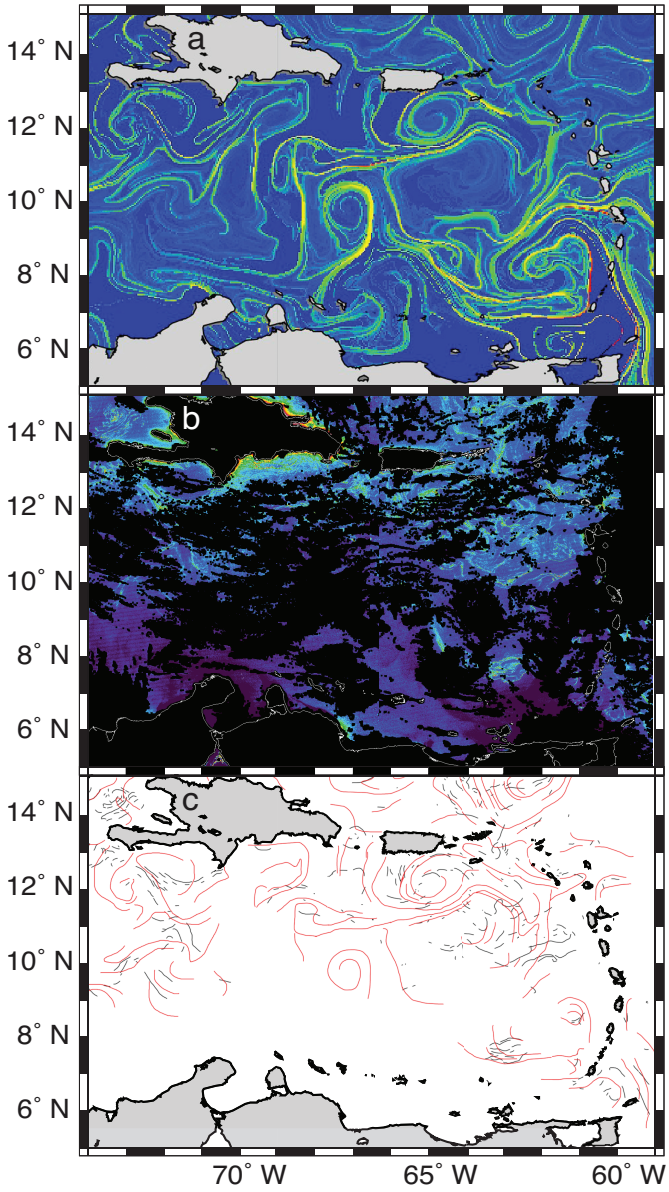

Figure 3.2 Deflection angle measurement of observations. The FSLE field (a) and AFAI (courtesy of the *Sargassum* Watch System) (b) were independently traced. Measurements of deflection angle were made where lines of FSLE (red) and *Sargassum* (black) approached each other near underlying circulation features (c).

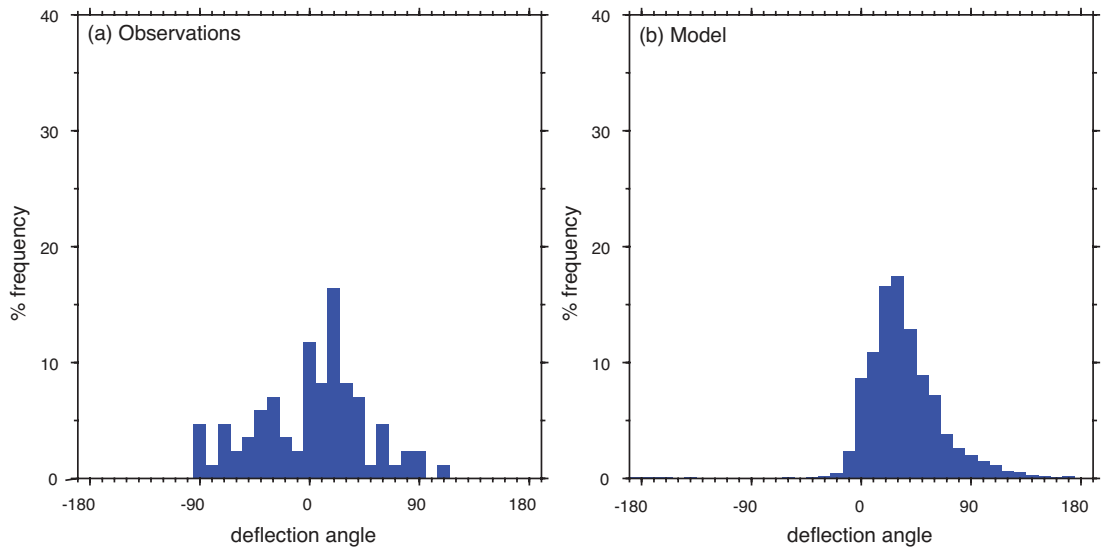

Figure 3.3 Histograms of (a) observed and (b) modeled deflection angle, used to estimate *Sargassum* effective radius.

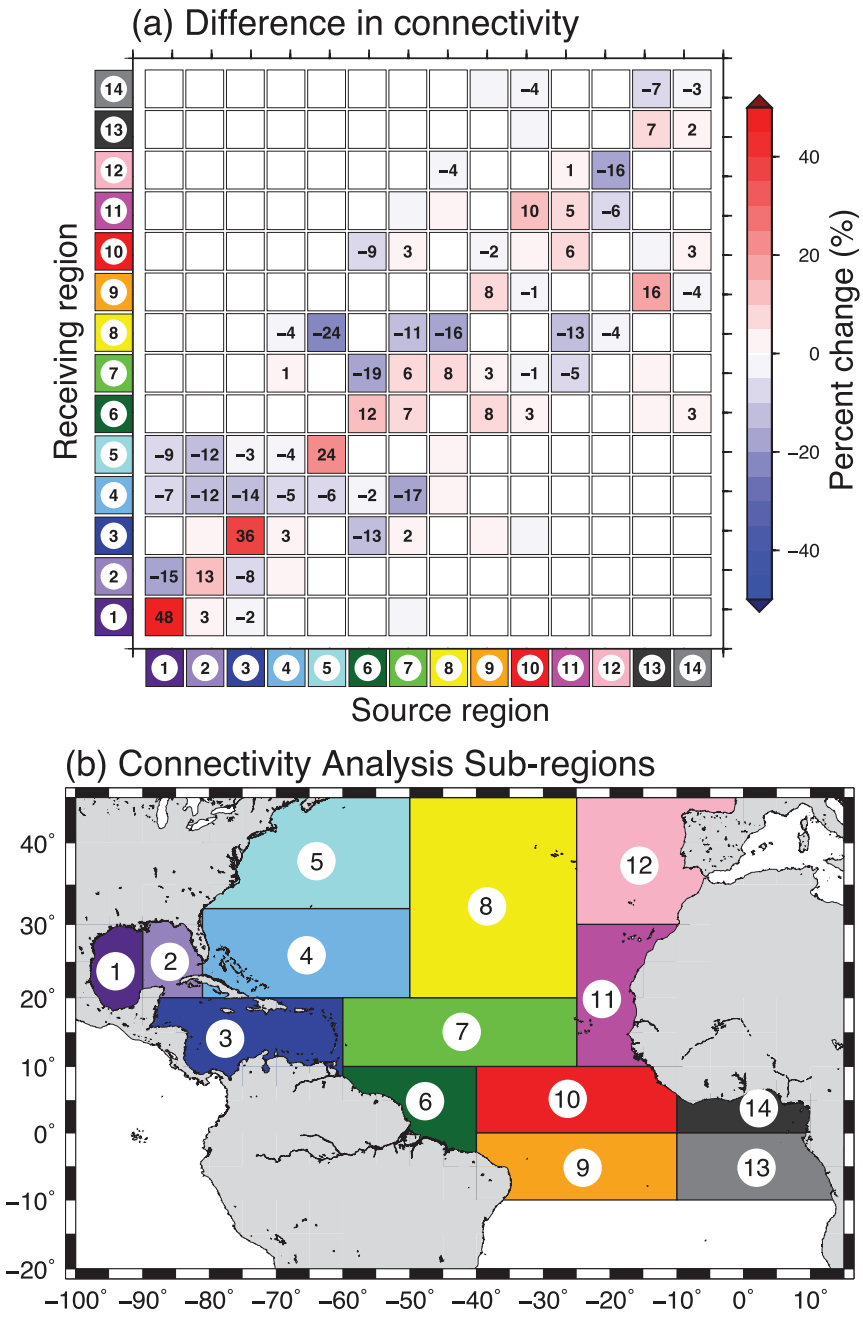

Figure 3.4 Effect of inertia on *Sargassum* trajectories and distribution throughout its range. (a) Changes in connectivity between regions when inertia is considered. Values are shown for changes of 1% or greater. (b) Sub-regions of the model domain used in this analysis.

Chapter 4: Inertial and eddy effects on *Sargassum* growth and persistence

4.1 Introduction

The Atlantic Ocean, Gulf of Mexico, and Inter-American Sea are home to the uniquely holopelagic macroalgae species, *Sargassum fluitans* and *Sargassum natans.* The pelagic *Sargassum* species serve as habitat and refuge for a diverse range of invertebrates (Coston-Clements et al. 1991, Huffard et al. 2014), fish (Wells & Rooker 2004, 2009), and even reptiles (Carr & Meylan 1980; Witherington et al. 2012). However, in recent years, coastal communities have experienced high volume *Sargassum* beaching events that threaten local economies and ecosystems (De Széchy et al. 2012; Ackah-Baidoo 2013; Smetacek & Zingone 2013; Maurer et al. 2015; Louime et al. 2017). The underlying causes behind these wash-up events are not fully understood, but evidence of changing temperatures (Huffard et al. 2014), nutrients (Djakouré et al. 2017), wind and circulation patterns (Franks et al. 2011; Sanchez-Rubio et al. 2018) have been advanced as hypotheses. Additional evidence pointing towards a potential regime shift stems from an increase in tropical Atlantic *Sargassum* biomass (Gower & King 2011, Wang et al. 2018) with a concurrent surge in a previously-rare morphotype of *Sargassum* (Schell et al. 2015; Amaral-Zettler et al. 2017).

Modeling studies highlight the importance of both ocean circulation (Franks et al. 2016; Putman et al. 2018) and *Sargassum* physiology and reproduction in accurately simulating the distribution of pelagic *Sargassum* (Brooks et al. 2018). In

addition to these processes, the inertial forces caused by the finite size and mass of floating objects cause them to move differently from the water they are being advected with (Maxey & Riley, 1983; Beron-Vera et al., 2015). Although the density of healthy *Sargassum* appears to be very close to that of surface tropical sea water (Brooks et al. 2019), its slight buoyancy is sufficient to increase the likelihood that it crosses eddy boundaries, and becomes entrained in cyclonic eddies in particular (Cartwright et al. 2010; Beron-Vera et al. 2015; Brooks et al. 2019). In theory, these eddies tend to move toward the northwest in the North Atlantic (Early et al., 2011; Morrow et al., 2004), which could help reinforce the connectivity between the *Sargassum* population in the tropics with the Caribbean and Gulf of Mexico (Brooks et al. 2019).

Nonlinear flow associated with eddies can generate localized increases in vertical velocities that alter nutrient concentrations. Cyclonic eddies can also influence growth through raising the depth of the thermocline in their interiors into the euphotic zone (Falkowski et al., 1991; Lévy et al., 1998; Martin & Richards, 2001). In the Gulf of Mexico, cyclonic features tend to be enriched in nitrate relative to anticyclones (Biggs 1992). These upwelled nutrients can lead to enhanced phytoplankton production (McGillicuddy et al. 1999; Seki et al. 2001) as well as correspondingly higher standing stocks of zooplankton and some small nekton (Zimmerman & Biggs 1999). Even the role *Sargassum* itself plays in the food web can differ, with a higher fraction of organic matter sourced from *Sargassum* (and associate epiphytes) than phytoplankton within anticyclones in the Gulf of Mexico (Wells et al. 2017).

These biological eddy effects have the potential to alter the *Sargassum* distribution and may explain, in part, the growth of *Sargassum* as it travels from the tropics to the northwest. Seasonal or age-related changes in *Sargassum* buoyancy due to growth conditions or colonization by epi-flora and -fauna may also influence the annual cycle of *Sargassum* throughout its range. In this study, we apply coupled biological and physical modeling approaches to investigate the interactions and possible feedbacks between *Sargassum* physiology and its entrainment in eddies. A simple *Sargassum* model, (Brooks et al. 2018), is first used to isolate inertial effects on *Sargassum* growth and distribution. Then a more complex *Sargassum* physiology model that includes feedbacks between growth and buoyancy is used to explore how the interaction of inertia, mode of vegetative propagation, and nutrient storage contribute to the genesis of a self-sustaining *Sargassum* population in the Atlantic.

4.2 Methods

4.2.1 Physical and biogeochemical framework

Ocean circulation was modeled using HYCOM, the Hybrid Coordinate Ocean Model, that can employ pressure vertical coordinates in the upper ocean to resolve the mixed layer, density coordinate layers in the ocean interior to more directly represent iso- and diapycnal mixing, and terrain-following vertical coordinates over topography to ensure representation of the bottom boundary layer (Chassignet et al. 2003; Bleck 2002). The simulations in this study used a 1/4° resolution model domain in the Atlantic from 15° S to 62° N and 100° W to 15° E. The model is forced with 6-hourly

surface forcing based on the European Centre for Medium-Range Weather Forecasts (ECMWF) reanalysis (Uppala et al. 2005) for the years 1979 – 1985.

Nutrient and light availability for *Sargassum* growth were provided from a biogeochemical model nested within the HYCOM simulations. This model, fully described by Brooks et al. (2018), includes three nutrient types (nitrate, ammonium, and dissolved inorganic phosphorus), as well as two phytoplankton assemblages, one zooplankton functional group, and two detrital pools. Nutrient concentrations from the Eulerian HYCOM model were interpolated to the locations of the Lagrangian *Sargassum* physiology model, and light attenuated by absorption from water and phytoplankton biomass was similarly interpolated to the particle position.

The advection of *Sargassum* rafts was simulated using the HYCOM particle tracking code (Garraffo et al. 2001; Halliwell et al. 2003). A horizontal turbulent advection velocity was applied, with a variance scale of 4.63 $x10^{-6}$ m^2 s^{-2} and an inverse decorrelation time scale of 1 d^{-1}. Modifications were made to the standard code to allow for inertial effects due to size and density as applied to a spherical particle in large scale ocean flow (Beron-Vera et al. 2015; Brooks et al. 2019). An "effective" radius for model *Sargassum* rafts was fixed at 0.95 m following the inverse tuning to remote sensing *Sargassum* distributions of Brooks et al. (2019). Raft density was initialized at 92% of the density of ambient water (Brooks et al. 2019) but, in some experiments, was allowed to vary with the physiological state of the *Sargassum* as detailed in the methods for the *Sargassum* physiology model below.

Additional modifications were made to the standard particle tracking code to modify the simulation of particle movement in the mixed layer. The original model

contained no increases in vertical velocity variability for particles in the mixed layer to represent turbulence. Here, we treated vertical motions due to sub-grid scale turbulence within the mixed layer as uncorrelated due to the relatively long timestep of the velocity fields input to the Lagrangian particle models (online 3600 sec, offline 86400 sec). The base of the mixed layer was first determined as the top of the first model layer with a density difference of greater than 0.2 kg/m^3 from the surface layer, consistent with the model mixed layer determination. A random number generator was used to apply a turbulent addition to particle vertical velocity within the mixed layer. This random component scaled linearly with mixed layer depth, up to double the surface value at a depth of 200 m to ensure that particles were moved throughout the mixed layer with larger velocities associated with deeper mixed layers and increased turbulent mixing.

4.2.2 *Sargassum* physiology model

This study utilized two *Sargassum* physiology models with differing hierarchies of complexity (Table 4.1). Both models were configured to be run within a Lagrangian particle. Each particle is a super-individual raft of *Sargassum*, with a general parameterization that represents an aggregate of both *Sargassum fluitans* and *Sargassum natans.* In the first model (SM-SIMPLE, Table 4.1), described fully in Brooks et al. (2018), *Sargassum* growth is a function of light, temperature, and nitrogen concentration in the biogeochemical model. Particle age is used to modify light availability, as a proxy for epiphyte growth and loss of buoyancy, however the particle does not move vertically in the water column. Growth and fragmentation in

SM-SIMPLE are assumed to be contained within a particle over the lifespan of a *Sargassum* raft. Vegetative propagation generates a new *Sargassum* raft only when older ones succumb to age-related sinking.

The second *Sargassum* physiology model (SM-COMPLEX, Table 4.1) explicitly modeled changes in raft buoyancy due to physiological state. This allows for feedbacks between the macroalgal biology and the inertial physics of the model particles. *Sargassum* growth rate influences its buoyancy in SM-COMPLEX, which affects both its position in the water column and alters advection in regions of vertical shear as well as the inertial effects on its trajectory. In this model, vegetative propagation occurs at high biomass and generates new *Sargassum* particles that can be advected independently from their parent rafts. A complete description of the SM-COMPLEX equations follows.

Light and temperature effects

Light attenuation due to depth and chlorophyll concentration were calculated within the HYCOM-based biogeochemical model (Brooks et al. 2018). Light limitation of *Sargassum* photosynthesis is a function of available light (I) and the light saturation tolerance (I_k):

$$f(I) = 1 - e^{-(I/I_k)}.$$

The optimum temperature ranges of *S. fluitans* and *S. natans* differ slightly, with *S. natans* tolerating water as cold as 18 °C while *S. fluitans* growth becomes limited below 24 °C (Hanisak and Samuel, 1987). Here we simulated a mixed

population containing both species. Temperature limitation of growth occurs below this range, with a formulation following Hadley et al. (2014):

$$f(T) = 1 / (1+e^{-(T-To)/Tr})$$

where To is the midpoint of the optimum temperature range (21 °C), and Tr is the width of that range (+/- 3 °C).

Nutrient Uptake and Storage

Sargassum biomass can have highly variable ratios of carbon to nitrogen to phosphorus (Lapointe 1995), and rates of macroalgal nutrient uptake vary depending on the nutrient concentrations in their tissues (Fujita, 1985). Therefore SM-COMPLEX is designed to allow for internal storage of nitrogen and phosphorus. This improves nutrient uptake response and allows *Sargassum* to temporarily withstand critically low nutrient concentrations for brief durations if internal nutrient stores are replete. The nutrient uptake and storage equations are formulated following Solidoro et al. (1997). Uptake of nutrients is governed by nutrient quotas (Hanisak 1983), estimated from *Sargassum* nutrient composition (Lapointe et al. 2014; Wang et al. 2018) and measurements of other brown macroalgae (Fujita, 1985; Perini and Bracken, 2014). The same formulation is used for the uptake of both nitrogen and phosphorus. The uptake of each nutrient (N) is:

$$\text{Uptake}(N) = V_M N / (K_n + N) (Q_{max} - Q)/(Q_{max} - Q_{min}).$$

Where V_M is the maximum uptake rate, K_n is the nutrient uptake half-saturation, Q_{min} is the fraction of internal nutrient quota (Q) required for growth, and Q_{max} is the maximum nutrient storage capacity.

Internal nutrients are shared between two pools, stored (N_S) and fixed (N_F). The instantaneous nutrient quota is calculated as

$$Q = Q_{min} (1 + (N_S/N_F)).$$

Growth limitation occurs relative to the internal nutrient pool via

$$(Q - Q_{min}) / (Q - K_{sN}).$$

Minimum nutrient quotas for N and P were estimated using C:N:P ratios of nutrient-limited *Sargassum* (Lapointe et al. 2014) as a starting point. This resulted in Q_{minN} = 10 mg N (g dw)$^{-1}$ and Q_{minP} = 0.7 mg P (g dw)$^{-1}$ which are within the known range for other macroalgae (e.g. Solidoro et al. 1995, Lundberg et al. 1989).

Vegetative propagation

Vegetative propagation of pelagic *Sargassum* has been shown as a potential contributing factor to the maintenance of its distribution throughout the Atlantic in model studies (Brooks et al. 2018). Here we explicitly modeled this process as a function of *Sargassum* biomass within each particle. In this model, when the super-individual biomass is greater than twice its initial condition, it becomes available for breakage and propagation. This is governed by a random number generator, with a mean of one vegetative propagation every 20 days based on *Sargassum* doubling time (Hanisak and Samuel 1987; Brooks et al. 2018). When a raft breaks, a biomass equal to the initial condition is subtracted from the existing particle and added to a new *Sargassum* particle. This new particle is initialized at the location of the parent particle, with a random offset determined by the scale of the particle horizontal turbulent velocity parameter.

Buoyancy

The gas vesicles that keep *Sargassum* rafts afloat can be compromised by excursions as small as 20 m (Johnson and Richardson, 1977). Older vesicles are more likely to fail than young ones, however vesicles can recover if they are not irreversibly ruptured (Johnson and Richardson, 1977). Based on these observations, *Sargassum* particle buoyancy was allowed to vary based on depth and physiological state in the model.

The buoyancy-induced vertical velocity of clumps of *Sargassum* can range from a positive (surfaceward) velocity of 0.09 m s^{-1} (B_P) (Johnson and Richardson, 1977) to a sinking rate of -0.035 m s^{-1} (B_N) (Schoener and Rowe, 1970). In the model, sinking rate is modified between these bounds by γ, a non-dimensional indicator of pneumatocyst integrity.

$$B_S = \gamma * B_p - (1-\gamma) * B_n$$

where

$$\gamma = \gamma_Z * \gamma_S$$

The loss of buoyancy due to compromise of floats with increasing pressure is based on the time it takes for *Sargassum* to reach negative buoyancy. Failure of *Sargassum* vesicles varies with depth (Johnson and Richardson, 1977). Float integrity is not affected above 30 m for time scales of days, however *Sargassum* rafts become negatively buoyant in less than one second below 145 m (Johnson and Richardson, 1977).

Depth modifies the float integrity (γ_Z) following the relationship derived by Johnson and Richardson (1977), where depth (z) has no effect above a minimum depth (z_{min}), and all floats rupture at some maximum depth (z_{max}), with a linear relationship between the two extremes.

$$\gamma_Z = \begin{cases} 1 & , 0\ m <= z < z_{min} \\ (z_{max} - z) / 115 & , z_{min} <= z <= z_{max} \\ 1 & , z > z_{max} \end{cases}$$

Physiological state further modifies the float integrity (γ_S) based on the ratio of the instantaneous growth rate (μ) to the maximum growth rate (μmax).

$$\gamma_S = (\mu / \mu max)$$

These changes to the float integrity affect not only the rate of rise or sinking of *Sargassum* through the water column, but also the density ratio value used for inertial calculations. The ratio of the density of *Sargassum* to ambient seawater is at a minimum of 0.92 (Brooks et al. 2019) when float integrity is at its maximum, and a maximum of 1.03 when float integrity is zero. As there are no existing density measurements of *Sargassum* with and without its buoyant bladders, we assume a linear relationship between these points consistent with that used for changes in vertical velocity.

Mortality and loss terms

Losses of *Sargassum* occur via senescence, grazing, and sinking. Sinking is explicitly modeled through buoyancy changes in the particle model discussed above. The other two sources of mortality are combined as one density-dependent term:

$$\text{Loss} = m_S * S^2 + \text{breakage}$$

Loss of *Sargassum* is equal to the mortality rate times the square of the *Sargassum* biomass. The squared closure term reflects that grazing and breakage are due to associated fauna, and this community is assumed to increase as *Sargassum* density increases. This quadratic loss term also incorporates disease or viral effects. Particle tracking is ceased for *Sargassum* particles with extremely low biomass (<10% of the initial condition), as well as those that sink below the depth at which buoyancy is permanently compromised. These particles are recycled for use in generating new super individuals that represent vegetative propagation. Finally, *Sargassum* biomass within a particle is also lost from particles in the process of breaking off to form new rafts, though biomass is conserved overall. When a new particle is spawned via vegetative propagation, that biomass is subtracted as breakage from the parent particle to conserve mass.

4.2.3 Parameter optimization and model validation

The SM-COMPLEX model was compared with monthly climatologies of satellite detections of *Sargassum* (Brooks et al. 2018) from the European Space Agency MERIS sensor (Rast et al. 1999) to evaluate model fit. This analysis was consistent with the validation approach used for the SM-SIMPLE model. Model biomass was normalized to its maximum value over one year of simulation for direct comparison with the satellite Maximum Chlorophyll Index (MCI). Only model biomass within 5m of the surface was used, since remote sensing does not detect subsurface *Sargassum*. Both model and satellite climatologies were gridded to 2° and

a weighted RMS difference was calculated. Regions with MCI less than 0.05 were weighted at 50%, to prioritize fit with high-*Sargassum* bloom regions and reduce errors associated with the uncertainty of the minimum biomass detectable via satellite. Parameter optimization was carried out for mortality rate and nutrient half-saturation and storage parameters. The final parameter values used for all subsequent model experiments are listed in Table 4.2.

4.2.4 Model experiments

The first model experiment examines how inertia affects *Sargassum* growth and distribution. For one model year, 140 non-inertial particles, representing control *Sargassum* aggregates, were initialized daily. These particles were randomly distributed over the model domain. Each particle was tracked for an additional year for a total of two years of simulation. This simulation was then repeated for inertial *Sargassum* particles with an identical initial distribution. Comparison of the inertial and non-inertial particles allows us to evaluate the role of inertia in steering particles into eddies with potentially different mean advection patterns as well as the altered light and nutrient conditions that result from inertial steering of the *Sargassum* represented in the SM-SIMPLE model.

This pair of simulations was run again using the SM-COMPLEX model to compare the effects of adaptive buoyancy on the inertial propagation and also how the mechanism of vegetative propagation differed. Differences in annual and monthly mean biomass, growth rate, distribution, and entrainment in eddies were calculated

between the inertial and non-inertial *Sargassum* simulations and between SM-SIMPLE and SM-COMPLEX.

Determination of whether a *Sargassum* particle was within an eddy was automated, using particle looping as an indicator (Richardson, 2005; Chérubin and Richardson, 2007). The change in orientation of each particle trajectory was calculated daily and a running 5-day sum was tallied. Looper particles were defined as those particles completing 180° of rotation within 5 days. This running sum was computed over the life of the particle, allowing for determination of when particles entered and exited eddies over the full span of their trajectories.

4.3 Results and Discussion

4.3.1 Inertial effects

In simulations using SM-SIMPLE there was a significant (Student's t-test, $p < 0.01$) difference in the annual mean biomass between inertial and non-inertial *Sargassum*. The annual mean biomass in the inertial simulation was 8% larger than the non-inertial, and was higher for all monthly means as well (Figure 4.1a). Likewise, growth rates more frequently approached the maximum growth rate (0.12 d^{-1}) in the inertial simulation, and inertial *Sargassum* had a more pronounced seasonal cycle in growth rate (Figure 4.1b). The inertial *Sargassum* also had slightly higher rates of survival. The mean lifespan, from start date to loss by sinking, mortality, exiting the domain, or running aground, of *Sargassum* in inertial particles was 33.25 d versus 32.30 d for non-inertial particles. Inertial *Sargassum* was advected more often into regions with ideal conditions for growth such as the Caribbean, Gulf of Mexico,

and tropical Atlantic (Figure 4.2), consistent with previous results (Brooks et al. 2019).

There were also significant differences in the number of inertial versus non-inertial *Sargassum* particles entrained in eddies. *Sargassum* in the inertial simulation spent 42.6% of the time entrained in eddies, compared with 34.5% in the non-inertial. This difference demonstrates itself in the patchier nature of the surface distribution in Figure 4.2b as compared with Figure 4.2a. *Sargassum* was more likely to be entrained in cyclonic eddies in both the inertial and non-inertial simulations. However, this difference was much more striking in the inertial *Sargassum* particles, with >80% of eddy-entrained particles in cyclonic eddies, versus 64% of the eddy-entrained non-inertial particles.

In both simulations, the biomass and growth rates of *Sargassum* inside eddies was not significantly different from those outside of eddies. This suggests that in this model, eddy entrainment does not contribute directly to increased *Sargassum* growth. Rather, increased entrainment in eddies, in conjunction with other changes in trajectories due to inertial effects, appears to yield increased *Sargassum* biomass and growth rates by advecting *Sargassum* into more optimal habitat.

Sargassum simulated with SM-COMPLEX spent less time entrained in eddies than when simulated with SM-SIMPLE, but showed the same pattern of increased entrainment in the inertial simulation, with a 12% increase in entrainment in the inertial simulation. The overall lower entrainment in SM-COMPLEX is due to multiple factors. The feedback between *Sargassum* physiological state and its buoyancy in SM-COMPLEX means that on average it will experience weaker inertial

effects than that in SM-SIMPLE. This is because when it is not growing optimally its density approaches that of seawater.

An examination of a sample pair of trajectories illustrates how inertia contributes to changes in *Sargassum* growth and distribution in the SM-COMPLEX model. An inertial and non-inertial particle initialized at the same location in the tropical Atlantic follow different trajectories (Figure 4.3a). The non-inertial particle gets advected into the Sargasso Sea, while its inertial counterpart gets advected to the Caribbean. Both *Sargassum* particles encounter eddies, although the inertial particle spends longer entrained within them. The non-inertial particle experiences two dips in biomass associated with propagation events, but otherwise the biomass in both particles remains similar over the course of the year (Figure 4.3b). Their growth rates also start out similar (4.3c). However, the non-inertial *Sargassum* growth declines over time, while the inertial *Sargassum* growth starts to increase as it gets advected into the western tropics.

4.3.2 Vegetative propagation and inter-model comparison

The effects of the more complex physiology and mode of vegetative propagation in SM-COMPLEX were evaluated by comparing model RMS error compared with satellite climatologies of *Sargassum* observations (Gower and King 2013; Brooks et al. 2018). Due to the patchy nature of *Sargassum* biomass in the Atlantic, a weighted RMS error was used that prioritized the fit of regions with strong *Sargassum* signals at twice the weight of regions with no *Sargassum* detections.

In SM-SIMPLE, vegetative propagation occurs when older aggregations begin to fail and are more susceptible to breakage, while in SM-COMPLEX propagation occurs when biomass is high and can no longer remain in a single aggregation. Vegetative propagation occurs most frequently in the Sargasso Sea in SM-SIMPLE, and in the tropics in SM-COMPLEX. This contributes to a 15% reduction in error between model and observations in SM-COMPLEX compared with SM-SIMPLE (Figure 4.4), and is evident in the increased biomass in the tropics in figure 4.2b. The annual mean weighted RMS error for SM-SIMPLE is 0.20 and for SM-COMPLEX is 0.17. May model biomass is enhanced in the tropics, Caribbean and Gulf of Mexico, consistent with observations (Figure 4.5a,b). By September, observed biomass is lower in the Gulf of Mexico, and higher in the Gulf Stream and North Atlantic Current, and this pattern is captured in the model simulations (Figure 4.5c,d). The model tropical biomass is somewhat lower in September than observed, however it is higher than in the SM-SIMPLE model. The mean basin-wide normalized biomass is increased by 30% in SM-COMPLEX compared to SM-SIMPLE. This is a reflection of increased growth rates, which average 50% of their maximum in SM-COMPLEX compared with only 30% of their maximum in SM-SIMPLE. Overall SM-COMPLEX more accurately captures the seasonal distribution, especially in the Caribbean and Gulf of Mexico

4.3.3 Self-sustaining *Sargassum* population

Previous work with the SM-SIMPLE model showed that seeding in the Gulf of Mexico and Western Tropical Atlantic was required to maintain the seasonal

distribution of *Sargassum* year after year. To test whether changes in trajectories due to inertial processes are sufficient to generate a self-sustaining population, the inertial SM-SIMPLE simulation was allowed to run for an additional two years with no new *Sargassum* particles initialized aside from those generated by vegetative propagation. By the last year of simulation, fewer than 20 *Sargassum* rafts remained viable. However, the distribution of *Sargassum* particles is much more conducive to regenerating the seasonal distribution than that of non-inertial *Sargassum* after this length of time (Figure 4.6). Non-inertial *Sargassum* is concentrated in the Sargasso Sea with no return pathway to the tropics. *Sargassum* in the inertial experiment maintains small populations in the Caribbean and Gulf of Mexico where they have more opportunities for growth and transport before being trapped in the convergent subtropical gyre.

Sargassum in SM-COMPLEX also did not maintain a self-sustaining population. However, the pattern of increased vegetative propagation in the tropics highlighted a phenomenon that was present, but less severe in SM-SIMPLE. The location of *Sargassum* loss from the system is very different between the inertial and non-inertial *Sargassum* rafts. Non-inertial *Sargassum* mainly accumulates in the Sargasso Sea and is lost from the system there, via sinking. Inertial *Sargassum*, however, is more than 5 times more likely to run aground. This increased beaching of *Sargassum* happens mainly in the tropics, on the western edge of the basin (Figure 4.7).

4.4 Conclusions

Inertial processes alter the advection pathways by which *Sargassum* is transported throughout its range (Brooks et al. 2019). When inertial processes are accounted for, *Sargassum* tends to be entrained in cyclonic mesoscale eddies more frequently. This eddy entrainment contributes to *Sargassum* being advected more often into the Caribbean and Gulf of Mexico and out of the Sargasso Sea compared with water parcels with the same starting location.

Although in this model system *Sargassum* within eddies does not experience higher growth rates than rafts outside of eddies, the changes in trajectories associated with eddy propagation result in overall higher growth and biomass. This interaction between transport and growth is not accounted for in other simulations of *Sargassum* distributions and could help better predict the severity of potential beaching events.

The comparison of modes of vegetative propagation also yields new testable hypotheses regarding how and where *Sargassum* reproduces. In these models, *Sargassum* that propagates when growth and biomass are high has a better fit with observations than *Sargassum* that splits as it ages. Fragmentation and vegetative propagation in the tropics, Caribbean, and Gulf of Mexico is more beneficial to maintaining the *Sargassum* population than reproduction in the Sargasso Sea.

Buoyancy response is also important in the distribution of *Sargassum* throughout the basin. Normalized growth rates and biomass are both higher in inertial simulations where *Sargassum* buoyancy, and thus inertial response, are dynamically responsive to physiological state. *Sargassum* is uniquely adapted to its habitat and geographical range, and accounting for its biological-physical feedbacks results in

more realistic simulations. Reproduction and physiological state interact with patterns of surface circulation and mesoscale features via buoyancy and inertial processes. These interactions help transport and maintain *Sargassum* in regions where its growth potential is highest, and provide a mechanism for transport out of the Sargasso Sea and back to the tropics where it can perpetuate its annual cycle.

4.5 Tables and Figures

Table 4.1: *Sargassum* physiology models used in this study. *Sargassum* model 1 (SM-SIMPLE) (Brooks et al. 2018) and *Sargassum* model 2 (SM-COMPLEX) differ in how they handle nutrient uptake, light limitation, buoyancy, and vegetative propagation.

	SM-SIMPLE	**SM-COMPLEX**
Nutrient storage	Direct uptake for growth only	Uptake and internal storage pools
Age effects	Light limitation, vegetative propagation	--
Buoyancy	Static	Modified by *Sargassum* health as a function of growth and vertical mixing - depth
Vegetative propagation trigger	Age- and mortality-based	Biomass-based

Table 4.2: SM-COMPLEX parameters.

Symbol	Parameter	Value	Units
I_k	Growth-Irradiance parameter	70	W m^{-2}
T_o	*Sargassum* optimum temperature	21.0	°C
T_r	Width of optimum temperature range	3.0	°C
V_{MN}	Nitrogen maximum uptake rate	2.0	mgN(g $dw^{)-1}$ d^{-1}
V_{MP}	Phosphorus maximum uptake rate	2.0	mgP(g $dw^{)-1}$ d^{-1}
K_N	Nitrogen uptake half-saturation	0.7	mmol N m^{-3}
K_P	Phosphorus uptake half-saturation	0.4	mmol P m^{-3}
Q_{minN}	Fraction of internal nitrogen quota required for growth	10.0	mgN(g $dw^{)-1}$
Q_{minP}	Fraction of internal phosphorus quota required for growth	0.7	mgP (g $dw^{)-1}$
Q_{maxN}	Maximum nitrogen storage capacity	50.0	mgN(g $dw^{)-1}$
Q_{maxP}	Maximum phosphorus storage capacity	3.7	mgP(g $dw^{)-1}$
μ_{max}	Maximum growth rate	0.12	d^{-1}
m_S	Mortality rate	0.02	d^{-1}
B_p	Maximum positive rate of rise	0.09	m s^{-1}
B_n	Maximum sinking rate	0.035	m s^{-1}
z_{max}	Maximum depth before vesicle rupture	145	m
z_{min}	Minimum depth for pressure effects	30	m

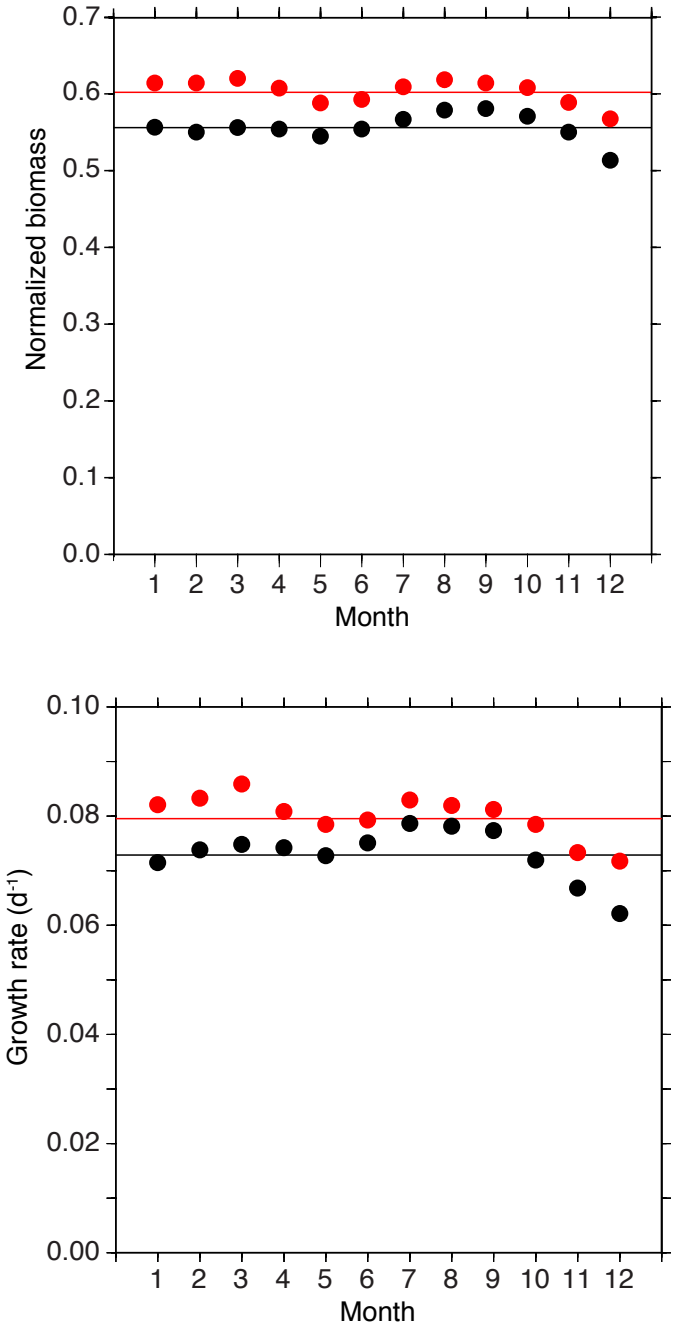

Figure 4.1. Inertial influences on *Sargassum* (a) biomass and (b) growth rate in SM-SIMPLE. Black points are non-inertial monthly means, red points are inertial monthly means. Lines are non-inertial (black) and inertial (red) annual means. Normalized biomass is normalized to the maximum in-particle biomass in the non-inertial simulation.

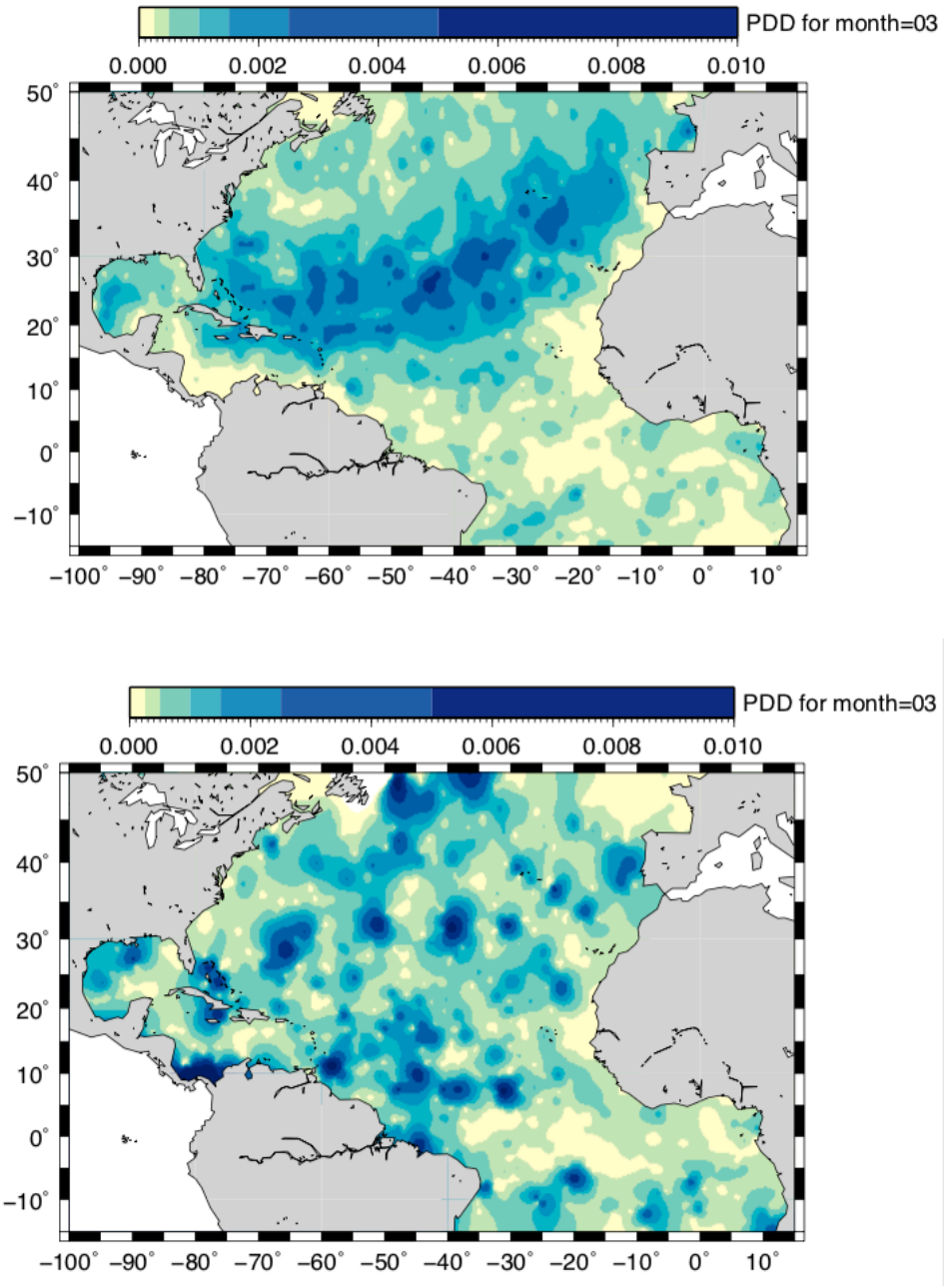

Figure 4.2 Particle density distributions without accounting for biomass, for (a) non-inertial and (b) inertial *Sargassum* particles in SM-SIMPLE for the month of March.

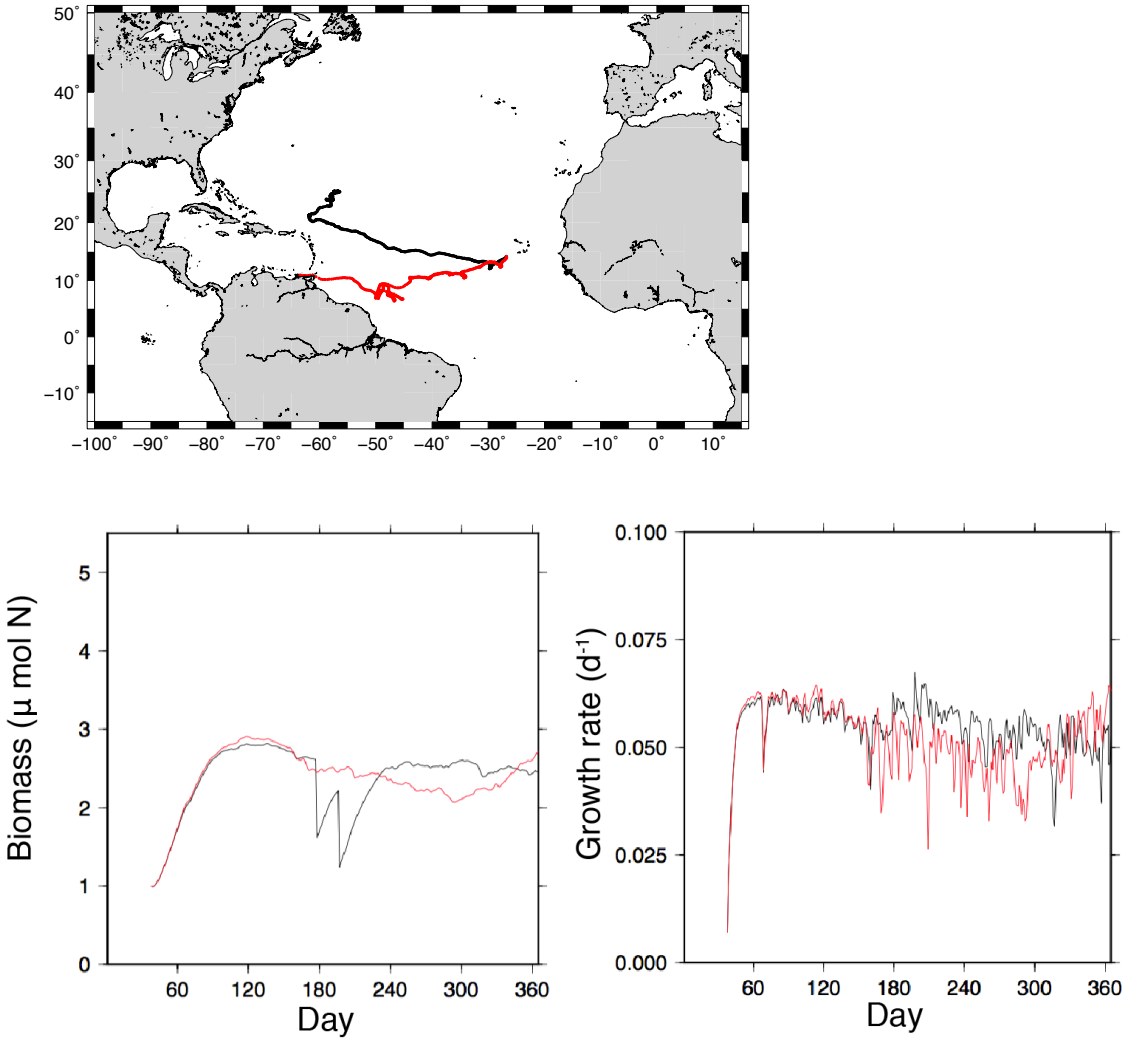

Figure 4.3 Comparison of inertial (red) and non-inertial (black) particle trajectories (a), biomass (b), and growth rate (c).

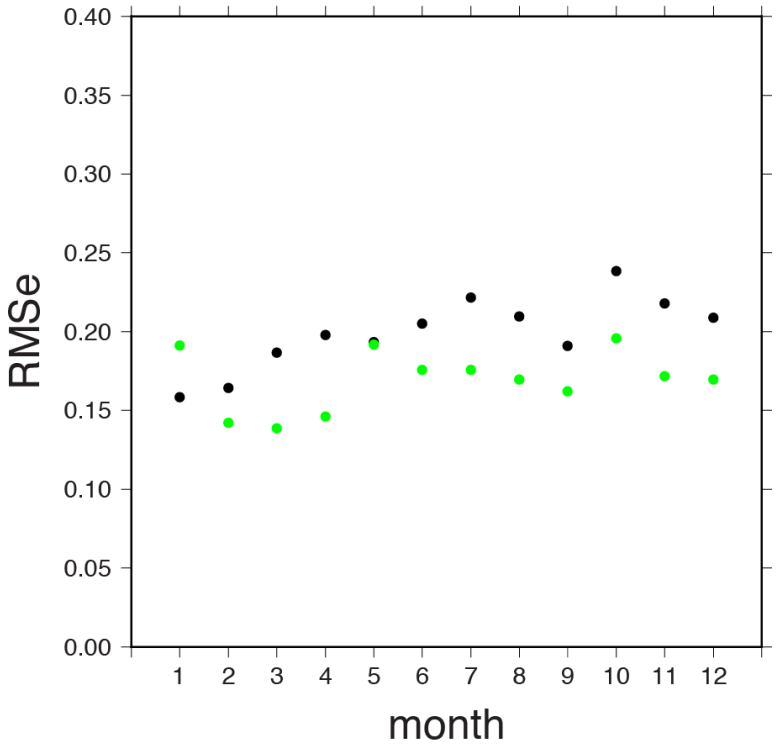

Figure 4.4 Comparison of model fit for SM-SIMPLE (black) and SM-COMPLEX (green). RMS error is calculated between normalized model biomass and monthly climatologies of satellite observations (Gower and King, 2013; Brooks et al., 2018).

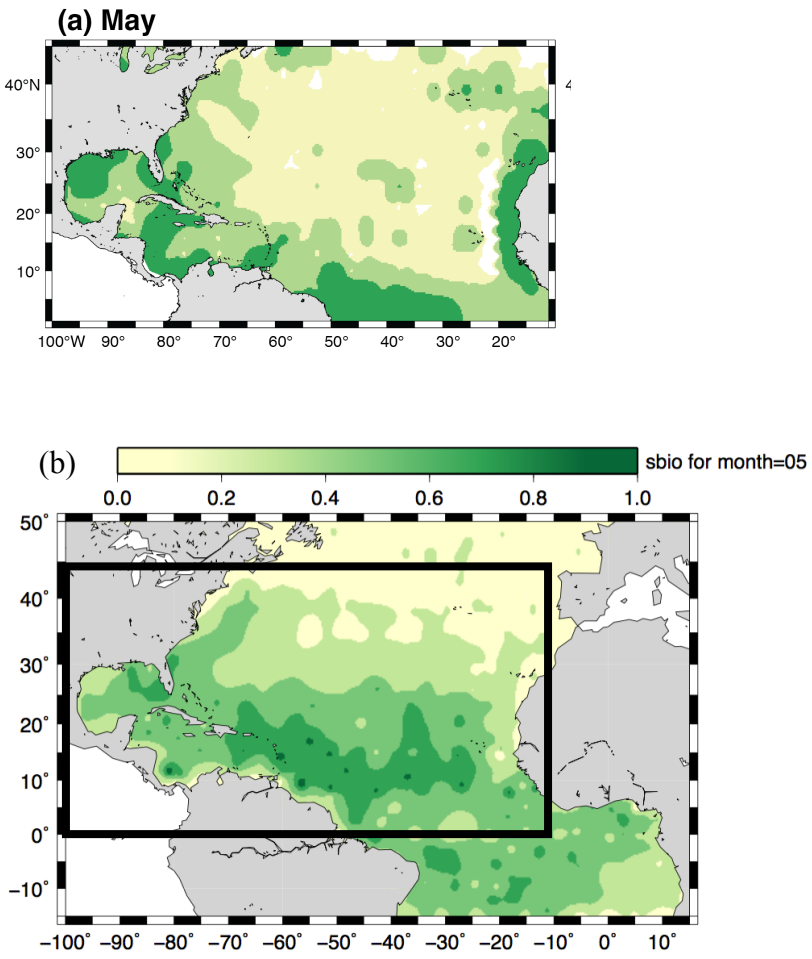

Figure 4.5 (continued on next page)

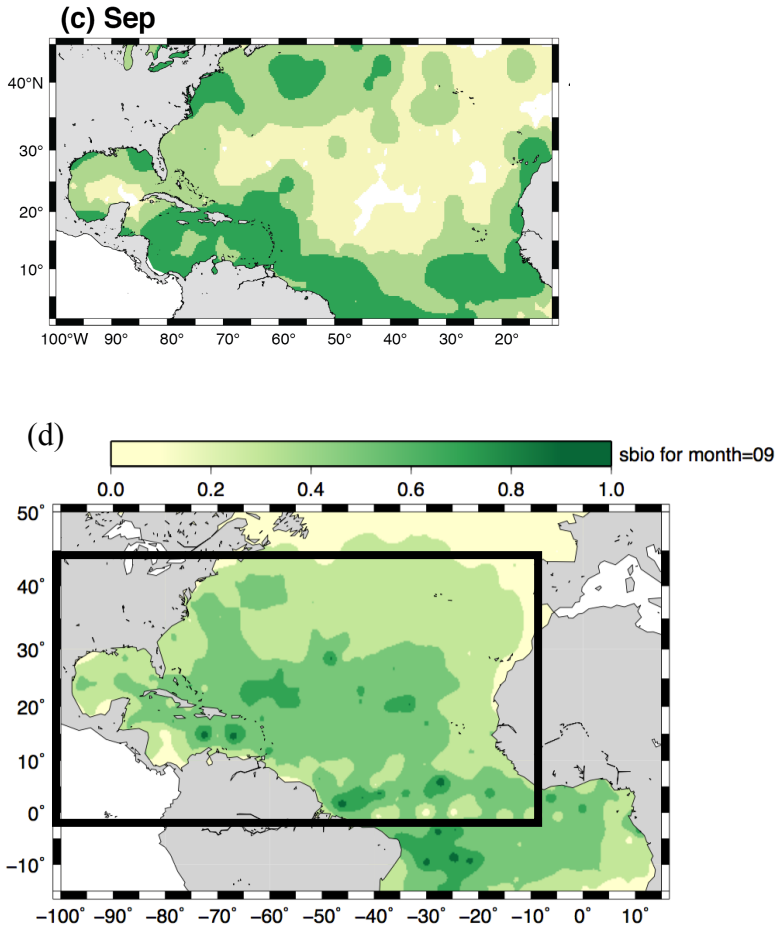

Figure 4.5 Satellite climatology of *Sargassum* observations (a,c) and normalized *Sargassum* biomass in SM-COMPLEX (b, d). (a) and (b) show May, and (c) and (d) show September. Black box in (b,d) outlines the region where satellite observations were available.

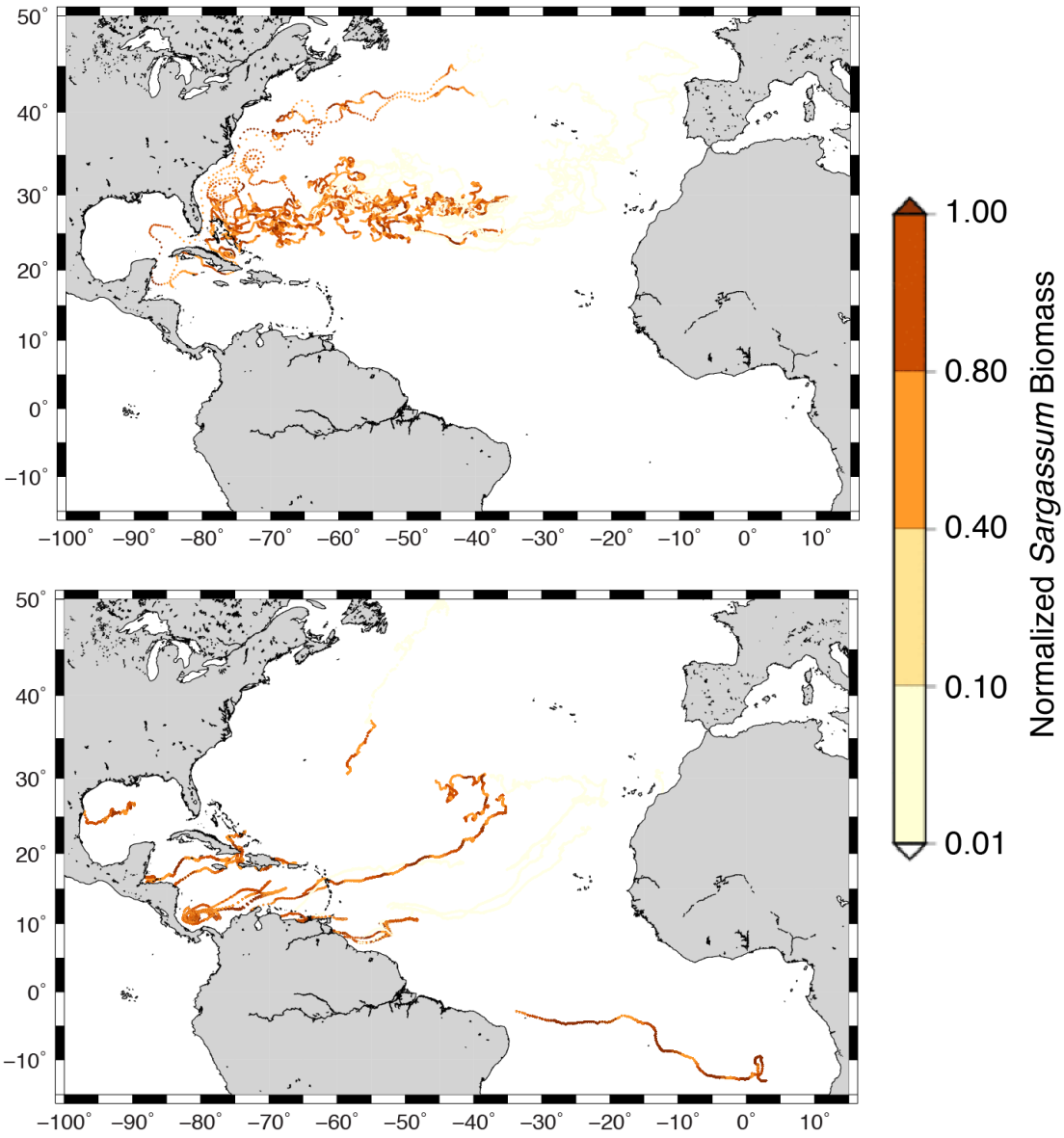

Figure 4.6 Trajectories of non-inertial (a) and inertial (b) *Sargassum* particles in SM-SIMPLE for the third year after initialization with no external renewal of particles.

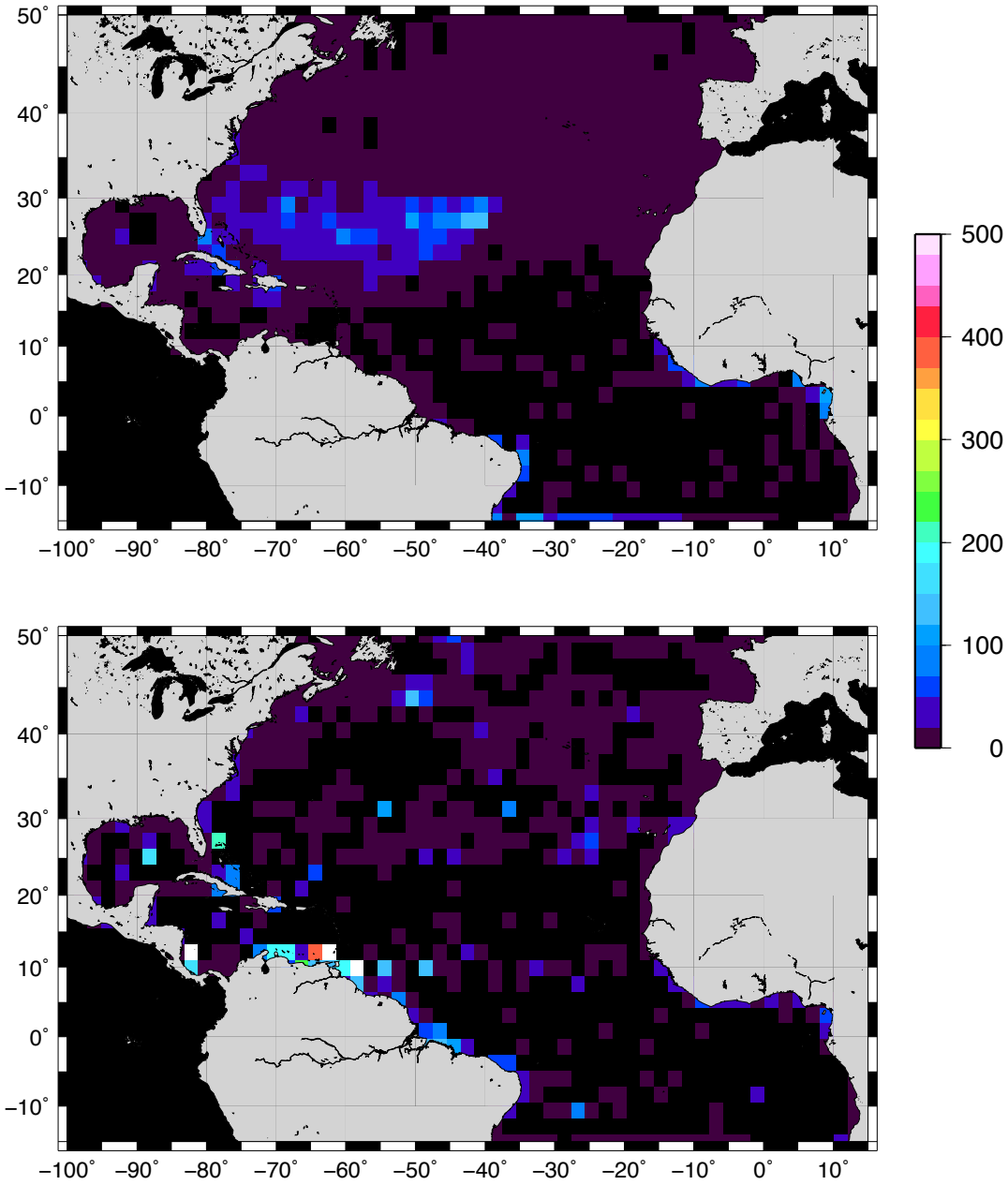

Figure 4.7 Number of *Sargassum* particles lost in SM-COMPLEX with (a) non-inertial and (b) inertial *Sargassum*.

Chapter 5: Synthesis and Conclusions

Across these studies, I have used a multiscale modeling system to investigate the interactions between algal physiology, biogeochemistry, and ocean physics that drive the growth and distribution of pelagic *Sargassum*. This research has shown that focusing on only one of these drivers is insufficient to capture the dynamics of this unique organism across spatial and temporal scales.

Since the putative regime shift to increasing *Sargassum* biomass in the tropical Atlantic in 2011, several hypotheses have been put forward to explain it in terms of changing growing conditions ocean circulation, and wind (e.g. Louime et al., 2017; Sanchez-Rubio et al., 2018; Langin 2018; Smetacek and Zingone, 2013). However, other modeling efforts to date have focused solely on the physical processes affecting *Sargassum* transport (Franks et al. 2016; Putman et al. 2018). This study bridges the knowledge gap and examines both physical and biological processes affecting *Sargassum*.

Chapter 2 showed the importance of including both physical and biological processes when considering *Sargassum* distribution over seasonal scales. Models of floating debris show how inert buoyant objects tend to accumulate in the subtropical gyres (Lebreton et al. 2012). Considering advection alone in models of *Sargassum* results in distributions that more closely resemble those of plastic debris than *Sargassum* observations (Law et al. 2010). Accounting for growth, mortality, and reproduction provided a better fit with remote sensing observations, especially at seasonal and longer time scales. These simulations suggested that vegetative

propagation is one of the mechanisms that contributes to the persistence of *Sargassum* throughout the Atlantic at annual time scales. In addition, the Gulf of Mexico and western tropical Atlantic were found to be key regions whose *Sargassum* populations drive the basin-wide distribution of this organism.

Chapter 3 introduced an inverse technique for estimating the effective radius of *Sargassum* rafts based on remote sensing observations and density measurements of *Sargassum* samples. The resulting values were used to parameterize a model that accounted for inertial effects on *Sargassum* trajectories. These effects alter the pathways *Sargassum* travels around the Atlantic, causing more to reach the Caribbean and Gulf of Mexico and increasing the potential for a return pathway from the Sargasso Sea back to the tropics.

Chapter 4 showed that the above inertial effects also yield changes in *Sargassum* growth and biomass. Inertial trajectory changes and increases in entrainment and retention in eddies lead to increased growth and biomass through transport of *Sargassum* rafts to regions like the Gulf of Mexico and Caribbean. This work also showed that in this model system, vegetative propagation by means of disaggregation of rafts when biomass is high yields distributions more consistent with observations than when vegetative propagation occurs when rafts are older and structurally weakened.

A recurring theme in this dissertation is that both biological and physical processes are acting on *Sargassum,* across temporal and spatial scales. Physical advection alone can explain more than half of the *Sargassum* distribution, but only at time scales on the order of 1-2 months. Beyond that scale, growth plays an

increasingly important role as biomass has time to either accumulate or die and sink out of surface waters. Likewise, inertial impacts can alter the trajectories of *Sargassum* rafts by tens of kilometers at weekly time scales, while reproduction has greater impacts at monthly and seasonal scales.

The interactions between inertial effects and patterns of organismal growth and distribution may not be unique to *Sargassum*. Although small, larval fish and other planktonic organisms may experience some changes in trajectories due to inertia. As this study showed, even small differences between organism density and that of the ambient water can drive large changes in distribution over time. Even larger, mobile organisms such as turtles and marine mammals may be influenced by these forces during periods of reduced swimming activity. These effects should be more noticeable in organisms living at higher latitudes where changes in trajectory due to the Earth's rotation are more pronounced.

The trajectories of *Sargassum* rafts and connectivity between regions of its known habitat provide insight into the source of the biomass that has been washing up on Caribbean and Gulf of Mexico beaches with increasing frequency and severity in recent years. Despite being its namesake and being closely associated since its discovery, *Sargassum* in the Sargasso Sea appears to be at a nearly dead-end. There are some pathways of escape but overall that region of the North Atlantic Subtropical Gyre is highly retentive and provides only a small source of *Sargassum* to other regions. The newly emerging paradigm of *Sargassum* transport minimizes the role of the Sargasso Sea in favor of two other areas. The Western Gulf of Mexico and the Western Tropical Atlantic are both significant source regions that influence the

Sargassum distribution throughout the Atlantic year-round. The growth potential in these regions is high, and inertial processes and entrainment in eddies help increase the transport to and retention in these locations.

Modeling efforts could be further refined by the inclusion of two-way coupling between *Sargassum* growth and ambient nutrient concentrations. This should increase the disparity of success between *Sargassum* rafts that stay in the tropics and Caribbean and those that get advected into the oligotrophic Sargasso Sea. This feedback may be especially important for predicting how *Sargassum* populations are likely to change in a changing climate, since ocean stratification is expected to increase as temperatures rise. Increasing temperatures could even lead to seasonal incursions of *Sargassum* to more northern latitudes where we currently see evidence of advection but mortality due to temperature limitation. Meanwhile, *Sargassum* also shows reductions in growth above its optimum temperature range (Hanisak and Samuel, 1987), which could negatively impact the population at low latitudes with temperature increases of 2°C.

One application of the modeling approach of this study would be to test the hypothesis that the relatively new prevalence of *Sargassum* biomass in the tropics represents a distinct population. If growth and nutrient kinetics measurements are made for individual *Sargassum* species or morphotypes, the *Sargassum* physiology models used in this study could be parameterized to distinguish between them. This could further improve bloom predictions, and give insights into the root causes of the regime shift in the tropics.

In the future, the coupled model system developed here may help improve prediction of *Sargassum* beaching events. Existing prediction systems either focus on short-term early warnings based on satellite observations (e.g. SAWS 2018, Webster and Linton 2013), or statistical prediction based on *Sargassum* detection in hot spots early in the growing season (Wang and Hu, 2017). Including both physical and biological processes in a numerical simulation provides a pathway toward predicting high bloom conditions farther in advance based on the distribution in the previous growing season and predicted oceanographic conditions.

To facilitate this predictive capacity, future studies would benefit from the development of data assimilation techniques for biogeochemical variables such as nutrient concentrations. Additionally, model experiments at higher, eddy-resolving resolutions would help uncover whether there are eddy impacts on *Sargassum* growth that cannot be detected at the lower, eddy-permitting resolutions used in this study.

Appendix I: Biogeochemical model details

Biogeochemical model equations

The biogeochemical model uses ten state variables to track the flow of nitrogen and phosphorous. This model operates in nitrogen units, with a basic structure adapted from Fennel et al. (2006) with additional light and grazer parameterizations adapted from Hood et al. (2001) and Stukel et al. (2014), respectively. Phytoplankton (P) biomass is a function of growth rate (μ_P), grazing rate (g_P), mortality rate (m_P), and aggregation into detrital particles (τ)

$$\frac{dP}{dt} = \mu_P P - g_P Z - m_P P - \tau(Ds + P)P \text{ , (Eqn S.1)}$$

where growth is a function of maximum growth rate (μ_{maxP}), nutrient limitation (L_{Ntot}, L_{DIP}), and light ($f(I)$).

$$\mu_P = \mu_{maxP} \cdot \min(L_{Ntot}, L_{DIP}) \cdot f(I). \quad \text{(Eqn S.2)}$$

Nitrogen and phosphorus limitation are given by

$$L_{Ntot} = L_P^N + L_P^A \quad \text{(Eqn S.3)}$$

where

$$L_P^N = \frac{NO3}{k_{NO3}+NO3} \cdot \frac{1}{1+\frac{NH4}{k_{NH4}}}, \quad L_P^A = \frac{NH4}{k_{NH4}+NH4}, \quad \text{(Eqns S.4, S.5)}$$

and

$$L_P^P = \frac{DIP}{k_{PDIP}+DIP}, \quad \text{(Eqn S.6)}$$

while light (I) dependence is determined via light saturation tolerance (I_P) and photoinhibition irradiance level ($I_{\beta P}$) by

$$f(I) = (1 - e^{-I/I_P})(e^{-I/I_{\beta P}}) \text{(Eqn S.7)}$$

after Hood et al. (2001).

Zooplankton grazing is density-dependent, with

$$g_P = g_{max} \frac{P^2}{k_P + P^2}. , \quad \text{(Eqn S.8)}$$

where g_{max} is zooplankton maximum grazing rate and k_P is the half-saturation constant for zooplankton grazing.

The modeled diazotroph, T is parameterized after *Trichodesmium*. It has similar growth rate (μ_T) and mortality (m_T) formulations as the other phytoplankton, although it is not limited by nitrogen availability. It also has a higher rate of self-aggregation (τ_T) and experiences a small leakage to the ammonium pool (α),

$$\frac{dT}{dt} = \mu_T T - m_T T - \tau_T T^2 - \alpha T . \quad \text{(Eqn S.9)}$$

$$\mu_T = \mu_{maxT} \cdot L_{TDIP} \cdot f_T(I). \quad \text{(Eqn S.10)}$$

with phosphorus limitation only,

$$L_T^P = \frac{DIP}{k_{TDIP} + DIP}, \quad \text{(Eqn S.11)}$$

and no photoinhibition,

$$f_T(I) = (1 - e^{-I/I_T}). \text{ (Eqn S.12)}$$

The rate of change of zooplankton is dependent on grazing (g_P), with assimilation efficiency (β), basal metabolism (l_{BM}), assimilation-dependent excretion, and density-dependent mortality with maximum rate m_Z (Fennel et al. 2006).

$$\frac{dZ}{dt} = g_P \beta Z - l_{BM} Z - l_E \frac{P^2}{k_P + P^2} \beta Z - m_Z Z^2 \ . \qquad \text{(Eqn S.13)}$$

Model nitrate is dependent on phytoplankton uptake and nitrification (n)

$$\frac{dN}{dt} = -\mu max_P f_P(I) L_P^N P + nA \ , \qquad \text{(Eqn S.14)}$$

while change in ammonium concentration is dependent on phytoplankton uptake, nitrification, zooplankton metabolism and assimilation, remineralization from small and large detrital pools, and losses from the *Trichodesmium* pool.

$$\frac{dA}{dt} = -\mu max_P f_P(I) L_P^A P - nA + l_{BM} Z + l_E \frac{P^2}{k_P + P^2} \beta Z + r_{DSN} D_S^N + r_{DLN} D_L^N + \alpha T$$

(Eqn S.15)

Dissolved inorganic phosphorus is depleted via phytoplankton and *Trichodesmium* uptake, and replenished via zooplankton excretion and remineralization of detritus

$$\frac{dDIP}{dt} = -\mu max_P f_P(I) L_P^P P - \mu max_T f_T(I) L_T^P T + l_{BM} Z + l_E \frac{P^2}{k_P + P^2} \beta Z \qquad \text{(Eqn S.16)}$$

$$+ r_{DSP} D_S^P + r_{DLP} D_L^P \ .$$

Detritus is tracked as four different pools to allow for differential remineralization (r) of nitrogen and phosphorus, and of different size classes. The rates of change of these pools are given by

$$\frac{dD_S^N}{dt} = m_P P + m_T T + m_Z Z^2 - \tau(D_S^N + P)D_S^N - r_{DSN} D_S^N \quad \text{(Eqn S.17)}$$

$$\frac{dD_S^P}{dt} = m_P P + m_T T + m_Z Z^2 - \tau(D_S^N + P)D_S^N - r_{DSP} D_S^P \quad \text{(Eqn S.18)}$$

$$\frac{dD_L^N}{dt} = \tau(Ds + P)^2 + \tau_T T^2 - r_{DLN} D_L^N \qquad \text{(Eqn S.19)}$$

$$\frac{dD_L^P}{dt} = \tau(Ds + P)^2 + \tau_T T^2 - r_{DLP} D_L^P \,, \qquad \text{(Eqn S.20)}$$

with the small pools gaining contributions from the living compartments via mortality, and the large pools growing via aggregation, and all detrital pools diminished via remineralization.

Table A1.1 Biogeochemical Model Parameters

Symbol	Parameter	Value	Units
μmax_P	Phytoplankton maximum growth rate	2.0	d^{-1}
μmax_T	*Trichodesmium* maximum growth rate	0.15	d^{-1}
k_{NO3}	Phytoplankton NO3 uptake half saturation	0.5	mmol N m^{-3}
k_{NH4}	Phytoplankton NH4 uptake half saturation	0.5	mmol N m^{-3}
k_{PDIP}	Phytoplankton DIP uptake half saturation	0.0125	mmol P m^{-3}
k_{TDIP}	*Trichodesmium* DIP uptake half saturation	0.0125	mmol P m^{-3}
I_P	Phytoplankton light saturation	20.0	W m^{-2}
$I_{\beta P}$	Phytoplankton photoinhibition	400.0	W m^{-2}
I_T	*Trichodesmium* light saturation	70.0	W m^{-2}
τ	Phytoplankton and detritus aggregation parameter	0.005	(mmol N m^{-3})$^{-1}$ d^{-1}
τ_T	*Trichodesmium* aggregation parameter	0.001	(mmol N m^{-3})$^{-1}$ d^{-1}
α	*Trichodesmium* leakage to the NH4 pool	0.01	d^{-1}
m_P	Phytoplankton mortality	0.15	d^{-1}
m_T	*Trichodesmium* mortality	0.02	d^{-1}
m_Z	Zooplankton mortality	0.015	d^{-1}
g_{max}	Zooplankton maximum grazing rate	0.6	(mmol N m^{-3})$^{-1}$ d^{-1}
k_P	Half saturation of phytoplankton ingestion	2.0	(mmol N m^{-3})^2
β	Zooplankton assimilation efficiency	0.75	dimensionless
l_{BM}	Zooplankton basal metabolism-based excretion rate	0.1	d^{-1}
l_E	Zooplankton assimilation-related excretion	0.1	d^{-1}
n	maximum nitrification rate	0.05	d^{-1}
r_{DSN}	Remineralization of nitrogen in small detritus	0.03	d^{-1}
r_{DLN}	Remineralization of nitrogen in large detritus	0.01	d^{-1}
r_{DSP}	Remineralization of phosphorus in small detritus	0.2	d^{-1}
r_{DLP}	Remineralization of phosphorus in large detritus	0.2	d^{-1}

Appendix II: Supporting information for *Sargassum* density and radius calculations

Introduction

This supporting information document contains sampling locations for *Sargassum* density measurements, the data from those measurements, and the results of model sensitivity analysis and seasonal connectivity analysis. Results of deflection angle measurements are also included. All methods are as described in the main body of Chapter 3.

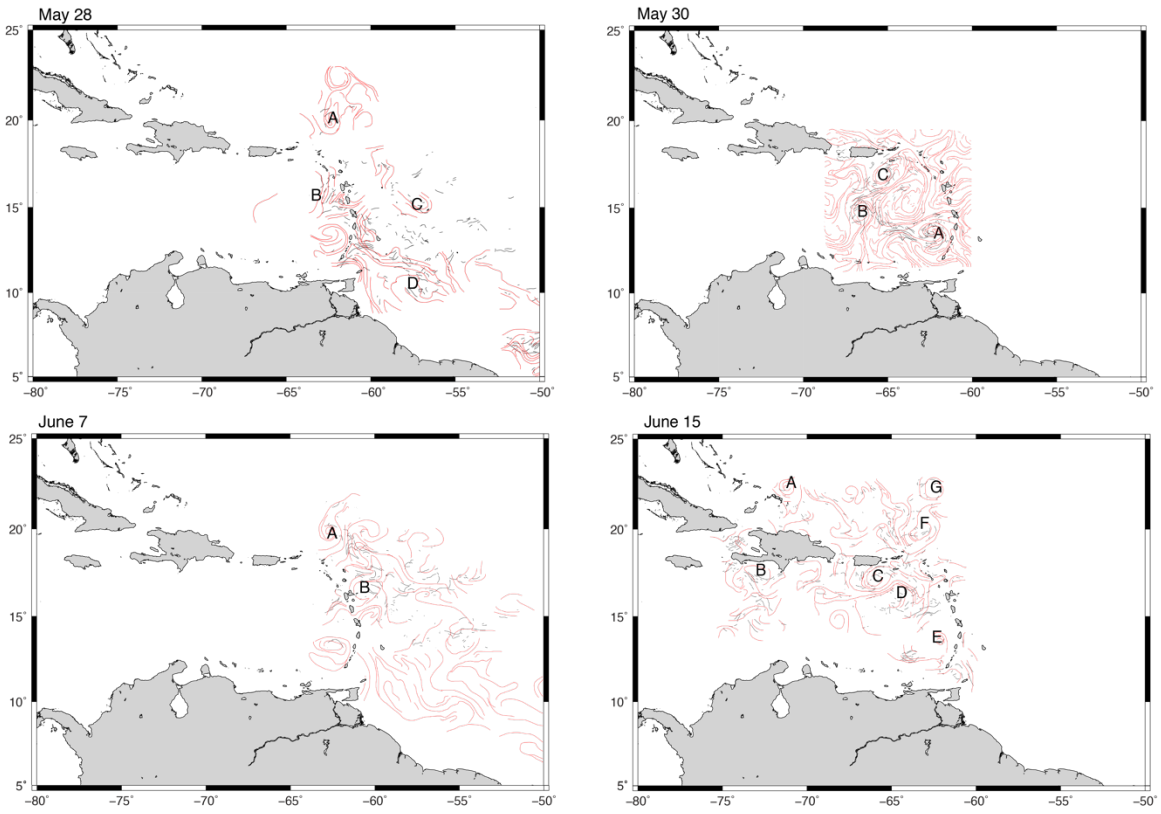

Figure A2.1 Feature locations for deflection angle analysis. Deflection angles were calculated for *Sargassum* lines near these features in May and June, 2018.

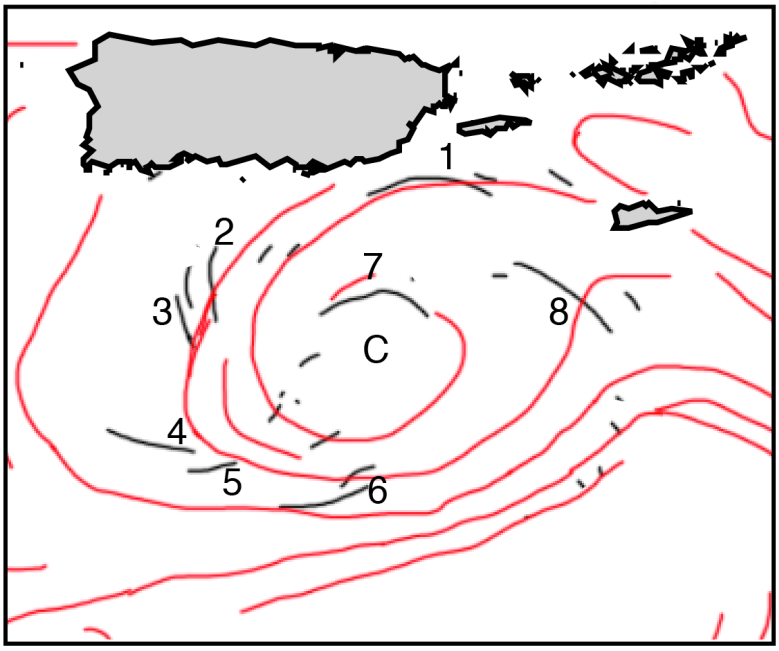

Figure A2.2 Example of *Sargassum* line selection. This magnification of feature "C" from June 15, 2018 highlights how only *Sargassum* lines with length greater than 20 km that approach within 10 km or cross FSLE lines were used for subsequent analysis.

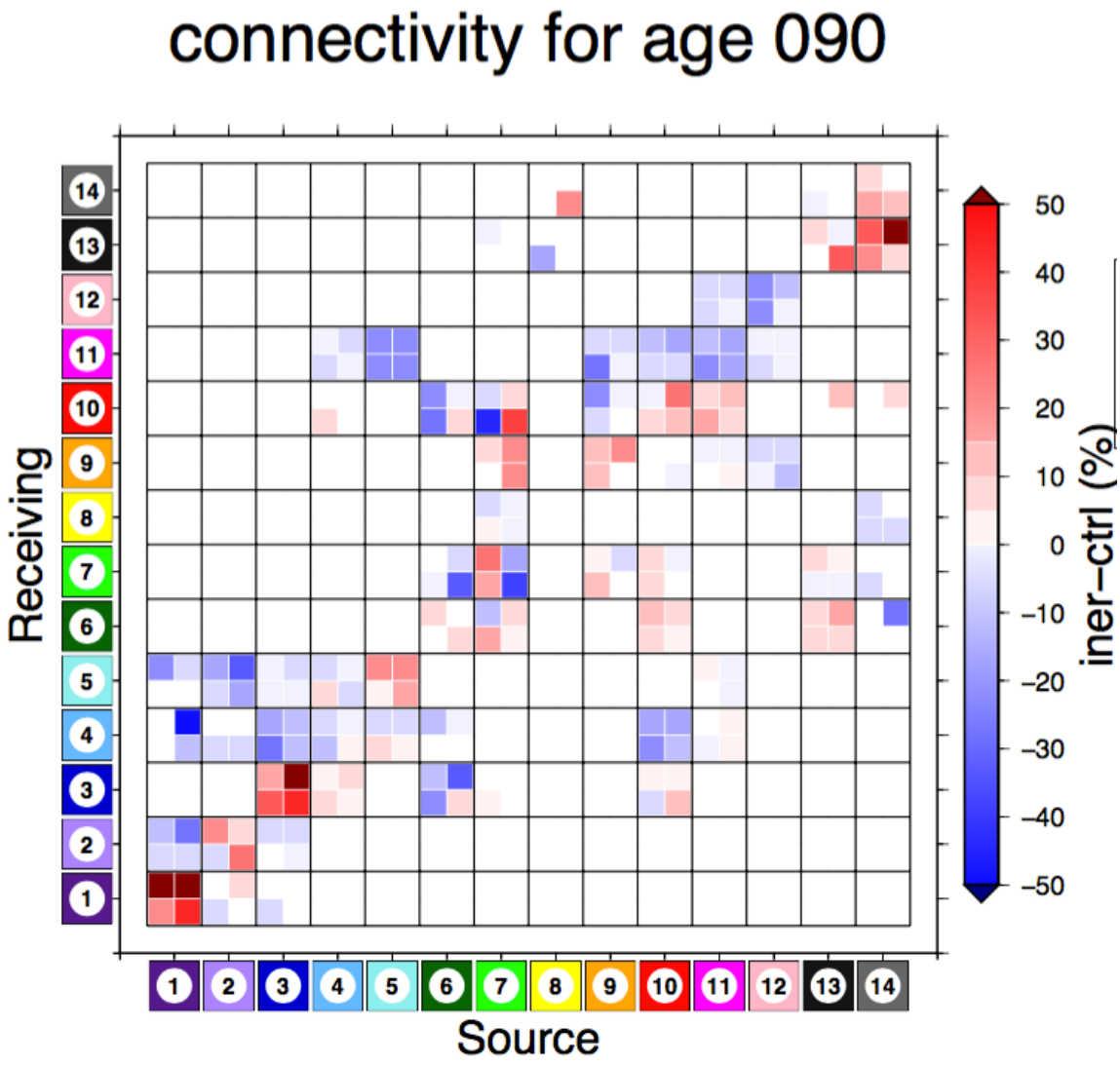

Figure A2.3 *S*easonal effect of inertia on connectivity of *Sargassum* throughout its range. Connectivity was calculated at a particle age of 90 d. Colors indicate the % change in connectivity from source region on the x-axis to each receiving region on the y-axis. Small sub-boxes are for particles launched in Fbruary, May, August, and November (clockwise from top left) for each source-receiving region pair.

Table A2.1 *Sargassum* sampling locations. All locations are St. Croix, U.S. Virgin Islands.

Sample Site	Latitude	Longitude	Location
Robin Bay	17.72523° N	64.63410° W	South side of St. Croix
Turner Hole	17.74384° N	64.60419° W	South side of St. Croix
Christiansted Harbor	17.74695° N	64.70726° W	North Side of St. Croix
Hibiscus Beach	17.76262° N	64.73180° W	North Side of St. Croix

Table A2.2 *Sargassum* density. *Sargassum* samples of 15g wet weight or less (*) were excluded from the calculation of mean density.

Sample	Mass (g)	Volume (mL)	Density (g mL^{-1})
RB01	20	23	0.87
RB02	20	22	0.91
RB03	30	32	0.94
RB04	20	22	0.91
RB05	40	41	0.97
RB06	5	11	0.45*
RB07	20	22	0.91
RB08	20	22	0.91
RB09	30	37	0.81
RB10	35	37	0.95
TH01	5	5	1.0*
TH02	10	7	1.4*
TH03	15	13	1.2*
TH04	25	28	0.89
TH05	15	17	0.88*
TH06	10	4	2.5*
TH07	15	7	2.1*
TH08	25	25	1.1
TH09	40	43	0.93
TH10	30	23	1.3
CH01	45	47	0.96
CH02	25	22	1.1
CH03	35	32	1.1
CH04	35	37	0.95
CH05	15	17	0.88*
CH06	25	27	0.92
CH07	40	47	0.85
CH08	40	42	0.95
CH09	20	22	0.91
CH10	30	31	0.97
HB01	20	31	0.65
HB02	50	52	0.96
HB03	20	22	0.91
HB04	40	42	0.95
HB05	35	37	0.95
HB06	30	27	1.1
HB07	20	22	0.91
HB08	25	27	0.92
HB09	20	22	0.91
HB10	60	67	0.97

Table A2.3 Model sensitivity analysis. Density ratio is the ratio of the particle density to the density of ambient sea water. Values are p-values of an Anderson-Darling k-sample test for whether the distributions of model and observed deflection angles are significantly different (**).

	Particle Density Ratio				
Particle Radius (m)	0.81	0.87	0.92	0.98	1.03
0.45	**	**	**	**	**
0.55	**	**	**	**	**
0.65	**	0.173	**	**	**
0.75	0.015	0.324	0.015	**	**
0.85	**	0.055	0.260	**	**
0.95	**	**	0.337	**	**
1.05	**	**	0.098	**	**
1.15	**	**	0.016	**	**
1.25	**	**	**	**	**
1.35	**	**	**	**	**

Table A2.4 Deflection angle measurements. This includes the date for each satellite observation, unique eddy and *Sargassum* line identifiers, the measured angles for each *Sargassum* line and its corresponding nearest contour of Finite Size Lyapunov Exponent, and the calculated deflection. Data on whether the eddy was cyclonic or anticyclonic, and the *Sargassum* line position relative to the center for the eddy is also shown. Quality Control (QC) values indicate the following quality requirements: clarity of the *Sargassum* lines in the satellite image, whether the lines were straight for >= 20 km, and whether they were touching a FLSE line. A QC value of 1 indicates the *Sargassum* line met all three criteria, a value of 2 indicates the line failed one criterion, and a value of 3 indicates it failed 2 of the criteria. Lines failing all three criteria were not considered in this analysis.

Date	Eddy	Line	Angles		Deflection (°)	Eddy rotation	Position relative to eddy center (°)	QC Value
			Sargassum (°)	FSLE (°)				
5/30/18	A	1	127.79	98.82	28.97	cyclonic	358	1
5/30/18	A	2	159.95	143.73	16.22	cyclonic	50	1
5/30/18	A	3	195.49	176.79	18.7	cyclonic	84	1
5/30/18	A	4	179.64	188.68	-9.04	cyclonic	114	2
5/30/18	A	5	166.91	135.28	31.63	cyclonic	146	2
5/30/18	A	6	206.38	233.09	-26.71	cyclonic	157	1
5/30/18	A	7	180.91	269.54	-88.63	cyclonic	169	1
5/30/18	A	8	5.45	303.7	61.75	cyclonic	184	1
5/30/18	A	9	23.56	346.87	36.69	cyclonic	210	2
5/30/18	A	10	14.17	15.76	-1.59	cyclonic	270	2
5/30/18	A	11	134.9	38.22	96.68	cyclonic	346	3
5/30/18	A	12	133.76	116.79	16.97	cyclonic	357	2
5/30/18	B	1	291.71	222.06	69.65	cyclonic	94	3
5/30/18	B	2	292.45	198.27	94.18	cyclonic	74	3
5/30/18	B	3	217.8	254.59	-36.79	cyclonic	141	2
5/30/18	B	4	199.53	234.89	-35.36	cyclonic	142	1
5/30/18	B	5	164.33	231	-66.67	cyclonic	114	2
5/30/18	B	6	233.25	293.17	-59.92	cyclonic	200	1
5/30/18	B	7	296.55	354.13	-57.58	cyclonic	70	1
5/30/18	B	8	208.73	241.57	-32.84	cyclonic	130	1
5/30/18	B	9	223.36	206.57	16.79	cyclonic	115	1
5/30/18	B	10	358.81	331.26	27.55	cyclonic	243	1
5/30/18	C	1	335.26	42.71	-67.45	cyclonic	52	1
5/30/18	C	2	330.55	43.3	-72.75	cyclonic	52	1
5/30/18	C	3	251.82	243.4	8.42	cyclonic	355	1

5/30/18	C	4	126.68	212.24	-85.56	cyclonic	318	2
5/30/18	C	5	240.08	221.83	18.25	cyclonic	330	2
5/30/18	C	6	151.63	126.71	24.92	cyclonic	215	2
5/30/18	C	7	136.85	136.57	0.28	cyclonic	224	3
5/28/18	A	1	185.4	275.35	-89.95	cyclonic	121	1
5/28/18	A	2	202.99	231.45	-28.46	cyclonic	90	1
5/28/18	A	3	124.06	97.93	26.13	cyclonic	353	2
5/28/18	A	4	294.63	298.74	-4.11	cyclonic	227	2
5/28/18	B	1	265.42	298.86	-33.44	anticyclonic	38	2
5/28/18	B	2	178.62	270.75	-92.13	anticyclonic	30	1
5/28/18	B	3	235.57	267.97	-32.4	anticyclonic	21	2
5/28/18	B	4	224.23	267.43	-43.2	anticyclonic	14	1
5/28/18	B	5	230.85	250.48	-19.63	anticyclonic	358	1
5/28/18	B	6	215.63	251.24	-35.61	anticyclonic	347	2
5/28/18	B	7	204.82	250.32	-45.5	anticyclonic	351	1
5/28/18	C	1	141.27	139.46	1.81	cyclonic	152	2
5/28/18	C	2	138.58	136.86	1.72	cyclonic	192	2
5/28/18	C	3	170.27	154.3	15.97	cyclonic	286	2
5/28/18	C	4	162.17	157.33	4.84	cyclonic	270	2
5/28/18	C	5	147.95	185.27	-37.32	cyclonic	221	1
5/28/18	D	1	179.71	170.32	9.39	cyclonic	131	1
5/28/18	D	2	149.76	175.54	-25.78	cyclonic	107	1
5/28/18	D	3	161.78	173.23	-11.45	cyclonic	92	1
5/28/18	D	4	181.85	165.3	16.55	cyclonic	55	2
5/28/18	D	5	172.07	167.39	4.68	cyclonic	55	3
5/28/18	D	6	175.27	86.84	88.43	cyclonic	27	1
6/15/18	A	1	323.8	272.94	50.86	cyclonic	199	2
6/15/18	B	1	147.3	134.98	12.32	anticyclonic	170	2
6/15/18	B	2	140.2	136.48	3.72	anticyclonic	173	2
6/15/18	B	3	136.26	122.84	13.42	anticyclonic	209	1
6/15/18	B	4	123.2	112.37	10.83	anticyclonic	217	2
6/15/18	B	5	146.73	110.53	36.2	anticyclonic	234	1
6/15/18	B	6	196.92	249.56	-52.64	anticyclonic	341	3
6/15/18	C	1	182.31	180.97	1.34	cyclonic	81	1
6/15/18	C	2	277.63	237.68	39.95	cyclonic	154	1
6/15/18	C	3	288.39	259.02	29.37	cyclonic	172	1
6/15/18	C	4	350.42	312.61	37.81	cyclonic	201	2
6/15/18	C	5	12.75	340.15	32.6	cyclonic	214	1
6/15/18	C	6	22.3	5.17	17.13	cyclonic	265	1
6/15/18	C	7	199.23	202.6	-3.37	cyclonic	96	2

6/15/18	C	8	141.86	64.45	77.41	cyclonic	16	1
6/15/18	D	1	130.62	37.16	93.46	anticyclonic	136	1
6/15/18	D	2	134.15	179.69	-45.54	anticyclonic	242	1
6/15/18	D	3	270.32	249.46	20.86	anticyclonic	302	2
6/15/18	D	4	230.76	250.93	-20.17	anticyclonic	323	2
6/15/18	D	5	193.3	260.36	-67.06	anticyclonic	340	1
6/15/18	D	6	196.82	272.04	-75.22	anticyclonic	7	1
6/15/18	D	7	338.33	318.88	19.45	anticyclonic	37	2
6/15/18	E	1	2.42	337.75	24.67	cyclonic	295	2
6/15/18	E	2	67.05	88.82	-21.77	cyclonic	13	1
6/15/18	F	1	312.19	233.79	78.4	cyclonic	161	1
6/15/18	F	2	354.72	298.14	56.58	cyclonic	214	1
6/15/18	F	3	25.28	323.06	62.22	cyclonic	228	1
6/15/18	F	4	32.74	23.99	8.75	cyclonic	299	2
6/15/18	F	5	96.87	74.88	21.99	cyclonic	0	2
6/15/18	F	6	118.06	74.81	43.25	cyclonic	8	2
6/15/18	G	1	174.01	170.23	3.78	cyclonic	102	2
6/15/18	G	2	238.4	240.63	-2.23	cyclonic	142	2
6/15/18	G	3	54.03	23.88	30.15	cyclonic	298	1
6/15/18	G	4	172.9	164.04	8.86	cyclonic	67	1
6/7/18	A	1	247.84	180.67	67.17	cyclonic	94	1
6/7/18	A	2	226.66	164.12	62.54	cyclonic	78	2
6/7/18	A	3	134.23	92.43	41.8	cyclonic	346	2
6/7/18	B	1	155.26	131.03	24.23	cyclonic	19	1
6/7/18	B	2	106.99	46.93	60.06	cyclonic	348	3
6/7/18	B	3	157.67	47	110.67	cyclonic	334	2

References

Ackah-Baidoo, A. (2013). Fishing in troubled waters: Oil production, seaweed and community-level grievances in the Western Region of Ghana. *Community Development Journal*, *48*(3), 406–420. https://doi.org/10.1093/cdj/bst022

AdobeSystems. (2011). Adobe Photoshop CS5 12.1. San Jose, CA: Adobe Systems Incorporated.

Amaral-Zettler, L. A., Dragone, N. B., Schell, J., Slikas, B., Murphy, L. G., Morrall, C. E., & Zettler, E. R. (2017). Comparative mitochondrial and chloroplast genomics of a genetically distinct form of *Sargassum* contributing to recent "Golden Tides" in the Western Atlantic. *Ecology and Evolution*, *7*(2), 516–525. https://doi.org/10.1002/ece3.2630

Beaugrand, G., Ibañez, F., Lindley, J. A., & Reid, P. C. (2002). Diversity of calanoid copepods in the North Atlantic and adjacent seas: Species associations and biogeography. *Marine Ecology Progress Series*, *232*, 179–195. https://doi.org/10.3354/meps232179

Beron-Vera, F. J., Olascoaga, M. J., & Lumpkin, R. (2016). Inertia-induced accumulation of flotsam in the subtropical gyres. *Geophysical Research Letters*, *43*, 1–6. https://doi.org/10.1002/2016GL071443

Beron-Vera, F. J., Olascoaga, M. J., Haller, G., Farazmand, M., Triñanes, J., & Wang, Y. (2015). Dissipative inertial transport patterns near coherent Lagrangian eddies in the ocean. *Chaos*, *25*(8). https://doi.org/10.1063/1.4928693

Bortone, S. A., Hastings, P. A., & Collard, S. B. (1977). The Pelagic-*Sargassum* Icthyofauna of the Eastern Gulf of Mexico. *Northeast Gulf Science*.

Brooks, M. T., Coles, V. J., Hood, R. R., & Gower, J. F. R. (2018). Factors controlling the seasonal distribution of pelagic *Sargassum*. *Mar. Ecol. Prog. Ser.*, *599*, 1–18. https://doi.org/https://doi.org/10.3354/meps12646

Brooks, M. T., Coles, V. J., Coles, W. C. (2019). Inertia influences pelagic *Sargassum* advection and distribution. *Geophysical Research Letters.* https://doi.org/10.1029/2018GL081489.

Butler, J. N., Morris, B. F., Cadwallader, J., & Stoner, A. W. (1983). *Studies of Sargassum and the Sargassum Community*. *Studies of Sargassum and the Sargassum Community*. Bermuda Biological Station Special Publication No. 22. The Bermuda Station for Biological Research, Inc.

Butler, J. N., & Stoner, A. W. (1984). Pelagic *Sargassum*: has its biomass changed in the last 50 years? *Deep Sea Research Part A. Oceanographic Research Papers*, *31*, 1259–1264. https://doi.org/10.1016/0198-0149(84)90061-X

Carpenter, E. J. (1972). Nitrogen fixation by a blue-green epiphyte on pelagic *Sargassum*. *Science*, *178*, 1207–1209.

Carpenter, E. J., & Cox, J. L. (1974). Production of pelagic *Sargassum* and a blue-green epiphyte in the western Sargasso Sea. *Limnology and Oceanography*, *19*(3), 429–436. https://doi.org/10.4319/lo.1974.19.3.0429

Carr, A. (1987). Perspective on the pelagic stage of sea turtle development. *Conservation Biology*, *1*(2), 103–121.

Carr, A., & Meylan, A. B. (1980). Evidence of Passive Migration of Green Turtle Hatchlings in *Sargassum*. *Copeia*, *1980*(2), 366–368.

Cartwright, J. H. E., Feudel, U., Károlyi, G., de Moura, A., Piro, O., & Tél, T. (2010). Dynamics of finite-size particles in chaotic fluid flows. In M. et al. Thiel (Ed.), *Nonlinear Dynamics and Chaos: Advances and Perspectives* (pp. 51–87). https://doi.org/10.1007/978-3-642-04629-2

Casazza, T. L., & Ross, S. W. (2008). Fishes associated with pelagic *Sargassum* and open water lacking *Sargassum* in the Gulf Stream off North Carolina. *Fishery Bulletin*, p*106*.

Cavender-Bares, K. K., Karl, D. M., & Chisholm, S. W. (2001). Nutrient gradients in the western North Atlantic Ocean: Relationship to microbial community structure and comparison to patterns in the Pacific Ocean. *Deep Sea Research Part I: Oceanographic Research Papers*, *48*(11), 2373–2395. https://doi.org/10.1016/S0967-0637(01)00027-9

Chassignet, E. P., Smith, L. T., & Halliwell, G. R. (2003). North Atlantic Simulations with the Hybrid Coordinate Ocean Model (HYCOM): Impact of the Vertical Coordinate Choice, Reference Pressure, and Thermobaricity. *Journal of Physical Oceanography*, *33*, 2504–2526.

Chassignet, E., Hurlburt, H., Metzger, E. J., Smedstad, O., Cummings, J., Halliwell, G., Bleck, R., Baraille, R., Wallcraft, A.J., Lozano, C., Tolman, H.L., Srinivasan, A., Hankin, S. Cornillon, P., Weisberg, R, Barth, A., He, R., Werner, F., and Wilkin, J. (2009). US GODAE: Global Ocean Prediction with the HYbrid Coordinate Ocean Model (HYCOM). *Oceanography*, *22*(2), 64–75. https://doi.org/10.5670/oceanog.2009.39

Coles, V. J., & Hood, R. R. (2007). Modeling the impact of iron and phosphorus limitations on nitrogen fixation in the Atlantic Ocean. *Biogeosciences*, *4*(4), 455–479. https://doi.org/10.5194/bg-4-455-2007

Coles, V. J., Brooks, M. T., Hopkins, J., Stukel, M. R., Yager, P. L., & Hood, R. R. (2013). The pathways and properties of the Amazon River Plume in the tropical North Atlantic Ocean. *Journal of Geophysical Research: Oceans*, *118*(12), 6894–6913. https://doi.org/10.1002/2013JC008981

Conover, J. T., & Sieburth, J. M. (1964). Effect of *Sargassum* distribution on its epibiota and antibacterial activity. *Botanica Marina*, *6*, 147–157.

Coston-Clements, L. R., Settle L. R., Hoss D. E., & Cross F. A. (1991). *Utilization of the Sargassum habitat by marine invertebrates and vertebrates - A review*. *NOAA Tecnical Memorandum* (Vol. NMFS-SEFSC). NMFS-SEFSC-296.

Cummings, J. A. (2005). Operational multivariate ocean data assimilation. *Quarterly Journal of the Royal Meteorological Society*, *131*(613), 3583–3604. https://doi.org/10.1256/qj.05.105

Cummings, J. A., & Smedstad, O. M. (2013). Variational Data Assimilation for the Global Ocean. In S. K. Park & L. Xu (Eds.), *Data Assimilation for Atmospheric, Oceanic and Hydrologic Applications (Vol. II)* (Vol. II, pp. 303–343). Berlin Heidelberg: Springer-Verlag. https://doi.org/10.1007/978-3-642-35088-7_13

D'Ovidio, F., DeMonte, S., Penna, A. Della, Cotté, C., & Guinet, C. (2013). Ecological implications of eddy retention in the open ocean : a Lagrangian approach. *Journal of Physics A: Mathematical and Theoretical*, *46*, 254023. https://doi.org/10.1088/1751-8113/46/25/254023

d'Ovidio, F., Fernández, V., Hernández-García, E., & López, C. (2004). Mixing structures in the Mediterranean Sea from finite-size Lyapunov exponents. *Geophysical Research Letters*, *31*(17), 1–4. https://doi.org/10.1029/2004GL020328

de Széchy, M. T. M., Guedes, P. M., Baeta-Neves, M. H., & Oliveira, E. N. (2012). Verification of *Sargassum natans* (Linnaeus) Gaillon (Heterokontophyta: Phaeophyceae) from the Sargasso Sea off the coast of Brazil, western Atlantic Ocean. *Check List*, *8*(July 2011), 638–641.

Deacon, G. E. R. (1942). The Sargasso Sea. *The Geographical Journal*, *99*(1), 16–28.

Dickson, H. N. (1894). Recent Contributions to Oceanography. *The Geographical Journal*, *3*(4), 302–310.

Dooley, J. K. (1972). Fishes associated with the pelagic *Sargassum* complex, with a discussion of the *Sargassum* community. *Contributions in Marine Science*, *16*, 1–32.

Ducet, N., & Traon, L. (2001). A comparison of surface eddy kinetic energy and Reynolds systems from merged TOPEX / Poseidon and ERS-1 / 2 altimetric data. *Journal of Geophysical Research*, *106*, 16603–16622.

Early, J. J., Samelson, R. M., & Chelton, D. B. (2011). The Evolution and Propagation of Quasigeostrophic Ocean Eddies. *Journal of Physical Oceanography*, *41*(8), 1535–1555. https://doi.org/10.1175/2011JPO4601.1

Elliott, B. a. (1982). Anticyclonic Rings in the Gulf of Mexico. *Journal of Physical Oceanography*. https://doi.org/10.1175/1520-0485(1982)012<1292:ARITGO>2.0.CO;2

Falkowski, P. G., Ziemann, D., Kolber, Z., & Bienfang, P. K. (1991). Role of eddy pumping in enhancing primary production in the ocean. *Nature*, *352*(6330), 55–58. https://doi.org/10.1038/352055a0

Fennel, K., Wilkin, J., Levin, J., Moisan, J., O'Reilly, J., & Haidvogel, D. (2006). Nitrogen cycling in the Middle Atlantic Bight: Results from a three-dimensional model and implications for the North Atlantic nitrogen budget. *Global Biogeochemical Cycles*, *20*(3), GB3007. https://doi.org/10.1029/2005GB002456

Franks, J. S., Johnson, D. R., Ko, D. S., Rubio, G. S., Hendon, J. R., & Lay, M. (2011). Unprecedented Influx of Pelagic *Sargassum* along Caribbean Island Coastlines during Summer 2011. *Proceedings of the Gulf and Caribbean Fisheries Institute*, *64*, 6–8.

Franks, J. S., Johnson, D. R., & Ko, D. S. (2016). Pelagic *Sargassum* in the Tropical North Atlantic. *Gulf and Caribbean Research*, *27*(1). https://doi.org/10.18785/gcr.2701.08

Fraser, C. I., Nikula, R., & Waters, J. M. (2011). Oceanic rafting by a coastal community. *Proceedings. Biological Sciences / The Royal Society*, *278*(1706), 649–655. https://doi.org/10.1098/rspb.2010.1117

Fujita, R. M. (1985). The role of nitrogen status in regulating ammonium transient uptake and nitrogen storage by macroalgae. *Journal of Experimental Marine Biology and Ecology*, *92*(2–3), 283–301. https://doi.org/10.1016/0022-0981(85)90100-5

Gao, J., Mu, L., Bao, X., Song, J., & Ding, Y. (2018). Drift analysis of MH370 debris in the southern Indian Ocean, *12* (January 2017), 468–480.

Garraffo, Z. D., Mariano, A. J., Griffa, A., Veneziani, C., & Chassignet, E. P. (2001). Lagrangian data in a high-resolution numerical simulation of the North Atlantic I. Comparison with in situ drifter data. *Journal of Marine Systems*, *29*, 157–176.

Gaube, P., McGillicuddy, D., Chelton, D., Behrenfeld, M. J., & Strutton, P. (2014). Regional variations in the influence ofmesoscale eddies on near-surface chlorophyll. *Journal of Geophysical Research: Oceans*, *119*, 8195–8220. https://doi.org/10.1002/2014JC010111.

Gaube, P., Chelton, D. B., Samelson, R. M., Schlax, M. G., & O'Neill, L. W. (2015). Satellite Observations of Mesoscale Eddy-Induced Ekman Pumping. *Journal of Physical Oceanography*, *45*(1), 104–132. https://doi.org/10.1175/JPO-D-14-0032.1

Gower, J. F. R., & King, S. a. (2011). Distribution of floating *Sargassum* in the Gulf of Mexico and the Atlantic Ocean mapped using MERIS. *International Journal of Remote Sensing*, *32*(7), 1917–1929. https://doi.org/10.1080/01431161003639660

Gower, J., Hu, C., Borstad, G., & King, S. (2006). Ocean Color Satellites Show Extensive Lines of Floating *Sargassum* in the Gulf of Mexico. *IEEE Transactions on Geoscience and Remote Sensing*, *44*(12), 3619–3625.

Gower, J., Young, E., & King, S. (2013). Satellite images suggest a new *Sargassum* source region in 2011. *Remote Sensing Letters*, *4*(8), 764–773. https://doi.org/10.1080/2150704X.2013.796433

Häkkinen, S., Hátún, H., & Rhines, P. (2008). Satellite Evidence of Change in the Northern Gyre. In R. R. Dickson, J. Meincke, & P. Rhines (Eds.), *Arctic-Subarctic Ocean Fluxes* (pp. 551–567). Springer Science+Business Media.

Haller, G., & Sapsis, T. (2008). Where do inertial particles go in fluid flows? *Physica D: Nonlinear Phenomena*, *237*(5), 573–583. https://doi.org/10.1016/j.physd.2007.09.027

Halliwell, G. R., Weisberg, R. H., & Mayer, D. A. (2003). A synthetic float analysis of upper-limb meridional overturning circulation interior ocean pathways in the tropical/subtropical Atlantic. In *Interhemispheric Water Exchange in the Atlantic Ocean* (Elsevier O, pp. 93–136).

Hanisak, M. D., & Samuel, M. a. (1987). Growth rates in culture of several species of *Sargassum* from Florida, USA. *Hydrobiologia*, *151–152*(1), 399–404. https://doi.org/10.1007/BF00046159

Hansen, D., & Poulain, P.-M. (1996). Quality Control and Interpolations of WOCE-TOGA Drifter Data. *Journal of Atmospheric and Oceanic Technology*, *13*, 900–909.

Hemphill, A. (2005). Conservation on the High Seas — drift algae habitat as an open ocean cornerstone. High Seas Marine Protected Areas. *Parks*, *15*(3), 48–56.

Hoffmayer, E. R., Franks, J. S., Comyns, B. H., Hendon, J. R., & Waller, R. S. (2005). Larval and Juvenile Fishes Associated with Pelagic *Sargassum* in the Northcentral Gulf of Mexico. *50th Gulf and Caribbean Fisheries Institute*, 259–269.

Hood, R. R., Bates, N. R., Capone, D. G., & Olson, D. B. (2001). Modeling the Effect of Nitrogen Fixation on Carbon and Nitrogen Fluxes at BATS. *Deep-Sea Research*, 1–53.

Hu, C. (2009). A novel ocean color index to detect floating algae in the global oceans. *Remote Sensing of Environment*, *113*(10), 2118–2129. https://doi.org/10.1016/j.rse.2009.05.012

Hu, C., Feng, L., Hardy, R. F., & Hochberg, E. J. (2015). Spectral and spatial requirements of remote measurements of pelagic *Sargassum* macroalgae. *Remote Sensing of Environment*, *167*, 229–246. https://doi.org/10.1016/j.rse.2015.05.022

Huffard, C. L., von Thun, S., Sherman, a D., Sealey, K., & Smith, K. L. (2014). Pelagic *Sargassum* community change over a 40-year period: temporal and spatial variability. *Marine Biology*, *161*(12), 2735–2751. https://doi.org/10.1007/s00227-014-2539-y

Johnson, D. L., & Richardson, P. L. (1977). On the wind-induced sinking of *Sargassum*. *Journal of Experimental Marine Biology and Ecology*, *28*(3820), 255–267.

Laffoley, D. d'., Laffoley, D.d'A, Roe, H.S.J., Angel, M.V., Ardron, J., Bates, N. R., Boyd, I.L., Brooke, S., Buck, K.N., Carlson, C.A., Causey, B., Conte, M.H., Christiansen, S., Cleary, J., Donnelly, J., Earle, S.A., Edwards, R., Gjerde, K.M., Giovannoni, S.J., Gulick, S., Gollock, M., Hallett, J., Halpin, P., Hanel, R., Hemphill, A., Johnson, R.J., Knap, A.H., Lomas, M.W., McKenna, S.A., Miller, M.J., Miller, P.I., Ming, F.W., Moffitt, R., Nelson, N.B., Parson, L., Peters, A.J., Pitt, J., Rouja, P., Roberts, J., Seigel, D.A., Siuda, A.N.S., Steinberg, D.K., Stevenson, A., Sumaila, V.R., Swartz, W., Thorrold, S., Trott, T.M., & Vats, V.. (2011). *The Protection and Management of the Sargasso Sea: The golden floating rainforest of the Atlantic Ocean. Summary Science and Supporting Evidence Case*. Sargasso Sea Alliance.

Langin, K. (2018). Seaweed masses assault Caribbean islands. *Science*, *360*(6394), 1157–1158. https://doi.org/10.1126/science.360.6394.1157

Lapointe, B. E. (1986). Phosphorus-limited photosynthesis and growth of *Sargassum* natans and *Sargassum fluitans* (Phaeophyceae) in the western North Atlantic. *Deep-Sea Research*, *33*(3), 391–399.

Lapointe, B. E. (1995). A comparison of nutrient-limited productivity in *Sargassum natans* from neritic vs . oceanic waters of the western North Atlantic Ocean. *Limnology and Oceanography*, *40*(3), 625–633.

Lapointe, B. E., West, L. E., Sutton, T. T., & Hu, C. (2014). Ryther revisited: Nutrient excretions by fishes enhance productivity of pelagic *Sargassum* in the western North Atlantic Ocean. *Journal of Experimental Marine Biology and Ecology*, *458*, 46–56. https://doi.org/10.1016/j.jembe.2014.05.002

Law, K. L., Morét-Ferguson, S., Maximenko, N. A, Proskurowski, G., Peacock, E. E., Hafner, J., & Reddy, C. M. (2010). Plastic accumulation in the North Atlantic subtropical gyre. *Science (New York, N.Y.)*, *329*(5996), 1185–1188. https://doi.org/10.1126/science.1192321

Lebreton, L. C. M., Greer, S. D., & Borrero, J. C. (2012). Numerical modelling of floating debris in the world's oceans. *Marine Pollution Bulletin*, *64*(3), 653–661. https://doi.org/10.1016/j.marpolbul.2011.10.027

Lévy, M., Mémery, L., & Madec, G. (1998). The onset of a bloom after deep winter convection in the northwestern Mediterranean sea: Mesoscale process study with a primitive equation model. *Journal of Marine Systems*, *16*(1–2), 7–21. https://doi.org/10.1016/S0924-7963(97)00097-3

Lomas, M. W., Bates, N. R., Johnson, R. J., Knap, A. H., Steinberg, D. K., & Carlson, C. A. (2013). Two decades and counting: 24-years of sustained open ocean biogeochemical measurements in the Sargasso Sea. *Deep-Sea Research Part II: Topical Studies in Oceanography*, *93*, 16–32. https://doi.org/10.1016/j.dsr2.2013.01.008

Maréchal, J. P., Hellio, C., & Hu, C. (2017). A simple, fast, and reliable method to predict *Sargassum* washing ashore in the Lesser Antilles. *Remote Sensing Applications: Society and Environment*, *5*(May 2016), 54–63. https://doi.org/10.1016/j.rsase.2017.01.001

Martin, A. P., & Richards, K. J. (2001). Mechanisms for vertical nutrient transport within a North Atlantic mesoscale eddy. *Deep-Sea Research Part II: Topical Studies in Oceanography*, *48*(4–5), 757–773. https://doi.org/10.1016/S0967-0645(00)00096-5

Maxey, M. R., & Riley, J. J. (1983). Equation of motion for a small rigid sphere in a nonuniform flow. *Physics of Fluids*, *26*(4), 883–889. https://doi.org/10.1063/1.864230

McGillicuddy, D. J., Johnson, R., Siegel, D. A., Michaels, A. F., Bates, N. R., & Knap, A. H. (1999). Mesoscale variations of biogeochemical properties in the Sargasso Sea. *Journal of Geophysical Research: Oceans*, *104*(C6), 13381–13394. https://doi.org/10.1029/1999JC900021

Menzel, D. W., & Ryther, J. H. (1961). Nutrients limiting the production of phytoplankton in the Sargasso sea, with special reference to iron. *Deep Sea Research*, *7*(4), 276–281. https://doi.org/10.1016/0146-6313(61)90045-4

Michaels, A. F., Knap, A. H., & Rachael, L. (1994). Seasonal patterns of ocean biogeochemistry at the U . S . JGOFS Bermuda Atlantic Time-series Study site and STOMMEL ,. *Deep Sea Research Part I Oceanographic Research Papers*, *41*(7), 1013–1038.

Michaels, F., & Knap, H. (1996). Overview of the U . S . JGOFS Bermuda Atlantic Time-series Study and the Hydrostation S program. *Deep-Sea Research Part II: Topical Studies in Oceanography*, *43*(2–3), 157–198.

Mitchell, T. P., & Wallace, J. M. (1992). The annual cycle in equatorial convection and sea surface temperature. *Journal of Climate*. https://doi.org/10.1175/1520-0442(1992)005<1140:TACIEC>2.0.CO;2

Moore, C. M., Mills, M. M., Milne, A., Langlois, R., Achterberg, E. P., Lochte, K., Geider, R., & La Roche, J. (2006). Iron limits primary productivity during spring bloom development in the central North Atlantic. *Global Change Biology*, *12*(4), 626–634. https://doi.org/10.1111/j.1365-2486.2006.01122.x

Morrow, R., Birol, F., Griffin, D., & Sudre, J. (2004). Divergent pathways of cylonic and anti-cyclonic ocean eddies. *Geophysical Research Letters*, *31*(24), 1–5. https://doi.org/10.1029/2004GL020974

Muller-Karger, F. E., Smith, J. P., Werner, S., Chen, R., Roffer, M., Liu, Y., … Enfield, D. B. (2015). Natural variability of surface oceanographic conditions in the offshore Gulf of Mexico. *Progress in Oceanography*, *134*, 54–76. https://doi.org/10.1016/j.pocean.2014.12.007

North, E. W., & Gallego, A. Petitgas, P. (Eds.). (2009). *Manual of recommended practices for modelling physical-biological interactions during fish early life*. ICES Cooperative Research Report No. 295.

Ocean Color. (2018). Retrieved July 10, 2018, from http://oceancolor.gsfc.nasa.gov

O'Reilly, J. E., Maritorena, S., O'Brien, M. C., Siegel, D. A, Toole, D., Menzies, D., Smith, R.C., Mueller, J. L., Mitchell, B.G., Kahru, M., Chavez, F.P., Strutton, P., Cota, G.F., Hooker, S.B., Mcclain, C.R.,

Carder, K.L., Müller-Karger, F.E., Harding, L., Magnuson, A., Phinney, D., Moore, G.F., Aiken, J., Arrigo, K.R., Letelier, R., Culver, M. (2000). SeaWiFS Postlaunch Calibration and Validation Analyses, Part 3. *SeaWiFS Postlaunch Technical Report Series*, *11*, 51pp.

Oyesiku, O. O., & Egunyomi, A. (2014). Identification and chemical studies of pelagic masses of *Sargassum natans* (Linnaeus) Gaillon and *S* . *fluitans* (Borgessen) Borgesen (brown algae), found offshore in Ondo State , Nigeria. *African Journal of Biotechnology*, *13*(10), 1188–1193. https://doi.org/10.5897/AJB2013.12335

Parr, A. E. (1939). Quantitative observations on the pelagic *Sargassum* vegetation of the western North Atlantic. *Bull. Bingham Oceanogr. Coll.*, *6*, 1–94.

Putman, N. F., & He, R. (2013). Tracking the long-distance dispersal of marine organisms: sensitivity to ocean model resolution. *Journal of the Royal Society, Interface / the Royal Society*, *10*(81), 20120979. https://doi.org/10.1098/rsif.2012.0979

Putman, N. F., Goni, G. J., Gramer, L. J., Hu, C., Johns, E. M., Trinanes, J., & Wang, M. (2018). Simulating transport pathways of pelagic *Sargassum* from the Equatorial Atlantic into the Caribbean Sea. *Progress in Oceanography*, *165*(January), 205–214. https://doi.org/10.1016/j.pocean.2018.06.009

R Core Team. (2018). R: A Language and Environment for Statistical Computing. R Foundation for Statistical Computing, Vienna, Austria. https://www.R-project.org.

Rast, M., Bezy, J. L., & Bruzzi, S. (1999). The ESA Medium Resolution Imaging Spectrometer MERIS a review of the instrument and its mission. *International Journal of Remote Sensing*, *20*(9), 1681–1702. https://doi.org/10.1080/014311699212416

Redfield, A. C., Ketchum, B. H., & Richards, F. A. (1963). The Influence of Organisms on the Composition of Sea-Water. In M. N. Hill (Ed.), *The Sea: Ideas and Observations on Progress in the Study of the Seas Volume 2 The Composition of Sea-Water Comparative and Descriptive Oceanography* (pp. 26–77). New York: John Wiley & Sons, Inc.

Richardson, P. L., & Reverdin, G. (1987). Seasonal cycle of velocity in the Atlantic North Equatorial Countercurrent as measured by surface drifters, current meters,

and ship drifts. *Journal of Geophysical Research*, *92*(C4), 3691. https://doi.org/10.1029/JC092iC04p03691

Rooker, J. R., Holt, S.A., Wells, R. D., Turner, J. P., & Pratt, C. (2004). Retrospective determination of trophic relationships among pelagic fishes associated with *Sargassum* mats in the Gulf of Mexico. *55th Gulf and Caribbean Fisheries Institute*. 257-266.

Rothäusler, E., Gutow, L., & Thiel, M. (2012). Floating Seaweeds and Their Communities. In C. Wiencke & K. Bischof (Eds.), *Seaweed Biology, Ecological Studies 219* (pp. 359–380). Berlin: Springer-Verlag. https://doi.org/10.1007/978-3-642-28451-9

Rypina, I. I., Jayne, S. R., Yoshida, S., Macdonald, a. M., Douglass, E., & Buesseler, K. (2013). Short-term dispersal of Fukushima-derived radionuclides off Japan: modeling efforts and model-data intercomparison. *Biogeosciences*, *10*(7), 4973–4990. https://doi.org/10.5194/bg-10-4973-2013

Ryther, J. H., & Menzel, D. W. (1959). The seasonal and geographical range of primary production in the Western Sargasso Sea. *Deep Sea Research*, *6*, 235–238.

SaWS. (2018). University of South Florida Satellite-based *Sargassum* Watch System. Accessed July 10, 2018. https://optics.marine.usf.edu/projects.SaWS.html

Schell, J. M., Goodwin, D. S., & Siuda, A. N. S. (2015). Recent *Sargassum* inundation events in the Caribbean: Shipboard observations reveal dominance of a previously rare form. *Oceanography*, *28*(3), 8–10. https://doi.org/http://dx.doi.org/10.5670/oceanog.2015.70

Schoener, A., & Rowe, G. T. (1970). Pelagic *Sargassum* and its presence among the deep-sea benthos. *Deep-Sea Research*, *17*, 923–925. https://doi.org/10.1007/BF02767163

Schwartz, F. J. (1988). Aggregations of young hatchling loggerhead sea turtles in the *Sargassum* off North Carolina. *Marine Turtle Newsletter*, *42*, 9–10.

SeaWiFS Project. (2003). SeaWiFS Global Monthly Mapped 9 km Chlorophyll a. Ver. 1. CA, USA: PO.DAAC.

Shulzitski, K., Sponaugle, S., Hauff, M., Walter, K., D'Alessandro, E. K., & Cowen, R. K. (2015). Close encounters with eddies: oceanographic features increase growth of larval reef fishes during their journey to the reef. *Biology Letters*, *11*(1), 20140746. https://doi.org/10.1098/rsbl.2014.0746

Simons, R. D., Siegel, D. a., & Brown, K. S. (2013). Model sensitivity and robustness in the estimation of larval transport: A study of particle tracking parameters. *Journal of Marine Systems*, *119–120*, 19–29. https://doi.org/10.1016/j.jmarsys.2013.03.004

Sissini, M. N., de Barros Barreto, M. B. B., Széchy, M. T. M., de Lucena, M. B., Oliveira, M. C., Gower, J., … Horta, P. A. (2017). The floating *Sargassum* (Phaeophyceae) of the South Atlantic Ocean – likely scenarios. *Phycologia*, *56*(3), 321–328. https://doi.org/10.2216/16-92.1

Siuda, A. N. S. (2011). *Summary of Sea Education Association Long-term Sargasso Sea Surface Net Data*. Sargasso Sea Alliance Science Rep Ser 10. 18 pp.

Smetacek, V., & Zingone, A. (2013). Green and golden seaweed tides on the rise. *Nature*, *504*(7478), 84–88. https://doi.org/10.1038/nature12860

South Atlantic Fishery Management Council (SAFMC). (2002). *Fishery Management Plan for Pelagic Sargassum Habitat of the South Atlantic Region* (Vol. 4699) 153 pp.

Steele, M., Morley, R., & Ermold, W. (2001). PHC: A Global Ocean Hydrography with a High-Quality Arctic Ocean. *Journal of Climate*, *14*, 2079–2087. https://doi.org/10.1175/1520-0442(2001)014<2079:PAGOHW>2.0.CO;2

Stoner, A. W. (1983). Pelagic *Sargassum*: Evidence for a major decrease in biomass. *Deep Sea Research Part A. Oceanographic Research Papers*, *30*(4), 469–474.

Stoner, A. W., & Greening, H. (1984). Geographic variation in the macrofaunal associates of pelagic *Sargassum* and some biogeographic implications. *Mar. Ecol. Prog. Ser.*, *20*, 185--192.

Stramma, L., & Schott, F. (1999). The mean flow field of the tropical Atlantic Ocean. *Deep-Sea Res. II*, *46*(1–2), 279–303. https://doi.org/10.1016/S0967-0645(98)00109-X

Stukel, M. R., Coles, V. J., Brooks, M. T., & Hood, R. R. (2014). Top-down, bottom-up and physical controls on diatom-diazotroph assemblage growth in the Amazon River plume. *Biogeosciences*, *11*, 3259–3278. https://doi.org/10.5194/bg-11-3259-2014

Sturges, W. (2016). The Mean Upper-Layer Flow in the Central Gulf of Mexico by a New Method. *Journal of Physical Oceanography*, *46*, 2915–2924. https://doi.org/10.1175/JPO-D-16-0062.1

Sturges, W., & Leben, R. (2000). Frequency of Ring Separations from the Loop Current in the Gulf of Mexico: A Revised Estimate. *Journal of Physical*

Oceanography, *30*(7), 1814–1819. https://doi.org/10.1175/1520-0485(2000)030<1814:FORSFT>2.0.CO;2

Thiel, M., & Gutow, L. (2005). *The Ecology of Rafting in the Marine Environment . I. the Floating Substrata*. (R. N. Gibson, J. A. Atkinson, & J. D. M. Gordon, Eds.), *Oceanography and Marine Biology:An Annual Review* (Vol. 42). https://doi.org/10.1201/9781420037449.ch7

Tsukidate, J. (1984). Studies on the regenerative ability of the brown algae, *Sargassum muticum* (Yendo) Fensholt and *Sargassum tortile* C. Agardh. *Hydrobiologia*, *116–117*(1), 393–397. https://doi.org/10.1007/BF00027708

Uppala, S. M., Kållberg, P. W., Simmons, A. J., Andrae, U., da Costa Bechtold, V., Fiorino, M., Gibson, J. K., Haseler, J., Hernandez, A., Kelly, G. A., Li, X., Onogi, K., Saarinen, S., Sokka, N., Allan, R. P., Andersson, E., Arpe, K., Balmaseda, M. A., Beljaars, A. C.M., van de Berg, L., Bidlot, J., Bormann, N., Caires, S., Chevallier, F., Dethof, A., Dragosavac, M., Fisher, M., Fuentes, M., Hagemann, S., Hólm, E., Hoskins, B. J., Isaksen, L., Janssen, P. A.E.M., Jenne, R., McNally, A. P., Mahfouf, J. F., Morcrette, J. J., Rayner, N. A., Saunders, R. W., Simon, P., Sterl, A., Trenberth, K. E., Untch, A., Vasiljevic, D., Viterbo, P., & Woollen, J. (2005). The ERA-40 re-analysis. *Quarterly Journal of the Royal Meteorological Society*, *131*(612), 2961–3012. https://doi.org/10.1256/qj.04.176

Wang, M., & Hu, C. (2016). Mapping and quantifying *Sargassum* distribution and coverage in the Central West Atlantic using MODIS observations. *Remote Sensing of Environment*, *183*, 350–367. https://doi.org/10.1016/j.rse.2016.04.019

Wang, M., & Hu, C. (2018). On the continuity of quantifying floating algae of the Central West Atlantic between MODIS and VIIRS. *International Journal of Remote Sensing*, *39*(12), 3852–3869. https://doi.org/10.1080/01431161.2018.1447161

Wang, M., Hu, C., Cannizzaro, J., English, D., Han, X., Naar, D., Wang, M., Lapointe, B., Brewton, R., Hernandez, F. (2018). Remote sensing of *Sargassum* biomass, nutrients, and pigments. *Geophysical Research Letters*. https://doi.org/10.1029/2018GL078858

Weber, S. C., Carpenter, E. J., Coles, V. J., Yager, P. L., Goes, J., & Montoya, J. P. (2017). Amazon River influence on nitrogen fixation and export production in the western tropical North Atlantic. *Limnology and Oceanography*, *62*(2), 618–631. https://doi.org/10.1002/lno.10448

Webster, R. K., & Linton, T. (2013). Development and implementation of *Sargassum* Early Advisory System (SEAS). *Shore & Beach*, *81*(3), 1–6.

Wei, C. L., Rowe, G. T., Nunnally, C. C., & Wicksten, M. K. (2012). Anthropogenic "Litter" and macrophyte detritus in the deep Northern Gulf of Mexico. *Marine Pollution Bulletin*, *64*(5), 966–973. https://doi.org/10.1016/j.marpolbul.2012.02.015

Wells, R. J. D., Rooker, J. R., Quigg, A., & Wissel, B. (2017). Influence of mesoscale oceanographic features on pelagic food webs in the Gulf of Mexico. *Marine Biology*, *164*(4), 1–11. https://doi.org/10.1007/s00227-017-3122-0

Williams, A., & Feagin, R. (2010). *Sargassum* as a Natural Solution to Enhance Dune Plant Growth. *Environmental Management*, *46*(September), 738–747. https://doi.org/10.1007/s00267-010-9558-3

Winge, O. (1923). The Sargasso Sea, its boundaries and vegetation. *Report on the Danish Oceanographic Expeditions 1908-10 to the Mediterranean and Adjacent Seas*, *3*, 1–34.

Witherington, B., Hirama, S., & Hardy, R. (2012). Young sea turtles of the pelagic *Sargassum*-dominated drift community: Habitat use, population density, and threats. *Marine Ecology Progress Series*, *463*, 1–22. https://doi.org/10.3354/meps09970

Wolff, T. (1979). Macrofaunal utilization of plant remains in the deep sea. *Sarsia*, *64*, 117–136.

Woodcock, A. H. (1993). Winds subsurface pelagic *Sargassum* and Langmuir circulations. *Journal of Experimental Marine Biology and Ecology*, *170*(1), 117–125.

Wu, J., & Boyle, E. (2002). Iron in the Sargasso Sea : Implications for the processes controlling dissolved Fe distribution in the ocean. *Global Biogeochemical Cycles*, *16*(4), 1–8. https://doi.org/10.1029/2001GB001453

Wyrtki, K., Magaard, L., & Hager, J. (1976). Eddy energy in the oceans. *Journal of Geophysical Research*, *81*(15), 2641. https://doi.org/10.1029/JC081i015p02641

Xue, Z., He, R., Fennel, K., Cai, W.-J., Lohrenz, S., & Hopkinson, C. (2013). Modeling ocean circulation and biogeochemical variability in the Gulf of Mexico. *Biogeosciences*, *10*(11), 7219–7234. https://doi.org/10.5194/bg-10-7219-2013

Zhai, X., Greatbatch, R. J., & Kohlmann, J. D. (2008). On the seasonal variability of eddy kinetic energy in the Gulf Stream region. *Geophysical Research Letters*, *35*(24), 1–6. https://doi.org/10.1029/2008GL036412

Zhong, Y., Bracco, A., & Villareal, T. A. (2012). Pattern formation at the ocean surface: *Sargassum* distribution and the role of the eddy field. *Limnology & Oceanography: Fluids & Environments*, *2*, 12–27. https://doi.org/10.1215/21573689-1573372